Functional and Structural Insights into the First and Second Intracellular Domains for D_1-Class Dopaminergic Receptors

Boyang Zhang

This thesis is submitted to the Faculty of Graduate and Postdoctoral Studies as a partial fulfillment of the Ph.D. program in Neuroscience

Department of Cellular and Molecular Medicine
Faculty of Medicine
University of Ottawa

Abstract

Previous studies have shown that the subtype-specific pharmacological properties of D_1-class receptors (D_1R and D_5R) can be attributed to their third intracellular domain and C-terminal tail. However, the importance of their first and second intracellular domains (IC1 and IC2) has yet to be explored. Using mutagenesis and bioinformatics, we examine the functional and structural roles of Ser/Thr spanning IC1 and IC2—most of which are conserved not only among D_1-class receptors but also among other GPCRs. Mutant receptors of human D_1-class receptors (hD_1R and hD_5R) were constructed whereby all Ser and Thr were mutated to the respective Ala and Val in the IC1 region (termed ST1 mutant receptors) and in the IC2 region (termed ST2 mutant receptors). We found that hD_1-ST2 and hD_5-ST2 exhibited contrasting properties of agonist affinity, constitutive activity, and dopamine potency. On the other hand, both ST2 mutants underwent internalization as wild-type but displayed weakened desensitization abilities. Homology models, which have been refined under membrane simulations, illustrate that the conserved $Ser^{3.55}$ and $Thr^{3.65}$ utilize their side chains to anchor the loop regions of IC2 to cytoplasmic helices. We also found multiple functional alterations in the hD_1-ST1 and hD_5-ST2, but in a subtype-similar manner. Mutating the conserved $Thr^{2.39}$ recapitulated the ablated basal activity and drastic decrease in dopamine potency previously witnessed in the hD_1-ST1. Based on the recurring theme observed in crystal structures, the side-chain of $Thr^{2.39}$ may help to position IC2 to have proper contacts with the G protein. Mutating the conserved $Ser^{2.45}$ was found to be solely responsible for the elevated E_{max} (maximal response) of the hD_1-ST1. Using single point mutagenesis, we further found that breaking the potential molecular interactions of $Ser^{2.45}$ in hD_1R (i.e. with $Asn^{3.42}$ and

Trp$^{4.50}$) mimicked its elevated E_{max}. This elevated E_{max} was not found to be caused by altered abilities to undergo agonist-induced desensitization or internalization relative to hD_1R. Overall, our work highlights the important functional and structural roles of IC1 and IC2 that needs to be accounted for in our current canonical models of GPCR signalling. Given the conserved nature of these Ser/Thr, our work may also be pertinent towards understanding the roles of IC1 and IC2 for other GPCRs.

Table of Contents

List of Tables

List of Figures

List of Abbreviations

A_{2A}R: Adenosine A_{2A} receptor

AA: Ascorbic acid

AC: adenylyl cyclase

AMPA: α-amino-3-hydroxy-5-methyl-4-isoxazolepropionic acid

AT_{1A}R: Angiotensin II type 1A receptor

BSA: Bovine serum albumin

BRET: Bioluminescence resonance energy transfer

cAMP: Cyclic adenosine monophosphate

CHO: Chinese hamster ovarian

CME: Clathrin-mediated endocytosis

COMT: catechol-O-methyltransferase

CRE: cAMP response element

CT: C-terminus

D_1R: Dopamine D_1 receptor

D_2R: Dopamine D_2 receptor

D_3R: Dopamine D_3 receptor

D_4R: Dopamine D_4 receptor

D_5R: Dopamine D_5 receptor

DA: Dopamine

DARPP32: Dopamine and cAMP-regulated phosphoprotein, 32 kDa

DHX: Dihydrexidine

DMSO: Dimethyl sulfoxide

DRIP: Dopamine receptor-interacting protein

EC: Extracellular domain

EDTA: Ethylenediaminetetraacetic acid

ELISA: Enzyme-linked immunosorbent assay

Epac: Exchange protein directly activated by cAMP

ER: Endoplasmic reticulum

ERK: Extracellular signal-regulated kinase

ETCM: Extended ternary complex model

FBS: Fetal bovine serum

GDP: Guanosine diphosphate

GnRH: Gonadotropin-releasing hormone

GPCR: G protein-coupled receptor

GRK: G protein-coupled receptor kinase

GTP: Guanosine triphosphate

$G\alpha_s$AH: α-helical domain of $G\alpha_s$

$G\alpha_s$Ras: Ras-like GTPase domain of $G\alpha_s$

hD_1R: Human dopamine D_1 receptor

hD_5R: Human dopamine D_5 receptor

HEK: Human embryonic kidney

HEPES: 4-(2-hydroxyethyl)-1-piperazineethanesulfonic acid

IBMX: 3-isobutyl-1-methylxanthine

IC: Intracellular domain

IP3: Inositol 1,4,5-trisphosphate

kDa: Kilodalton

L-DOPA: L-3,4-dihydroxyphenylalanine

MAO: Monoamine oxidase

MD: Molecular dynamics

MEM: Minimum essential media

mGluR1: Metabotropic glutamate receptor 1

MSN: Medium-size spiny neurons

NAM: Negative allosteric modulator

NMDA: N-methyl-D-aspartate

NT: N-terminus

PBS: Phosphate-buffered saline

PIP2: Phosphatidylinositol 4,5-bisphosphate

PKA: Protein kinase A

PKC: Protein kinase C

PLCβ: Phospholipase Cβ

PMA: Phorbol 12-myristate 13-acetate

PP1: Protein phosphatase 1

PTH_1R: Parathyroid hormone type 1 receptor

PVDF: Polyvinylidene difluoride

RIPA: radioimmunoprecipitation assay buffer

RGS: Regulators of G protein signalling

RMSD: Root-mean-square deviation

STEP: Striatal-enriched tyrosine phosphatase

TBS-T: Tris-buffered saline with Tween-20

TM: Transmembrane

TSHR: Thyroid-stimulating hormone receptor

V_2R: Vasopressin type 2 receptor

VMAT: Vesicular monoamine transporter

VTA: Ventral tegmental area

WT: wild-type

β_1AR: β_1-adrenoceptor

β_2AR: β_2-adrenoceptor

Acknowledgements

This dissertation culminating my study as a Ph.D. candidate over the past six years would not have been possible without the support I have received from others.

I would like to first thank my supervisor Dr. Mario Tiberi. I am truly grateful for his constant guidance and for providing me the resources that I needed to succeed. His scientific knowledge and passion has often inspired me to persevere despite the failures I have encountered, to make that extra effort, and to think outside the box. Under his tutelage, I have matured not only as a scientist but also as a person. I am very fortunate to have been given the opportunity to work in his lab.

I would like to also thank my advisory committee members, Dr. Paul Albert, Dr. Jean-Claude Beique, and Dr. Antonio Colavita, for their helpful discussions and their critical assessment of my work.

I wish to also express my appreciation to the people whom I have worked with in the lab. In particular, I would like to thank Dr. Bianca Plouffe for teaching me techniques when I first came to the lab and also for initiating the ST1 project. I wish to extend my thanks to previous lab members, Andrew Charette, Awatif Albaker, Caroline Lefebvre, and to current members, Annette Gower and Bradley Mischuk for making the working environment creative and enjoyable. I would like to also thank Xiaodi Yang and Binhui Liang for their help and technical assistance. It has been an honour and pleasure working with you all. Thanks for all the laughs and memories. I also gratefully acknowledge scholarship support from OGS (Ontario Graduate Scholarship), QEII-GSST (Queen

Elizabeth II Graduate Scholarships in Science and Technology), and University of Ottawa excellence awards.

Last but not least, I need to thank my wonderful parents for their unwavering love and encouragement. They have been with me every step of this journey, and I thank them for their dedication.

List of Publications

I. **Zhang B**, Albaker A, Plouffe B, Lefebvre C, and Tiberi M (2014). Constitutive activities and inverse agonism in dopamine receptors. *Advances in Pharmacology*, 70: 175-214.

II. Sedaghat K, **Zhang B**, Yang X, Lefebvre C, and Tiberi M (2015). Study of dopamine D_1 receptor regulation by G protein-coupled receptor kinases using whole-cell phosphorylation and cross-linking methods. *Neuromethods*, 96: 101-138.

III. **Zhang B**, Yang X, and Tiberi M (2015). Functional importance of two conserved residues in intracellular loop 1 and transmembrane region 2 of Family A GPCRs: insights from ligand binding and signal transduction responses of D_1 and D_5 dopaminergic receptor mutants. *Cellular Signalling*, 27: 2014-25.

IV. **Zhang B** and Tiberi M (2016). Keys to unlocking human dopamine D_1 receptor signal transduction. *Atlas of Science*, http://atlasofscience.org/keys-to-unlocking-human-dopamine-d1-receptor-signal-transduction/.

V. **Zhang B**, Yang X, and Tiberi M (2017). Structural and functional evidence for a subtype-specific role of the second intracellular domain for dopamine D_1-class receptors (In preparation).

Introduction

1. General Principles of GPCRs

As popular drug targets, the superfamily of G protein-coupled receptors (GPCRs) is estimated to constitute 2% of all proteins in humans (Vassilatis *et al.*, 2003). GPCRs are able to capture external cues such as light, ordorant, and hormones and incorporate them into a cellular response by activating G proteins that trigger a cascade of downstream targets. They are found throughout the human body and participate in diverse physiological processes including vision, motor movements, and inflammatory responses.

1.1 - GPCR Topography and Taxonomy

All GPCR possess a common topology consisting of an extracellular N-terminus, seven transmembranes (TM), three extracellular loops, three intracellular loops, and an intracelluar C-terminus (CT)—joined in a serpentine fashion. The TMs are α-helical in structure and extend into the inner and outer regions of the plasma membrane. Consequently, the cytoplasmic extensions of TMs join with the three intracellular loops to form three intracellular domains (IC): IC1, IC2, and IC3. Similarly, three extracellular domains (EC) are formed, EC1, EC2, and EC3, from combining the exoplasmic extensions of TMs with the three extracellular loops **(Figure 1)**.

Human GPCRs are typically classified, based on sequence and structural similarities, into 5 families: Family A (rhodopsin-like), Family B (secretin-like), Family C (glutamate-like), adhesion, and frizzled/taste2 (Alexander *et al.*, 2015, Fredriksson *et al.*, 2003). By far the largest and most studied of the five, Family A is distinguished by receptors having conserved sequences such as the (E)DRY and NPXXY motifs (further

discussed in 1.3) and a relatively short N-terminus compared to receptors of Families B and C. Dopamine receptors and other biogenic amine receptors are members of Family A.

To compare Family A GPCRs at the primary structure level, the most prevalently used method has been the Ballesteros-Weinstein nomenclature (Ballesteros & Weinstein, 1995). In this method, a residue is denoted by A.B numbering scheme whereby A represents the TM number for which the residue is located, and B represents the number position relative to the most conserved residue, which is designated 50. For example, a proline is the most conserved residue in TM6 among Family A receptors and is denoted 6.50. Residues two positions before or after this proline would be 6.48 and 6.52, respectively. Because the most conserved TM residues are the same for the majority of Family A receptors, this method can be widely applicable. They are as follows, with % conservation among Family A in brackets: $Asn^{1.50}$ (98%), $Asp^{2.50}$ (90%), $Arg^{3.50}$ (95%), $Trp^{4.50}$ (97%), $Pro^{5.50}$ (78%), $Pro^{6.50}$ (99%), and $Pro^{7.50}$ (88%) (Isberg *et al.*, 2015). Although the Ballesteros-Weinstein nomenclature was designed for TM residues, it may also be implemented for residues in loop regions if sequence conservation is high.

1.2 - G protein Cycle and Signalling Pathways

At the heart of GPCR signalling is the G protein—heterotrimeric, composed of Gα, Gβ, and Gγ subunits. During the inactive state of the receptor, these subunits form a complex, with GDP occupying the guanine nucleotide binding region of Gα. Once the receptor becomes activated (e.g through agonist binding), conformational changes occur in both the receptor and Gα to facilitate the replacement of GTP for GDP in Gα (Pierce *et*

al., 2002). Subsequently, Gα dissociates from the complex to activate effectors that initiate signal transduction **(Figure 2)**. The freed Gβ and Gγ remain bound together at all times but can activate effectors as well. Following the hydrolysis of GTP to GDP by the GTPase domain of Gα, the GDP-bound Gα reassociates with Gβγ to form the inactive trimeric complex (Pierce *et al.*, 2002). The rate of Gα-GTP hydrolysis can be accelerated through interactions between Gα and certain effectors (Ross & Wilkie, 2000) or through the binding of RGS (regulators of G protein signalling) proteins to Gα (Dohlman & Thorner, 1997).

Like the diverse array of GPCRs, there exists a multitude of different G protein subunits. Gα subunits can be functionally divided into four families: G_s, $G_{i/o}$, $G_{q/11}$, and $G_{12/13}$ (Downes & Gautam, 1999, Wess, 1998). Members of the G_s family activate the effector, adenylyl cyclase (AC). They include α_s, which has four splice variants that are ubiquitously expressed; and α_{olf}, which is highly expressed in olfactory and neostriatal neurons. The $G_{i/o}$ family inhibit AC and is comprised of α_{i1}, α_{i2}, α_{i3}, α_o, α_{t1}, α_{t2}, α_{gust}, and α_z. Known as transducins, α_{t1} and α_{t2} are uniquely located in retinal rod and cone cells, respectively. α_{gust} can be found in taste buds. Members of $G_{q/11}$ family activate phospholipase Cβ (PLCβ) and consist of α_q, α_{11}, α_{14}, and $\alpha_{15/16}$. Forming the $G_{12/13}$ family are α_{12} and α_{13}, which have been reported to activate effectors such as Rho guanine exchange factor (Siehler, 2009) and phospholipase D (Plonk *et al.*, 1998).To date, six types of Gβ (including splice variants) and twelve types of Gγ have been identified (Downes & Gautam, 1999). It is therefore possible to have 72 permutations of Gβγ complexes; however, not all may exist in nature.

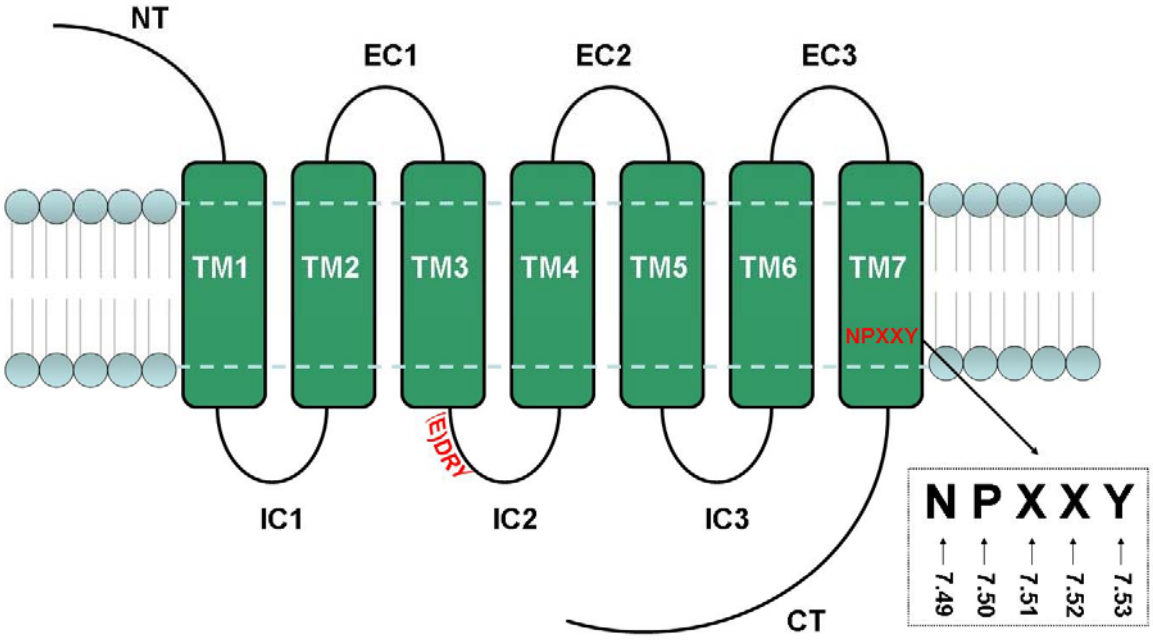

Figure 1. General topography of GPCRs.
The seven transmembrane domains are represented by green rectangles. Dashed lines represent membrane boundaries. Family A GPCRs are recognized by the (E)DRY motif located at the cytoplasmic extension of TM3 and the NPXXY motif located within TM7. An example of using the Ballesteros-Weinstein nomenclature is also shown for NPXXY motif. The proline in this motif is the most conserved residue in TM7 among Family A GPCRs and is denoted as 7.50. The preceding Asn (N) is denoted 7.49, and the downstream Tyr (Y) is given 7.53. X in the motif represents any amino acids. NT, N-terminus; IC, intracellular domain; EC, extracellular domain; CT, C-terminus.

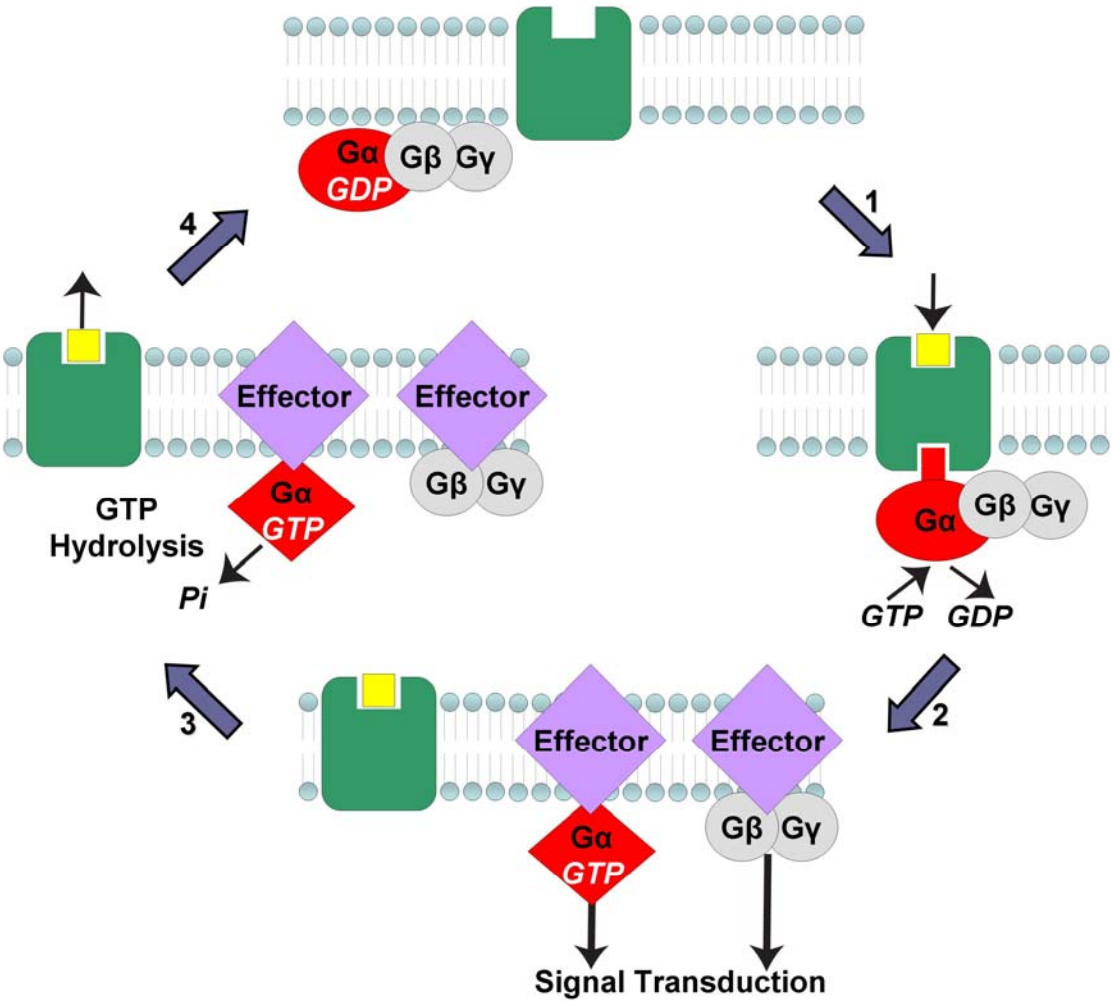

Figure 2. The G protein cycle.
There are four stages to the G protein cycle. Stage 1: Agonist binding to the receptor induces conformational changes that allow the G protein to couple to the receptor. This facilitates the exchange of GDP for GTP on Gα. Stage 2: GTP-bound Gα dissociates from Gβγ. Both activate effectors and initiate downstream signalling. Stage 3: GTP is hydrolyzed to GDP on Gα, which inactivates Gα. Stage 4: GDP-bound Gα reassociates with Gβγ to form the inactive trimeric complex.

The direct consequence of effector activation is the production of second messengers that amplify GPCR signalling. For instance, following G_s-mediated interaction and activation of the catalytic domain of AC, AC converts ATP to the secondary messenger cAMP (cyclic adenosine monophosphate). Subsequently, two molecules of cAMP bind to the two regulatory subunits of protein kinase A (PKA) to release its two catalytic subunits (Alberts *et al.*, 2008). One of the many effects exerted by PKA is the phosphorylation of cAMP response element-binding protein (CREB) that causes transcription of genes under the cAMP response element (CRE) promoter region (Shaywitz & Greenberg, 1999). In the $G_{q/11}$ signalling pathway, activated PLCβ converts phosphatidylinositol 4,5-bisphosphate (PIP2) to generate two secondary messengers: inositol 1,4,5-triphosphate (IP3) and diacylglycerol (Wettschureck & Offermanns, 2005). IP3 diffuses to the endoplasmic reticulum (ER) where it binds to IP3-gated Ca^{2+} channels to release calcium stores in the ER into the cytoplasm. On the other hand, diacylglycerol remains tethered to the plasma membrane where it cooperates with Ca^{2+} and phophatidylserine to activate protein kinase C (PKC). Like PKA, both Ca^{2+} release and activated PKC can subsequently proceed to mediate a diverse range of cellular effects.

1.3 - Theoretical and Structural Properties of GPCR Activation

Perhaps the most popular model to explain GPCR activation has been the extended ternary complex model (ETCM) (Samama *et al.*, 1993). In a setting comprised of only ligand, receptor, and G protein, the model proposes that the receptor can exists as two states, inactive R or active R*, in which only the R* couples to the G protein. With the addition of agonist binding to R*, the three components form a ternary complex. This

model, like the original ternary complex model, dictates that a receptor can transition from R to R* through agonist binding; however, it further dictates that R* can be achieved through the spontaneous isomerization of the receptor and therefore accounts for constitutive/basal activities among GPCRs. Furthermore, it describes that agonists preferentially bind (i.e. have high affinity) for the R* state and by binding, shifts the thermodynamic equilibrium towards the R* state. Conversely, inverse agonists preferentially bind and shift the equilibrium towards the R state and thereby reducing constitutive activity. Pure antagonists exhibit no preference for either R or R* state binding and possess no intrinsic activity.

Due to its simplicity, the ETCM has garnered much popularity; however, it is the same simplicity that has also contributed towards its limitations. For instance, the two-state model of ETCM cannot explain the multiple R* and R states thought to occur or the modulation of receptor activity by allosteric modulators, which can bind to the receptor separate from the orthosteric (primary) ligand binding site (Gether & Kobilka, 1998). As well, the ETCM does not account for biased agonism, whereby different agonists binding to one receptor can initiate different downstream signalling events (Rajagopal *et al.*, 2010).

The structural mechanism of how R state transitions to R* state, since the proposal of ETCM in 1992, has now begun to be unravelled due to a substantial increase in crystallized GPCR structures during this decade. Currently, the structure of receptor bound to a G protein (i.e full R*) has been obtained for the rhodopsin, adenosine A_{2A} ($A_{2A}R$), and β_2-adrenoceptor (β_2AR)—the former two bound to a truncated Gα and the latter bound to a heterotrimeric G_s. Furthermore, agonist-bound states that may represent

intermediate R* states are available for a number of GPCRs. When compared to their crystallized R states, the common conformational changes in (full) R* state are the outward "kick" of TM6 and movement of TM5, which collectively opens the cytoplasmic portion of the receptor to facilitate G protein coupling **(Figure 3)**. Specifically, TM6 moves as much as 6 Å in rhodopsin and 14 Å for both $A_{2A}R$ and β_2AR as they transition from R to R*.

The solved β_2AR-G_s complex also demonstrates that the $G\alpha_s$ subunit contains a Ras-like GTPase domain ($G\alpha_sRas$) and an α-helical domain ($G\alpha_sAH$), in which their joining interface creates the GDP/GTP binding site. During activation, it is proposed that the α5-helix of the $G\alpha_sRas$ first inserts into the receptor and then rotates 30^o in a crowbar-like manner to establish further receptor interactions (Katritch *et al.*, 2013, Rasmussen *et al.*, 2011). This triggers more conformational changes in $G\alpha_s$ and most importantly, a drastic rotation of $G\alpha_sAH$ from $G\alpha_sRas$ (127^o in the case of β_2AR-G_s complex) to release GDP from $G\alpha_s$. Furthermore, the β_2AR-G_s complex reveals that most of the contacts between receptor and G protein are IC2, TM5, and TM6 of the receptor with α5-helix and its neighbouring regions of $G\alpha_sRas$. One notable contact is the insertion of a conserved hydrophobic residue in IC2 ($Phe^{3.58}$ in β_2AR) into a hydrophobic pocket of $G\alpha_sRas$. Interestingly, no interactions were found between β_2AR and the two Gβγ subunits.

As previously mentioned, a signature of Family A GPCRs is the (E)DRY motif that is located in the cytoplasmic extension of TM3 and refers to a triad of residues: $Glu/Asp^{3.49}$, $Arg^{3.50}$, and $Tyr^{3.51}$. From the first crystallized GPCR, dark state (inactive) rhodopsin, it was suggested that $Arg^{3.50}$ of the (E)DRY motif may form an "ionic lock"

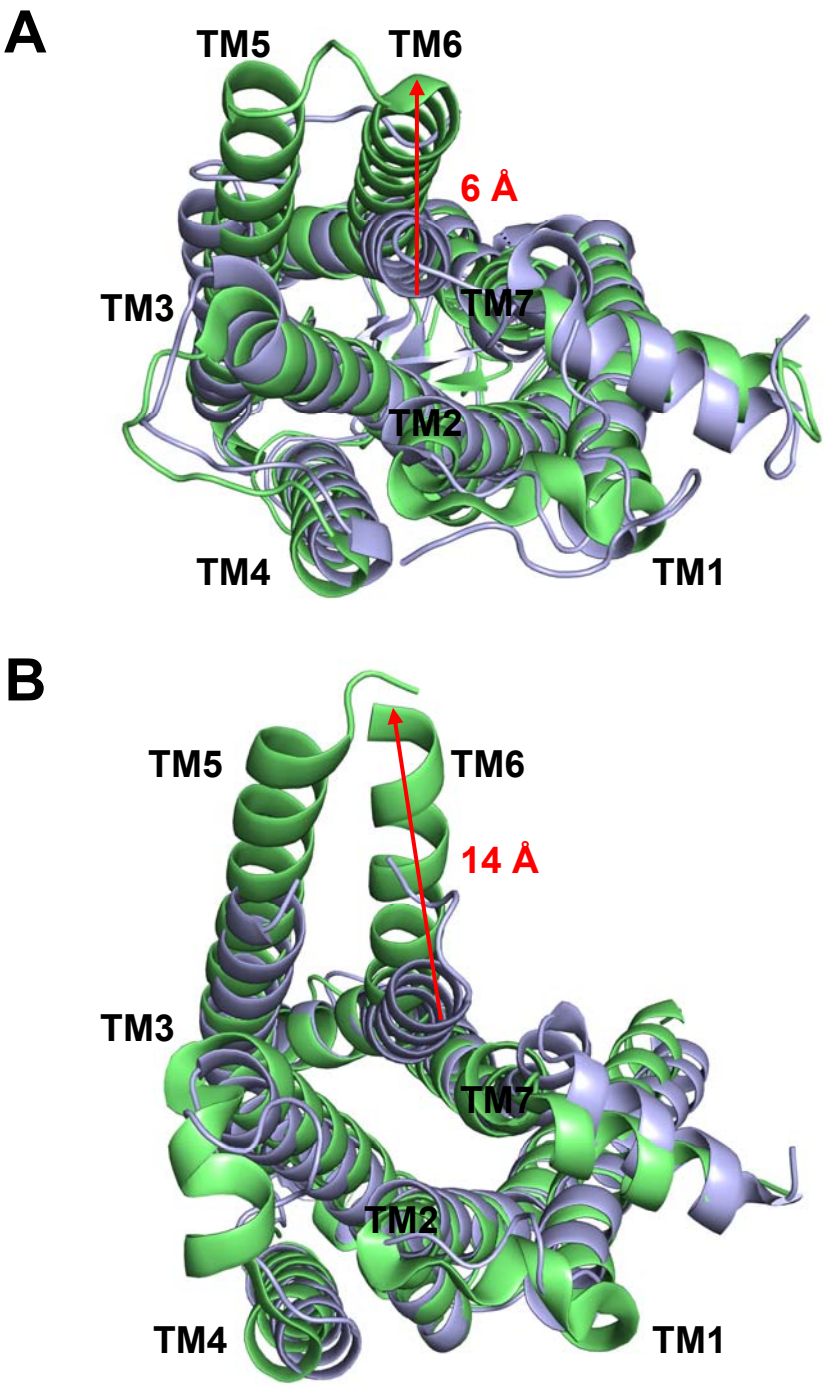

Figure 3. Common conformational changes from R to R*.
A) Inactive rhodopsin (grey; 1F88) aligned to rhodopsin bound to Gα fragment (green; 3PQR). B) Inactive β_2AR (grey; 2RH1) aligned to β_2AR bound to heterotrimeric G_s protein (green; 3SN6). The most significant movement is by TM6, which moves outward by 6 Å in A) and 14 Å in B). Another common change in A) and B) is the helical extension of TM5 upon transitioning to R*. G proteins have been removed for clarity.

with Asp/Glu$^{6.30}$ of TM6 that serves to keep the receptor inactive (Palczewski *et al.*, 2000). This ionic lock was indeed broken in the crystallized R* rhodopsin bound to a Gα fragment (Choe *et al.*, 2011, Scheerer *et al.*, 2008) **(Figure 4)**. However, the importance of this "ionic lock" for maintaining the R state is currently debatable because it is also broken in several crystallized GPCRs bound to either antagonists or inverse agonists. On the other hand, molecular dynamics (MD) simulations have demonstrated that despite being broken at start, the ionic lock can reform under microsecond timescales (Dror *et al.*, 2009, Vanni *et al.*, 2009). In addition, the other "ionic lock" between Glu/Asp$^{3.49}$ and Arg$^{3.50}$ within the (E)DRY motif is observed in all R and intermediate R* states (Katritch *et al.*, 2013). Only in the G protein-bound structures does this ionic lock break apart to allow Arg$^{3.50}$ to have electrostatic interactions with the G protein.

Another recognized hallmark for R* is the rotamer switch of the NPXXY motif within TM7 (where X represents any amino acid). In the inactive state, Tyr$^{7.53}$ of the NPXXY motif is oriented towards TM1 and TM2; however, upon receptor activation Tyr$^{7.53}$ rotates towards TM3, TM5, and TM6 **(Figure 4)**. This movement may serve to block the displaced TM6 from returning inward and therefore may stabilize the R* state. It is also interesting to note that in the G protein-bound $A_{2A}R$ and β_2AR, Tyr$^{7.53}$ forms cation-π interactions with Arg$^{3.50}$ of the (E)DRY motif. Consequently, this indirectly links the NPXXY motif to the G protein.

1.4 - Classical and Novel Events after GPCR Membrane Signalling

In broad strokes, the canonical life-cycle of a GPCR after initiating signalling can be defined by three stages: desensitization, internalization, and recycling/degradation

(Figure 5). This refractory period is highly regulated and serves to prevent potential cellular injury caused by sustained GPCR signalling. In homologous desensitization, the agonist-bound receptor becomes phosphorylated by G protein-coupled receptor kinases (GRK1-7), which increase receptor affinity for cytosolic arrestins (β-arrestin 1, β-arrestin 2, visual and cone arrestins). The binding of arrestin to the receptor sterically hinders the G protein from further coupling to the receptor (Gainetdinov *et al.*, 2004, Kelly *et al.*, 2008). Even without agonist occupancy, the receptor can be uncoupled from the G protein via phosphorylation by PKA and PKC that have been activated by another receptor signalling cascade. This is known as heterologous desensitization (Luttrell & Lefkowitz, 2002).

Although downstream events of heterologous desensitization are not well studied, it is established that following arrestin binding to the receptor, arrestin prepares the receptor for internalization by recruiting proteins such as clathrin and AP-2. Together, the receptor complex is targeted to clathrin-coated pits whereby the helical GTPase, dynamin, cleaves the budding vesicle for receptor internalization (Luttrell & Lefkowitz, 2002). This process is often referred to as clathrin-mediated endocytosis (CME). Additionally, some GPCRs can be internalized through arrestin-independent and dynamin-dependent pathway (i.e. caveolae) (Chini & Parenti, 2004) or through arrestin-independent and dynamin-independent pathway (Lamb *et al.*, 2001, Zhang *et al.*, 1996). Intracellular trafficking of GPCRs is also known to be orchestrated by different Ras-like GTPases of the Rab family. For instance, Rab5 mediates receptor endocytosis and sorting to early endosomes, while Rab7 regulates sorting from late endosomes to lysosomes for degradation (Seachrist & Ferguson, 2003).

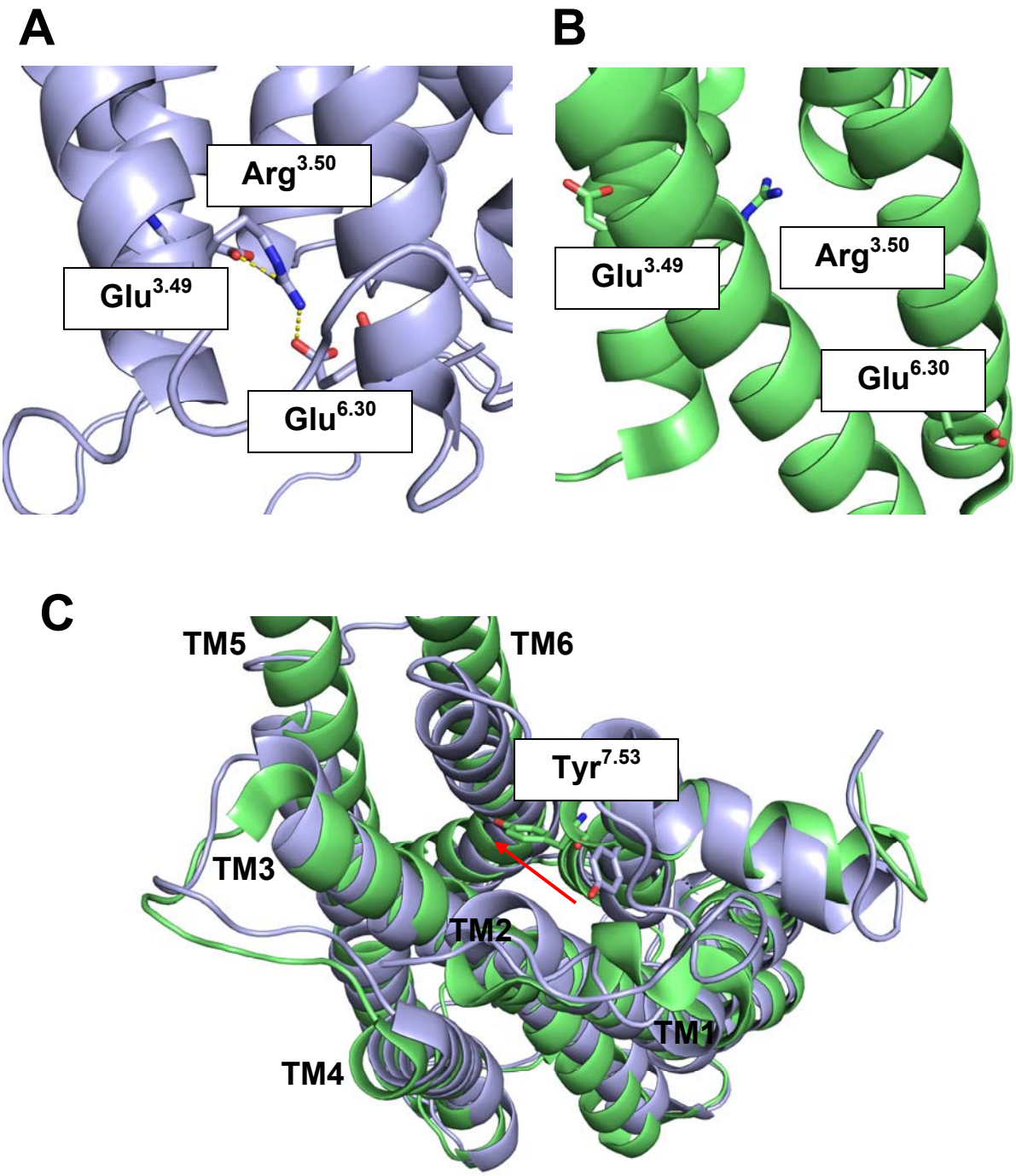

Figure 4. Molecular switches in GPCR activation.
A) $Arg^{3.50}$ forms ionic locks with $Glu^{6.30}$ and $Asp^{3.49}$ in inactive rhodopsin (1F88). B) Both ionic locks are broken in rhodopsin bound to $G\alpha_t$ (transducin) fragment (3PQR). C) Cytoplasmic view showing $Tyr^{7.53}$ of the NPXXY motif shifts towards TM3, TM5, and TM6 in R* state of rhodopsin (green; 3PQR) compared to its position facing TM1 and TM2 in R state of rhodopsin (grey; 1F88). Rotamer switch of $Tyr^{7.53}$ is also observed in R* states of A_2AR and β_2AR (not shown).

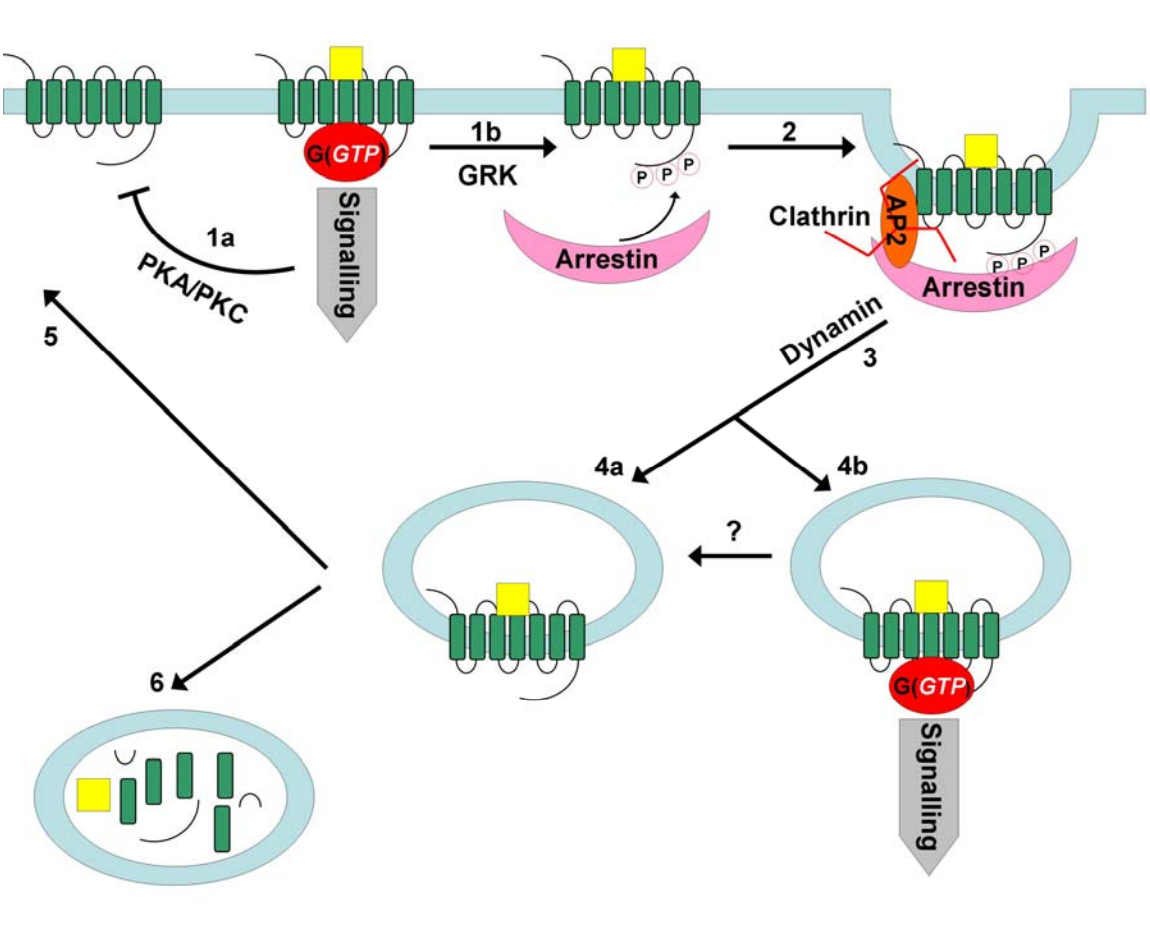

Figure 5. Canonical life-cycle of GPCR.
(1) Upon agonist-induced activation, the receptor couples to the G protein and initiates signalling at the membrane. Downstream activation of PKA/PKC phosphorylates other receptors to cause heterologous desensitization (1a). In some cases, PKA/PKC can also feedback phosphorylate and desensitize the signalling receptor (not shown). In homologous desensitization (1b), GRK phosphorylates the agonist-bound receptor typically at the CT followed by arrestin binding to the receptor. (2) Arrestin recruits other proteins such as AP2 and clathrin to complex with the receptor at clathrin-coated pits. (3) Dynamin cleaves the budding vesicle. (4a) In acidified endosomes, the receptor is dephosphorylated. (4b) Recent studies have demonstrated that the receptor can initiate a second wave of signalling from endosomes. How this pathway converges with (4a) is unknown. After (4a), the receptor can be recycled back to the plasma membrane (5) or be degraded by lysosomes (6).

Among Family A receptors, there exists a dichotomy regarding receptor trafficking traits that can be described by two groups: class A and class B (Oakley *et al.*, 2000, Pierce & Lefkowitz, 2001). Class A receptors such as β_2AR and μ opioid receptor have higher affinity for β-arrestin 2 compared to β-arrestin 1. Furthermore, class A receptors dissociate from β-arrestin at or near the cell surface following internalization into endosomes. In contrast, class B receptors such as vasopressin type 2 receptor (V_2R) and angiotensin II type 1A receptor (AT_{1A}R) possess similar high affinities for β-arrestin 2 and β-arrestin 1, and remain bound to β-arrestin following internalization. Class A receptors recycle quickly to the plasma membrane, upon undergoing dephosphorylation in acidified endosomes. Meanwhile, class B receptors recycle slower and are more likely to be degraded (Luttrell, 2008, Pierce & Lefkowitz, 2001). Mutagenesis studies have shown that the CT domain is a structural determinant for the differences in β-arrestin association/dissociation and recycling kinetics between class A and class B receptors (Oakley *et al.*, 1999, Oakley *et al.*, 2000, Oakley *et al.*, 2001, Zhang *et al.*, 1999).

Based on the classical paradigm, it was believed that GPCR signalling was only restricted to the plasma membrane. However, studies have suggested that some GPCRs, after initiating membrane signalling, can initiate a second wave of signalling from internalized endosomes—termed endosomal signalling. This has been implicated for recognized class B receptors: parathyroid hormone receptor type 1 (PTH_1R) (Ferrandon *et al.*, 2009), thyroid-stimulating hormone receptor (TSHR) (Calebiro *et al.*, 2009), and V_2R (Feinstein *et al.*, 2013). Upon brief treatment with certain agonists, these receptors were found to produce cAMP responses (detected using a fluorescent EPAC sensor) that

persisted for at least 20 mins, despite undergoing agonist-induced internalization within minutes. The observed intracelluar co-localization between fluorescent-tagged agonists and $G\alpha_s$ proteins further supported the idea of internal signalling (Calebiro *et al.*, 2009, Feinstein *et al.*, 2013, Ferrandon *et al.*, 2009). Interestingly, over-expressing subunits of the retromer complex, known to traffick receptors from endosomes to Golgi, attenuated the sustained signalling of PTH_1R and V_2R (Feinstein *et al.*, 2011, Feinstein *et al.*, 2013).

Class A receptors may also exhibit endosomal signalling but given their faster recycling to the surface, their endosomal signalling—if present— may operate within a faster time scale and thus may not be as pronounced as those reported for class B receptors. The few known examples include dopamine D_1 receptor (discussed later on) and the β_2AR, which has been shown by a novel approach with nanobodies. In this study, fluorescent nanobodies (Nb) were engineered to bind to agonist-bound β_2AR (Nb80) and the nucleotide-free form of $G\alpha_s$ (Nb37) (Irannejad *et al.*, 2013). Both nanobodies were recruited to the plasma membrane upon agonist treatment and later found in endosomes containing fluorescent-tagged β_2AR. In addition, Nb80 and Nb37 did not co-localize with β_2AR immediately after the β_2AR marker formed intracellular puncta (i.e. a sign for receptor endocytosis). These results suggest that β_2AR possesses two phases of signalling: one at the plasma membrane and another from endosomes—separated by an interval devoid of β_2AR signalling where CME occurs.

Recently, one study using various approaches including electron microscopy has identified the existence of a GPCR in complex with both G protein and β-arrestin (Thomsen *et al.*, 2016). The GPCR was a modified β_2AR (β_2V_2R) possessing the CT from V_2R. β-arrestin interacted with the CT of this chimeric receptor, while Gs

simultaneously interacted with the TM regions of the chimera. Contrary to the classical paradigm, this demonstrates that G protein coupling can occur even with β-arrestin binding, and can explain why class B receptors display endosomal signalling when bound to β-arrestin inside the cell. However, endosomal signalling for wild-type β_2AR was not detected in this study. Only when β_2AR was transformed to a class B receptor (i.e. β_2V_2R) could endosomal signalling be detected, suggesting that a stable interaction between receptor and β-arrestin is important for endosomal signalling. Nevertheless, endosomal signalling for class A receptors may be a fleeting occurrence as previously mentioned, but more evidence is needed in the future.

1.5 - GPCRs in Human Diseases

At present, over 30 human diseases have been associated with approximately 700 mutations in GPCRs leading to their malfunctioning (Schoneberg *et al.*, 2004). One of the first known cases was mutations in the rhodopsin gene linked to retinitis pigmentosa—a retinal dysfunction disease characterized by degeneration of rod photoreceptor cells. One etiology for this multifactorial disease is due to poor trafficking of rhodopsin to the cell surface. This can be attributed to mutations in the TM and EC regions of rhodopsin that also interfere with the binding of 11-*cis*-retinal (Sung *et al.*, 1991). Mutations in TM1 and the CT of rhodopsin can manifest into retinitis pigmentosa, by retaining rhodopsin intracellularly, but these mutant receptors are capable of binding to 11-*cis*-retinal (Sung *et al.*, 1994, Tam *et al.*, 2000). Given the well-conserved nature of the DRY motif among Family A GPCRs, it is not surprising that mutations in this region leads to pathologies. For the V_2R, mutating $Arg^{3.50}$ retains normal binding to vasopressin, but abrogates its

ability to initiate G_s-mediated signalling. Consequently, this lack of responsiveness to vasopressin results in excess urine production and dehydration due to the inability of kidneys to conserve water, a disorder known as nephrogenic diabetes insipidus (Rosenthal *et al.*, 1993). Replacing $Arg^{3.50}$ with His in the gonadotropin-releasing hormone receptor has been shown in hypogonadotropic hypogonadism (i.e. impaired production of sex hormones). This mutant receptor is expressed on the cell surface but fails to bind to agonists and is therefore unable to induce signalling (Costa *et al.*, 2001). Other examples of human diseases linked to genetic mutations in GPCRs include narcolepsy, hypothyroidism, Hirschsprung's disease, dwarfism, ocular albinism, juvenile periodontitis, and X-linked mental retardation (Schoneberg *et al.*, 2004).

2. Dopamine Receptors

2.1 - The Dopamine Neurotransmitter

In the 1950s, reserpine was known to cause depletion of noradrenaline and 3-hydroxytyramine, although its ability to block vesicular monoamine transporter (VMAT) was not yet discovered. It was also believed that 3-hydroxytyramine acted only as a precursor to the synthesis of noradrenaline with no direct effects by itself. In 1958, Arvid Carlsson and colleagues injected reserpine-treated rabbits with L-3,4-dihydroxyphenylalanine (L-DOPA) and saw an reversal of reserpine-mediated effects and an increase in 3-hydroxytyramine in the brain. They also found noradrenaline levels remained depleted and thus for the first time, showed that 3-hydroxytyramine could be an endogenous signalling compound (Carlsson *et al.*, 1957, Carlsson *et al.*, 1958). Today, this compound is known as dopamine (DA).

The synthesis of DA in the brain occurs near pre-synaptic terminals and is a two-step process that begins with the amino acid tyrosine. In the cytosol, tyrosine is converted to L-DOPA by tyrosine hydroxylase and is the rate-limiting step. The aromatic amino acid decarboxylase converts L-DOPA to DA, which is then transported into storage vesicles by VMAT (Daubner *et al.*, 2011). An action potential at the pre-synaptic terminal causes voltage-gated Ca^{2+} channels to open, resulting in Ca^{2+} influx, and vesicle fusion with the pre-synaptic membrane to release DA. The neurotransmitter then diffuses and activate DA receptors located either pre-synaptically (autoreceptors) or post-synaptically. DA in the synaptic cleft can be reuptaken into pre-synaptic neuron through DA transporters or be metabolised by either monoamine oxidase (MAO) in pre-synaptic terminal or catechol-O-methyltransferase (COMT) found in post-synaptic membrane (Munoz *et al.*, 2012).

In the brain, there are four major pathways for dopaminergic neurotransmission. In the mesolimbic pathway, neuronal cell bodies in the ventral tegmental area (VTA) project their axons that terminate and release DA at the limbic areas such the nucleus accumbens. Also known as the "reward pathway", stimulant drugs like cocaine and natural rewards like food and sex increase mesolimbic DA release (Adinoff, 2004). Repeated administration of stimulant drugs also induces psychosis and supports the hypothesis that hyperactivity of this pathway contributes to the positive systems of schizophrenia (e.g. hallucinations and delusions) (Brisch *et al.*, 2014). Dopaminergic neurons in the VTA also project to the frontal cortex. This pathway, known as the mesocortical pathway, is important for working memory, and its hypoactivity has been implicated in the negative deficits of schizophrenia (e.g. cognitive deficits and lack of

motivation) (Brisch *et al.*, 2014, Castner *et al.*, 2004). The nigrostriatal pathway involves dopaminergic projections from the substantia nigra pars compacta to the striatum and basal ganglia. This pathway is essential for locomotion, and as witnessed in Parkinson's disease, degeneration of dopaminergic neurons in the substantia nigra pars compacta leads to severe motor deficits (Dauer & Przedborski, 2003). Lastly, the tuberoinfundibular pathway consists of dopaminergic neurons, originating from the hypothalamus, that project their axonal terminals to the anterior pituitary to inhibit prolactin release (Fuxe, 1964, Lyons *et al.*, 2012).

Dopamine activates five receptors in mammals that can be grouped into two subclasses: D_1-class (D_1 and D_5; see **Figure 6** for snake plots) and D_2-class (D_2, D_3, and D_4). This classification was originally developed to differentiate the coupling of $G\alpha_{s/olf}$ and activation of AC by D_1 receptor (D_1R) from the coupling of $G_{i/o}$ and inhibition of AC by the D_2 receptor (D_2R) (Kebabian & Calne, 1979, Missale *et al.*, 1998). Following the discovery of D_3, D_4, and D_5 subtypes, this classification withstood because each subclass shared commonalities including high sequence homology among TMs and high affinity for selective ligands (Missale *et al.*, 1998). Furthermore, D_1-class receptors exhibit a short IC3 and long CT when compared to D_2-class receptors, which exhibit a long IC3 and a short CT. Unlike the intron-less genes for D_1-class receptors, D_2-class receptor genes have many introns and consequently, there exist splice variants for D_2-class receptors. Notably, there are two isoforms of D_2R, D_2R_{long} and D_2R_{short}, in which the latter has 29 amino acids in IC3 removed (Giros *et al.*, 1989). The D_2R_{long} are mostly expressed post-synaptically, while the D_2R_{short} are found pre-synaptically where they can serve as autoreceptors (Usiello *et al.*, 2000).

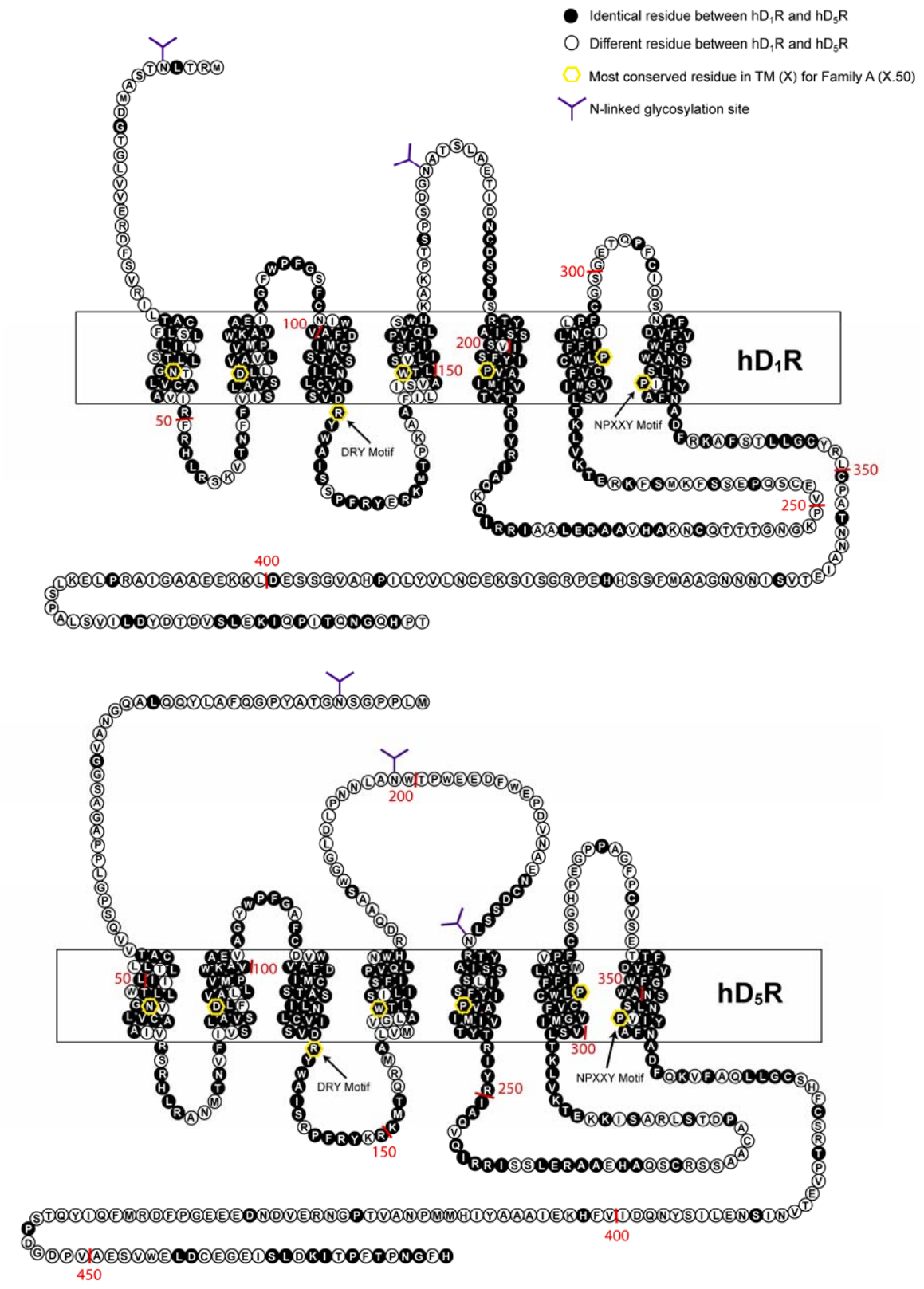

Figure 6. Snake plots of human D_1 and D_5 receptors (hD_1R and hD_5R).

2.2 - D_1-Class Receptor Signalling

D_1R is abundantly expressed throughout the brain with D_1R mRNA found in the neostriatum, nucleus accumbens, and olfactory bulb. D_1R mRNA are also found in cortex, hypothalamus, and thalamus but at lower levels (Meador-Woodruff *et al.*, 1991). D_5R mRNA are primarily found in the hippocampus and hypothalamus (Meador-Woodruff *et al.*, 1992, Neve *et al.*, 2004). In the neostriatum, where D_1R expression is most concentrated, abundant levels of α_{olf} and scarce levels of α_s restrict D_1R activation of AC through α_{olf} (Corvol *et al.*, 2001, Zhuang *et al.*, 2000). In other regions such as cortex and hippocampus where α_{olf} levels are much lower than α_s levels, D_1-class receptors likely couples to α_s (Herve *et al.*, 2001, Neve *et al.*, 2004). Although the $G\beta\gamma$ dimer(s) to which D_1-class receptors couple remains largely unknown, endogenous γ_7 subunit in HEK293 cells has been shown to be important for D_1R-G_s coupling (but not D_5R-G_s coupling) because diminishing γ_7 expression led to reduced β_1 expression and decreased D_1R activation of AC (Wang *et al.*, 2001).

Following the AC/cAMP/PKA cascade, a well-studied downstream target of D_1-class receptor signalling is DARPP32 (dopamine and cyclic adenosine 3',5'-monophosphate-regulated phosphoprotein, 32 kDa). Specifically, PKA phosphorylates DARPP32 at Thr34, which binds and blocks the active site of protein phosphatase 1 (PP1) (Kwon *et al.*, 1997). Inhibition of PP1 by DARPP32 prolongs dephosphorylation and acts synergistically with PKA phosphorylation to increase phosphorylation of NMDA, AMPA receptors, and L-type Ca^{2+} channels, resulting in increased channel activity (Blank *et al.*, 1997, Greengard *et al.*, 1999, Surmeier *et al.*, 1995, Yan *et al.*, 1999) **(Figure 7)**. In contrast, increased phosphorylation of Na^+ channels by PKA and

DARPP32/PP1 reduces their channel activity (Schiffmann *et al.*, 1995, Schiffmann *et al.*, 1998).

D_1R-mediated activation of DARPP32/PP1 cascade can also impact NMDA downstream targets **(Figure 7)**. In medium-size spiny neurons (MSNs) found in the neostriatum, activated MEK, through NMDA signalling, phosphorylates ERK. However, ERK is dephosphorylated by STEP (striatal-enriched tyrosine phosphatase), and this culminates into an unchanged net ERK phosphorylation. Because STEP is kept active through dephosphorylation by PP1, co-activation of D_1R in MSNs inactivates STEP through the DARP32/PP1 cascade, resulting in increased phosphorylation of ERK (Valjent *et al.*, 2005). On the other hand, D_1-class receptor signalling can also phosphorylate ERK using cAMP to directly activate exchange proteins (Epac1 and Epac2), which result in ERK phosphorylation via downstream targets of Epac (Beaulieu & Gainetdinov, 2011, New & Wong, 2007) **(Figure 7)**.

Aside from G_s coupling, D_1-class receptors may also signal through a G_q/PLC/IP3 pathway. Studies applying D_1-class selective agonists to crude renal membranes and brain slices have detected IP3 production. This was shown to be linked to G_q coupling through employing G protein inhibitors/antisera and GTPγS assays (Felder *et al.*, 1988, Jin *et al.*, 2001, Undie & Friedman, 1990). There is also evidence of heterodimerization between D_1R and D_2R to form a novel signalling complex that signals through G_q (Lee *et al.*, 2004, Rashid *et al.*, 2007). These two studies support a model where concurrent activation of D_1R and D_2R is required for G_q signalling. They conflict with the aforementioned studies, which found D_2R antagonists did not affect IP3 levels produced from D_1-class agonist treatment (Jin *et al.*, 2001, Undie & Friedman, 1990). Complex

still, IP3 production by D_1-class agonist stimulation was preserved in D_1R-knockout mice but reduced in D_5R knockout mice (Friedman *et al.*, 1997, Sahu *et al.*, 2009). Another study using heterologous expression systems did not detect IP3 production upon agonist activation of D_5R but could for the G_q-coupled α_{1B}-adrenergic receptor (Tiberi *et al.*, 1991). Because of these contradictory findings as well as others reviewed elsewhere (Lee *et al.*, 2014), G_q signalling by D_1-class receptors is currently controversial.

2.3 - Regulation of D_1-Class Receptor Trafficking and Signalling

In heterologous cells, D_1R is well-known to undergo agonist-induced desensitization in a matter of minutes and is believed to be mostly mediated by GRK isoforms (Gardner *et al.*, 2001, Jackson *et al.*, 2002, Kim *et al.*, 2004, Lamey *et al.*, 2002). Under basal conditions and in the presence of DA, GRK2, GRK3, and GRK5 have been shown to phosphorylate D_1R primarily on its CT (Gardner *et al.*, 2001, Jackson *et al.*, 2002, Lamey *et al.*, 2002, Sedaghat & Tiberi, 2011, Tiberi *et al.*, 1996). Whereas GRK2 and GRK3 phosphorylation of D_1R led to a rightward EC_{50} shift in DA dose-response curve of D_1R, GRK5 phosphorylation imposed a stronger D_1R desensitizing response that included a rightward EC_{50} shift and a 40% decrease in maximal cAMP accumulation (Tiberi *et al.*, 1996). Furthermore, GRK4α has been shown to constitutively phosphorylate D_1R, specifically Thr428 and Ser431 of its CT, resulting in reduced maximal cAMP responses by D_1R (Rankin *et al.*, 2006).

D_1R possesses four putative PKA phosphorylation sites: Thr135 in IC2, Ser229 and Thr268 in IC3, and Ser380 in CT (Jiang & Sibley, 1999). Whether PKA contributes to D_1R desensitization is currently unclear due to conflicting studies where some have

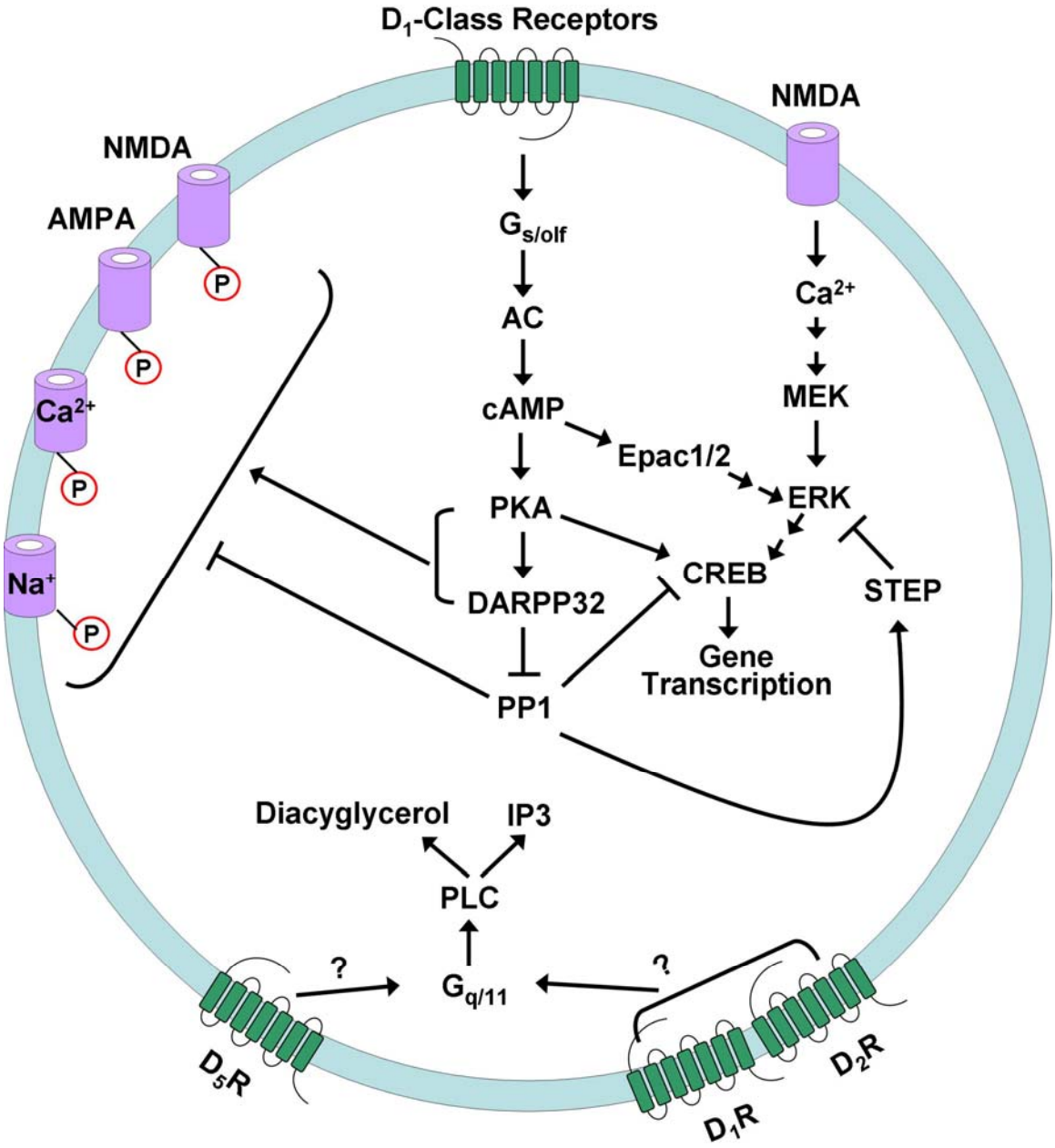

Figure 7. D_1-class receptor signalling cascade.
D_1-class receptors primarily signal through the $G_{s/olf}$ coupled pathway. Some responses include activation of ERK pathway, gene transcription, and phosphorylation of ion channels. D_1-class receptors may also signal through the $G_{q/11}$-coupled pathway. This may involve heterodimerization between D_1R and D_2R.

indicated involvement of PKA (Jiang & Sibley, 1999, Ventura & Sibley, 2000, Zhou *et al.*, 1991) but others have opposed (Lewis *et al.*, 1998, Mason *et al.*, 2002). In particular, one study showed that of the four putative PKA sites on D_1R, solely mutating Thr268 to Ala268 caused attenuations towards the rate of DA-induced desensitization (Jiang & Sibley, 1999). However, another study found mutating Thr268 to Ala268 did not alter DA-induced desensitization kinetics of D_1R (Mason *et al.*, 2002). This discrepancy might be accounted by differences in the species of D_1R and cell lines used (Mason *et al.*, 2002).

Upon agonist treatment, biotinylation assays using heterologous cells and striatal neurons with endogenous D_1R have demonstrated that a majority of D_1R internalize in 5 mins, mostly likely through the CME pathway (Macey *et al.*, 2005, Vickery & von Zastrow, 1999). Immunohistochemical studies using striatal neurons have also reported D_1R internalization in dendrites, soma, and axons occur within 5 mins of agonist treatment (Dumartin *et al.*, 1998, Martin-Negrier *et al.*, 2000). The most recent study, employing a live imaging approach, has shown that many D_1R can internalize even quicker in heterologous cells and striatal neurons: under 1 min of DA treatment (Kotowski *et al.*, 2011). Like desensitization, the CT has been shown to be a structural determinant for agonist-induced internalization of D_1R. Alanine mutations at Ser431, Thr439, and Thr446 reduced agonist-induced internalization of D_1R but did not affect D_1R desensitization (Lamey *et al.*, 2002). Conversely, mutating either Glu359 or Thr360 in the proximal CT region abolished the ability of D_1R to desensitize without affecting its ability to internalize (Lamey *et al.*, 2002). This implies that D_1R desensitization and internalization are two independent processes. Another mutagenesis study, using a

truncation approach, found residues between Cys351 and Gly379 of D_1R played an important role for agonist-induced internalization (Jackson *et al.*, 2002). However, removing the last 21 residues of CT, which encompasses Ser431, Thr439, and Thr446, was not found to alter agonist-induced internalization of D_1R (Jackson *et al.*, 2002).

Studies have found that D_1R possesses a higher affinity for β-arrestin 2 compared to β-arrestin 1 in both heterologous cells and striatal neurons endogenously expressing D_1R (Macey *et al.*, 2005, Oakley *et al.*, 2000). Activated D_1R in transfected cells was observed to interact with β-arrestin 2 at the plasma membrane, but quickly dissociated from β-arrestin 2 as it trafficked into endosomes (Zhang *et al.*, 1999). One study proposed that activated D_1R is phosphorylated first at CT and then IC3, which creates separation between CT and IC3 to allow β-arrestin 2 to bind to IC3 and promote D_1R desensitization (Kim *et al.*, 2004).

The internalized D_1R is known to recycle back to plasma membrane and not be subjected to rapid degradation. This is in tune with its internalization properties, which together categorize D_1R as a class A GPCR in terms of trafficking. Depending on the assay used (either with heterologous cells or striatal neurons with endogenous D_1R), the time for D_1R recovery to the plasma membrane ranges from 5 mins to 60 mins after agonist removal (Kotowski *et al.*, 2011, Martin-Negrier *et al.*, 2006, Vargas & Von Zastrow, 2004, Vickery & von Zastrow, 1999). Although it is classically presumed that the internalized D_1R undergoes dephosphorylation within acidic endosomes, inhibiting agonist-mediated endocytosis of D_1R with concanavalin A and hypertonic sucrose did not affect the dephosphorylation of agonist-treated D_1R in transfected cells (Gardner *et al.*, 2001). Another study, through truncating the CT of D_1R, found residues 360-382 was

required for D_1R recycling (Vargas & Von Zastrow, 2004). Furthermore, fusing these residues to the CT of the δ-opioid receptor not only prevented agonist-induced degradation normally observed for this receptor when internalized, but also enabled the receptor to recycle efficiently to the plasma membrane. However, it should be noted that the truncated CT mutants of D_1R used in this study showed wild-type abilities to undergo agonist-induced internalization. This potentially conflicts with other studies (Jackson *et al.*, 2002, Kotowski *et al.*, 2011, Lamey *et al.*, 2002) that have shown specific residues within these truncations are important for agonist-induced internalization of D_1R.

D_1-class receptor signalling and trafficking can also be regulated by PKC. In HEK293 cells, studies have demonstrated distinct responses between D_1R and D_5R upon heterologous activation of PKC by phorbol 12-myristate 13-acetate (PMA). PMA was shown to potentiate the maximal cAMP response elicited by DA in D_1R without significantly affecting its constitutive activity. In opposing fashion, PMA decreased DA potency, DA-mediated maximal cAMP response, and constitutive activity of D_5R (Jackson *et al.*, 2005). It was later found that these contrasting responses could be switched between D_1R and D_5R if their IC3 regions were exchanged (Plouffe *et al.*, 2012). PMA has also been demonstrated to induce D_5R but not D_1R internalization, and this may contribute to the subtype-specific signalling responses of D_1R and D_5R imposed by PMA (Thompson & Whistler, 2011). D_5R endocytosis in the presence of PMA was not found to depend on β-arrestin unlike DA-mediated endocytosis of D_5R. Furthermore, Ser271 within the IC3 of D_5R was shown to be critical for PMA-mediated endocytosis of D_5R. Mutating the corresponding residue in D_1R (i.e. Asn240 to Ser240) granted D_1R the novel ability to undergo PMA-mediated endocytosis (Thompson & Whistler, 2011).

PMA can also potentiate forskolin- and DA-mediated cAMP responses in cultured striatal neurons, although through which dopamine receptor is unknown (Schinelli *et al.*, 1994). As well, other work has showed that activation of group I metabotropic glutamate receptor in striatal neurons potentiates DA-induced cAMP response in a PKC-dependent manner (Paolillo *et al.*, 1998).

Presently, D_1R is one of the few GPCRs in which there exists evidence for endosomal signalling. One study utilized a fluorescent EPAC sensor to detect the early cAMP response that occurred less than 2 mins after D_1R activation (Kotowski *et al.*, 2011). This early cAMP response was attenuated through various methods to block D_1R endocytosis including using hypertonic sucrose and dynasore, knockdown of clathrin, and deleting residues 360-382 within CT of D_1R. Because inhibiting D_1R recycling did not affect this early cAMP response, it was reasoned that D_1R possessed another signalling phase from the endosomes that occurred quickly after D_1R endocytosis. This was further supported by co-localization of D_1R with AC and G_s puncta in endosomal compartments (Kotowski *et al.*, 2011).

2.4 - Dopamine Receptor-Interacting Proteins (DRIPs)

It is becoming increasingly evident that D_1-class receptor signalling complex is diversely structured. There are various DRIPs—besides the G proteins, GRKs, and arrestins mentioned thus far—capable of modulating D_1-class receptor function. Trafficking of D_1R from ER to the plasma membrane has been shown to require the ER protein calnexin, which interacts with D_1R in a glycan dependent and independent manner (Free *et al.*, 2007). Blocking D_1R glycosylation reduced D_1R interaction with

calnexin and impaired D_1R trafficking to the cell surface. This also occurred when calnexin was overexpressed whereby more D_1R were retained in the ER (Free *et al.*, 2007). Export of D_1R from ER has also been shown to be dependent on the FxxxFxxxF motif, located at the proximal CT and well-conserved among GPCRs (Bermak *et al.*, 2001). The ER protein DRIP78 was identified to interact with D_1R via this FxxxFxxxF motif. Sequestering endogenous DRIP78 or overexpressing DRIP78 increased retention of D_1R in the ER (Bermak *et al.*, 2001). Thus, it appears proper D_1R trafficking requires a fine balance of calnexin and DRIP78, whose endogenous levels have been pre-optimized by nature.

D_1R, but not D_5R, is recognized to directly interact with NMDA channels via its CT (Lee *et al.*, 2002, Pei *et al.*, 2004). Some studies report this interaction relies on activation of NMDA, but not D_1R (Pei *et al.*, 2004, Scott *et al.*, 2006). Formation of the D_1R-NMDA complex resulted in a potentiation of the agonist-induced cAMP response by D_1R that could be explained by increased insertion of intracellular D_1R to the cell surface (Pei *et al.*, 2004). On the other hand, the CT of D_5R but not D_1R interacts with $GABA_A$ receptor. In cells co-expressing D_5R and $GABA_A$ receptor, activation of $GABA_A$ receptor was found to diminish the agonist-induced cAMP response of D_5R (Liu *et al.*, 2000).

The CT and IC3 of D_1R have been shown to interact with the scaffold proteins PSD-95 and neurofilament-M, respectively. PSD-95 increased D_1R constitutive internalization via a dynamin-dependent fashion and consequently decreased cell surface levels of D_1R and D_1R-mediated cAMP accumulation (Zhang *et al.*, 2007). Similarly, co-expression with neurofilament-M impaired D_1R trafficking to the cell surface, although

the underlying mechanism was not investigated. This was linked to decreased D_1R-mediated cAMP response, and interestingly, abolished agonist-induced desensitization of D_1R (Kim *et al.*, 2002).

2.5 - Pharmacology of D_1-Class Receptors

Given the structural similarities among DA and other catecholamines, it is expected that the pharmacophore of D_1-class receptors should mimic those belonging to other catecholamine receptors. The TM5 of D_1-class receptors contains a cluster of conserved serines ($Ser^{5.42}$, $Ser^{5.43}$, and $Ser^{5.46}$), which is recognized as a hallmark feature among receptors binding to catecholamines. Indeed, mutating $Ser^{5.43}$ and $Ser^{5.46}$ to Ala decreased D_1R affinity for DA, with the latter mutation producing a stronger effect (Pollock *et al.*, 1992). Mutating $Ser^{5.42}$ to Ala in D_1R presumably disrupted binding to the radioligand [^{3}H]-SCH23390 and thus, DA affinity could not be assessed. However in cAMP assays stimulated with DA, the $Ser^{5.42}$Ala mutant receptor produced the largest rightward EC_{50} shift compared to $Ser^{5.43}$Ala and $Ser^{5.46}$Ala mutant receptors, suggesting a loss in DA affinity (Pollock *et al.*, 1992). Computational studies with D_1R homology models have shown that the catechol moiety of DA primarily hydrogen bonds with $Ser^{5.42}$ and $Ser^{5.46}$, and rarely with $Ser^{5.43}$ (Malo *et al.*, 2012, Mente *et al.*, 2015). Furthermore, the conserved aspartic acid of TM3 ($Asp^{3.32}$) in D_1R was shown to form a salt bridge with the amino group of DA. This is similar to what has been observed for $Asp^{3.32}$ in other catecholamine receptors (Malo *et al.*, 2012, Mente *et al.*, 2015) **(Figure 8)**. Other characteristics of D_1R-DA interface include polar interactions between $Asn^{6.55}$ and the catechol moiety of DA as well as π-π interactions between $Phe^{6.51}$/$Phe^{6.52}$ and the

aromatic ring of DA (Mente *et al.*, 2015). Functional assays involving D_2R have also demonstrated the importance of $Phe^{6.51}$ and $Phe^{6.52}$ towards DA binding (Cho *et al.*, 1995). The common DA binding motifs described for D_1R are likely to exist in the D_5R-DA interface; however, the subtleties discriminating D_1R and D_5R ligand binding pockets have remained elusive and may ultimately require crystal structures of D_1R and D_5R. This will guide in developing a subtype-specific ligand for D_1-class receptors in the future.

Although D_1R and D_5R share over 80% sequence identity within their TM domains, D_5R is distinguished from D_1R by exhibiting enhanced affinity and potency for agonists, lower affinity for inverse agonists, and higher basal signalling compared to the D_1R (Tiberi & Caron, 1994). In this aspect, D5R can be regarded as a more constitutively active counterpart of D_1R (Samama *et al.*, 1993).

Previous studies have demonstrated that swapping $Phe^{6.52}$ in the distal portion of IC3 of D_5R with $Ile^{6.52}$ of D_1R, reversed the subtype-specific properties observed between D_1-class receptors. Specifically, DA affinity, DA potency, and basal activity were diminished in the D_5 mutant receptor, but were increased in the D_1 mutant receptor (Charpentier *et al.*, 1996). Nevertheless, these properties were not fully reversed, which hinted at potential contributions by other regions. Indeed, exchanging the CT domain between D_1R and D_5R led to a full switch of DA affinity and basal activity (Jackson *et al.*, 2000), although DA potency was not reversed. The effects from interchanging CT was found to be mimicked by swapping the proximal portion of CT, a region also known as helix-8 due to its propensity to form an α-helical fold (Tumova *et al.*, 2004). As described earlier, the IC3 has also been shown to be influential in dictating the unique

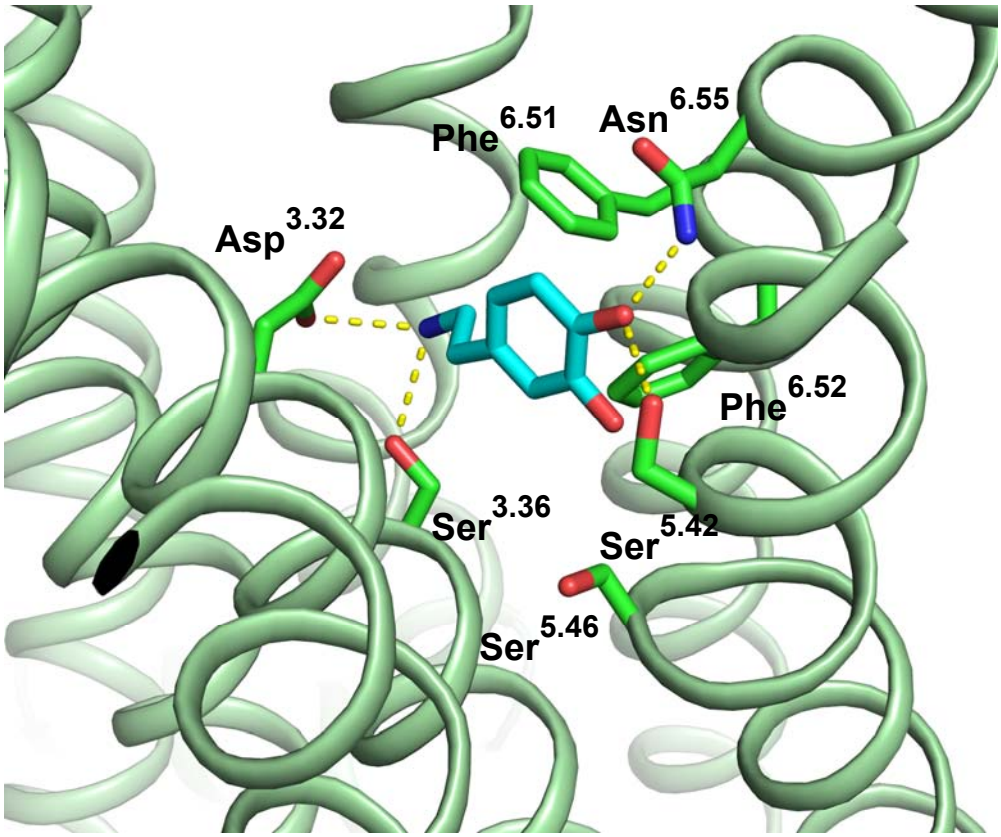

Figure 8. Simulation snapshot of DA bound to a homology model of D_1R.
DA (shown in cyan) makes hydrogen bonds (represented by yellow dashed lines) with $Asp^{3.32}$, $Ser^{3.36}$, $Ser^{5.42}$, and $Asn^{6.55}$. $Phe^{6.51}$ and $Phe^{6.52}$ makes hydrophobic contacts with the benzene ring of DA. $Phe^{6.52}$ also makes π-π interactions with DA. Parts of EC2 have been removed for clarity purposes.

PMA and PKC responses of D_1R and D_5R (Plouffe *et al.*, 2012, Thompson & Whistler, 2011). Collectively, these findings underscore important functional roles of IC3 and CT for D_1-class receptors. On the other hand, the significance of the remaining intracellular regions, IC1 and IC2, in contributing to the functional and possibly subtype-specific properties of D_1-class receptors remains to be determined.

3. First and Second Intracellular Domains (Rationale)

The IC1 and IC2 of D_1-class receptors share remarkable homology both in length and amino acid sequence with those among other GPCRs **(Figure 9)**. With regards to IC2, previous studies have already demonstrated the role of some of these conserved structural elements among biogenic amine receptors **(Figure 9A)**. As mentioned earlier, the (E)DRY motif is theorized to confine the receptor in its inactive conformation through an "ionic lock" between the $Arg^{3.50}$ of this motif and an aspartic/glutamic acid of TM6 (Palczewski *et al.*, 2000). Positioned a few amino acids downstream from the (E)DRY motif is a conserved $Val/Ile^{3.54}$ that has been shown to exhibit a role in G protein coupling (Burstein *et al.*, 1998, Moro *et al.*, 1993). Furthermore, $Ala^{3.53}$ is occasionally found to precede $Val/Ile^{3.54}$; replacing both hydrophobic residues with charged residues resulted in a loss of G protein coupling (Hajjhussein *et al.*, 2013). Five to six amino acids downstream from the (E)DRY motif resides a conserved $Pro^{3.57}$. It has been reported to promote β-arrestin 2 binding and subsequent receptor internalization upon agonist stimulation (Marion *et al.*, 2006). Lastly, adjacent to the proline tends to be a hydrophobic amino acid (Phe, Leu, Met, Ile, Val at position 3.58) that could function as a critical site for G protein coupling. This has been confirmed by the crystal structure of

β_2AR-G_s complex, whereby $Phe^{3.58}$ was illustrated to have direct contact with the hydrophobic pocket within the G_s protein (Rasmussen *et al.*, 2011).

In the case of IC1, its role is unknown not only for D_1-class receptors but for many other GPCRs. In spite of the limited knowledge, one study showed that a well-conserved Leu near the centre of IC1 (at position 2.34 in **Figure 9B**) was required for ER export of β_2AR, α_{1b}/α_{2b}-adrenoceptors, and angiotensin II AT_1 receptors (Duvernay *et al.*, 2009). Another study found that a positively-charged residue ($Lys/Arg^{2.35}$ in **Figure 9B**) neighboring the conserved Leu, which exists in some GPCRs (e.g. D_1-class and opioid receptors), modulated receptor export to the plasma membrane (Fan *et al.*, 2012). Although it is unclear how conserved motifs of IC1 control receptor trafficking, earlier work found that ER export of the thromboxane A_2 receptor required an interaction between its IC1 and activated C-kinase 1 (Parent *et al.*, 2008).

4. General Hypothesis and Research Objectives

To expand further from these previous studies, the goal of my research was to identify novel structural determinants of IC1 and IC2 that may be pertinent to D_1-class receptor function. Due to the well-conserved nature of Ser/Thr of IC1 and IC2 observed among GPCRs (**Figure 9**), I have decided to focus on these residues in a holistic and individual manner. I hypothesized that some, if not all, Ser/Thr of IC1 and IC2 are functionally important for D_1-class receptors because their side chains can play dual putative roles through forming hydrogen bonds or being phosphorylated to engage in signal transduction.

Within the 23 amino acid stretch in IC2 and IC2/TM membrane junctures, both human D_1 and D_5 receptors (hD_1R and hD_5R) possess $Ser^{3.55}$ and $Thr^{3.65}$ within IC2 and $Ser^{3.47}$ at the IC2/TM3 membrane juncture (note: "IC/TM membrane juncture" herein refers to the intersection where the intracellular region meets the membrane-bound portion of the TM). hD_1R also has a non-conserved $Ser^{3.56}$ of IC2. As initial screening tools, two mutant receptors, hD_1-ST2 and hD_5-ST2, were constructed whereby all Ser and Thr in IC2 and IC2/TM3 membrane juncture were mutated to Ala and Val, respectively **(Figures 10 and 11)**. As well, D_1-class receptors possess three Ser/Thr in IC1 and its transition into membrane-bound TM regions. $Thr^{2.39}$ within IC1 and $Ser^{2.45}$ by the IC1/TM2 membrane juncture are conserved among D_1-class receptors. $Ser^{2.36}$ of hD_1R and $Ser^{2.31}$ of hD_5R within their IC1 are not conserved. Analogous to ST2 mutant receptors, ST1 mutant receptors were created whereby all Ser and Thr in IC1 and IC1/TM2 membrane juncture were mutated to Ala and Val, respectively **(Figures 10 and 11)**. The positioning of IC1 and IC2 Ser/Thr were predicted based on homology models of D_1-class receptors and crystal structures of other GPCRs.

My experimental strategy consisted of the following objectives:

- Objective 1: Characterize D_1-class ST1 and ST2 mutant receptors using binding and cAMP assays to assess receptor expression, agonist and antagonist affinities, constitutive activity, and DA-induced activation of AC.
- Objective 2: Use solved crystal structures and bioinformatics to predict potential structural roles of Ser/Thr of IC1 and IC2.

- Objective 3: Investigate the functional properties of single point mutant receptors to dissect the hD_1-ST1 phenotype and verify the existence of putative molecular interactions of $Thr^{2.39}$ and $Ser^{2.45}$.
- Objective 4: Investigate changes to cell-surface and total receptor expression, agonist-induced desensitization, and agonist-induced internalization properties of mutant receptors (particularly hD_1-S65A).

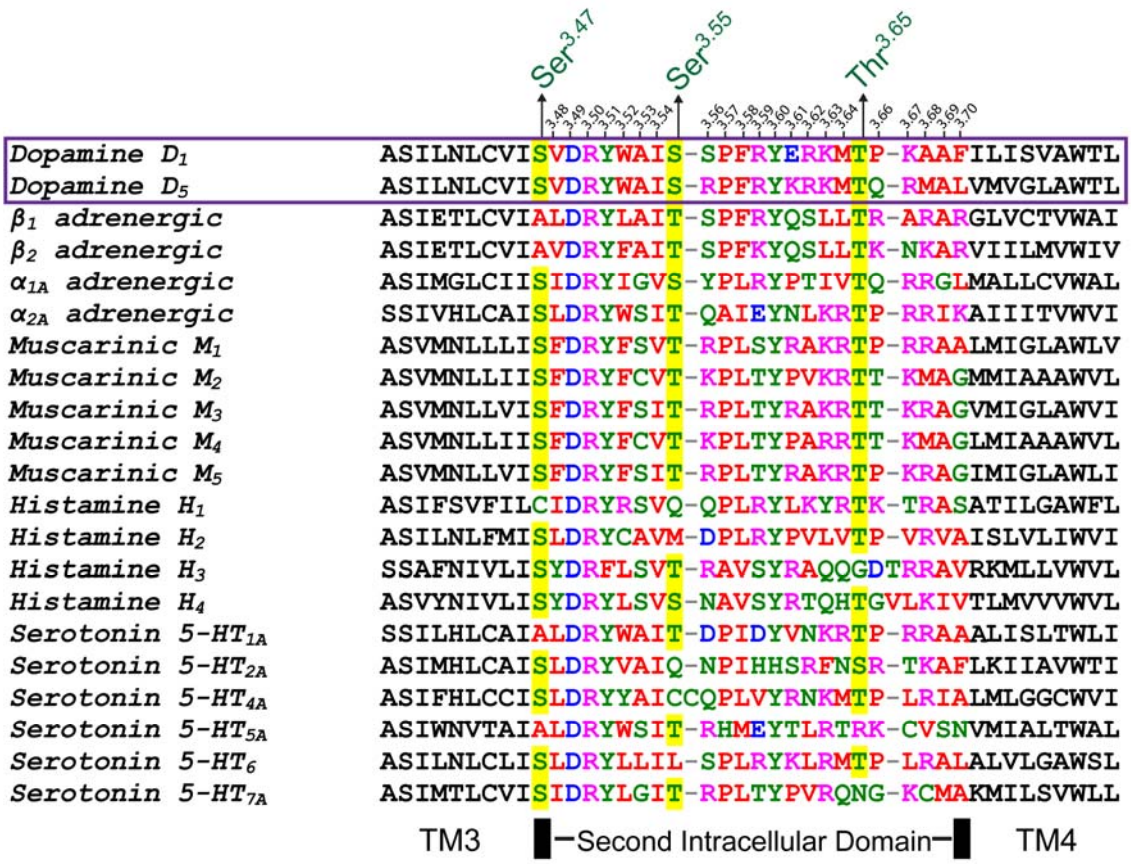
Ser3.47
Ser3.55
Thr3.65
3.48 3.49 3.50 3.51 3.52 3.53 3.54 3.56 3.57 3.58 3.59 3.60 3.61 3.62 3.63 3.64 3.66 3.67 3.68 3.69 3.70
Dopamine D1 ASILNLCVISVDRYWAIS-SPFRYERKMTP-KAAFILISVAWTL
Dopamine D5 ASILNLCVISVDRYWAIS-RPFRYKRKMTQ-RMALVMVGLAWTL
β1 adrenergic ASIETLCVIALDRYLAIT-SPFRYQSLLTR-ARARGLVCTVWAI
β2 adrenergic ASIETLCVIAVDRYFAIT-SPFKYQSLLTK-NKARVIILMVWIV
α1A adrenergic ASIMGLCIISIDRYIGVS-YPLRYPTIVTQ-RRGLMALLCVWAL
α2A adrenergic SSIVHLCAISLDRYWSIT-QAIEYNLKRTP-RRIKAIIITVWVI
Muscarinic M1 ASVMNLLLISFDRYFSVT-RPLSYRAKRTP-RRAALMIGLAWLV
Muscarinic M2 ASVMNLLIISFDRYFCVT-KPLTYPVKRTT-KMAGMMIAAAWVL
Muscarinic M3 ASVMNLLVISFDRYFSIT-RPLTYRAKRTT-KRAGVMIGLAWVI
Muscarinic M4 ASVMNLLIISFDRYFCVT-KPLTYPARRTT-KMAGLMIAAAWVL
Muscarinic M5 ASVMNLLVISFDRYFSIT-RPLTYRAKRTP-KRAGIMIGLAWLI
Histamine H1 ASIFSVFILCIDRYRSVQ-QPLRYLKYRTK-TRASATILGAWFL
Histamine H2 ASILNLFMISLDRYCAVM-DPLRYPVLVTP-VRVAISLVLIWVI
Histamine H3 SSAFNIVLISYDRFLSVT-RAVSYRAQQGDTRRAVRKMLLVWVL
Histamine H4 ASVYNIVLISYDRYLSVS-NAVSYRTQHTGVLKIVTLMVVVWVL
Serotonin 5-HT1A SSILHLCAIALDRYWAIT-DPIDYVNKRTP-RRAAALISLTWLI
Serotonin 5-HT2A ASIMHLCAISLDRYVAIQ-NPIHHSRFNSR-TKAFLKIIAVWTI
Serotonin 5-HT4A ASIFHLCCISLDRYYAICCQPLVYRNKMTP-LRIALMLGGCWVI
Serotonin 5-HT5A ASIWNVTAIALDRYWSIT-RHMEYTLRTRK-CVSNVMIALTWAL
Serotonin 5-HT6 ASILNLCLISLDRYLLIL-SPLRYKLRMTP-LRALALVLGAWSL
Serotonin 5-HT7A ASIMTLCVISIDRYLGIT-RPLTYPVRQNG-KCMAKMILSVWLL
TM3
Second Intracellular Domain
TM4

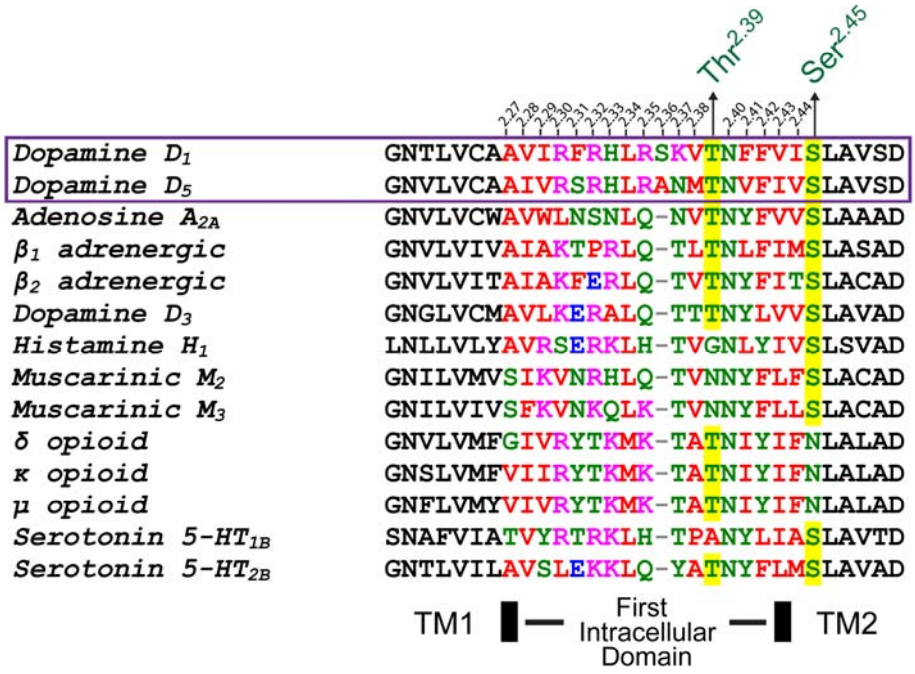

Figure 9. Sequence alignment of the second intracellular domain (A) and first intracellular domain (B) and their neighbouring TM regions among human Family A GPCRs.

Selected receptors in (A) are biogenic amine receptors. Selected receptors in (B) have their crystal structures solved (with the exception of D_1-class receptors). Color scheme for amino acids is denoted as follows: blue (acidic), magenta (basic), red (hydrophobic), green (polar and also includes glycine and cysteine). Black rectangular boxes mark the predicted junctures between IC2 with membrane-bound TM3 and TM4 (A) and between IC1 with membrane-bound TM1 and TM2 (B) based on homology models of hD_1R and hD_5R. The well-conserved Ser/Thr of IC2 and IC1 and their transition into membrane-bound TMs are highlighted in yellow and are denoted using Ballesteros Weinstein nomenclature. Alignment was performed using an online version of Clustal Omega (www.ebi.ac.uk/Tools/msa/clustalo/).

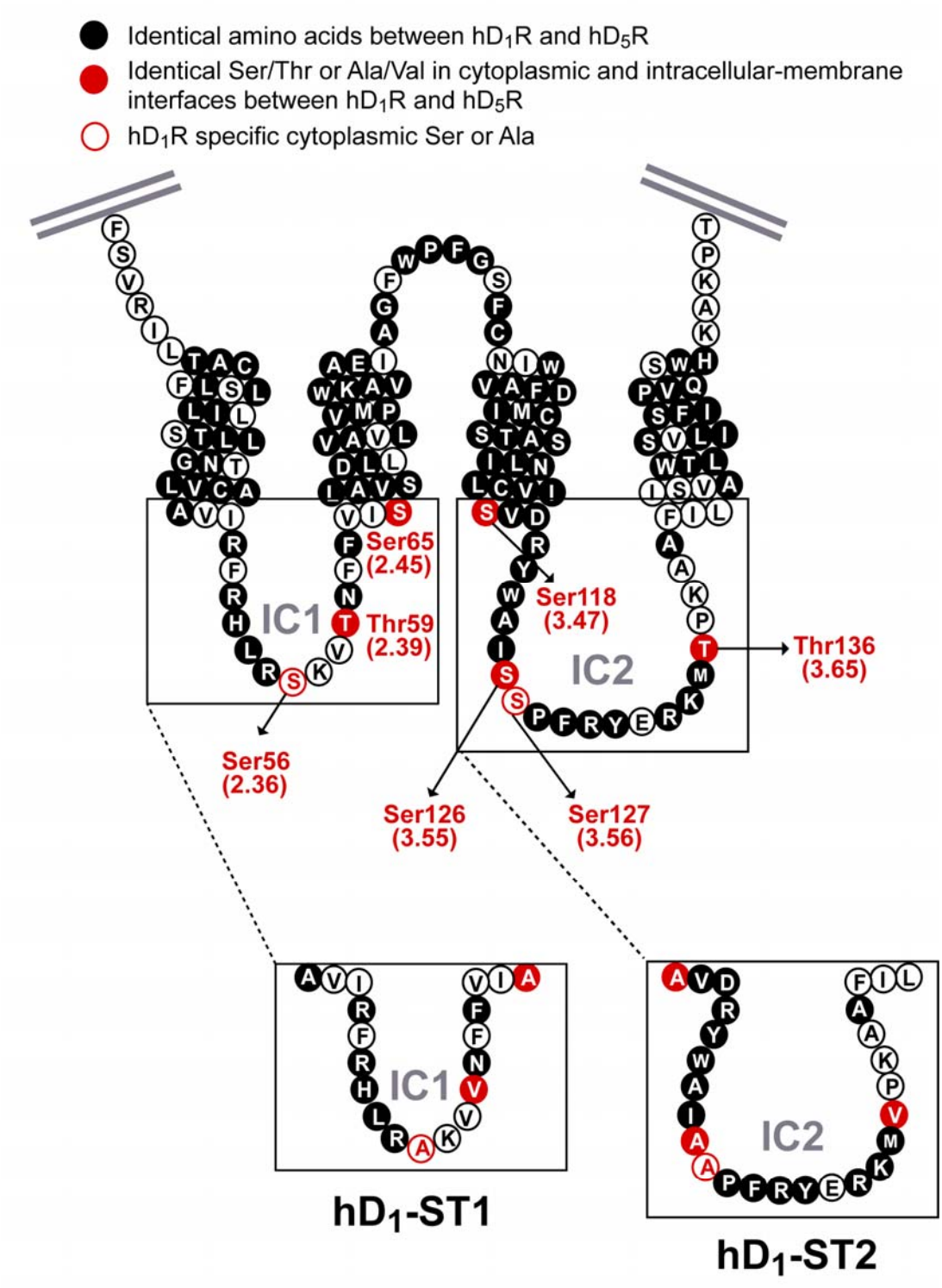

Figure 10. Amino acid sequence of the hD_1R and ST mutant receptors.
The hD_1-ST1 has $Ser^{2.36}$, $Thr^{2.39}$, and $Ser^{2.45}$ mutated to $Ala^{2.36}$, $Val^{2.39}$, and $Ala^{2.45}$, respectively. The hD_1-ST2 has $Ser^{3.47}$, $Ser^{3.55}$, $Ser^{3.56}$, and $Thr^{3.65}$ mutated to $Ala^{3.47}$, $Ala^{3.55}$, $Ala^{3.56}$, and $Val^{3.65}$, respectively.

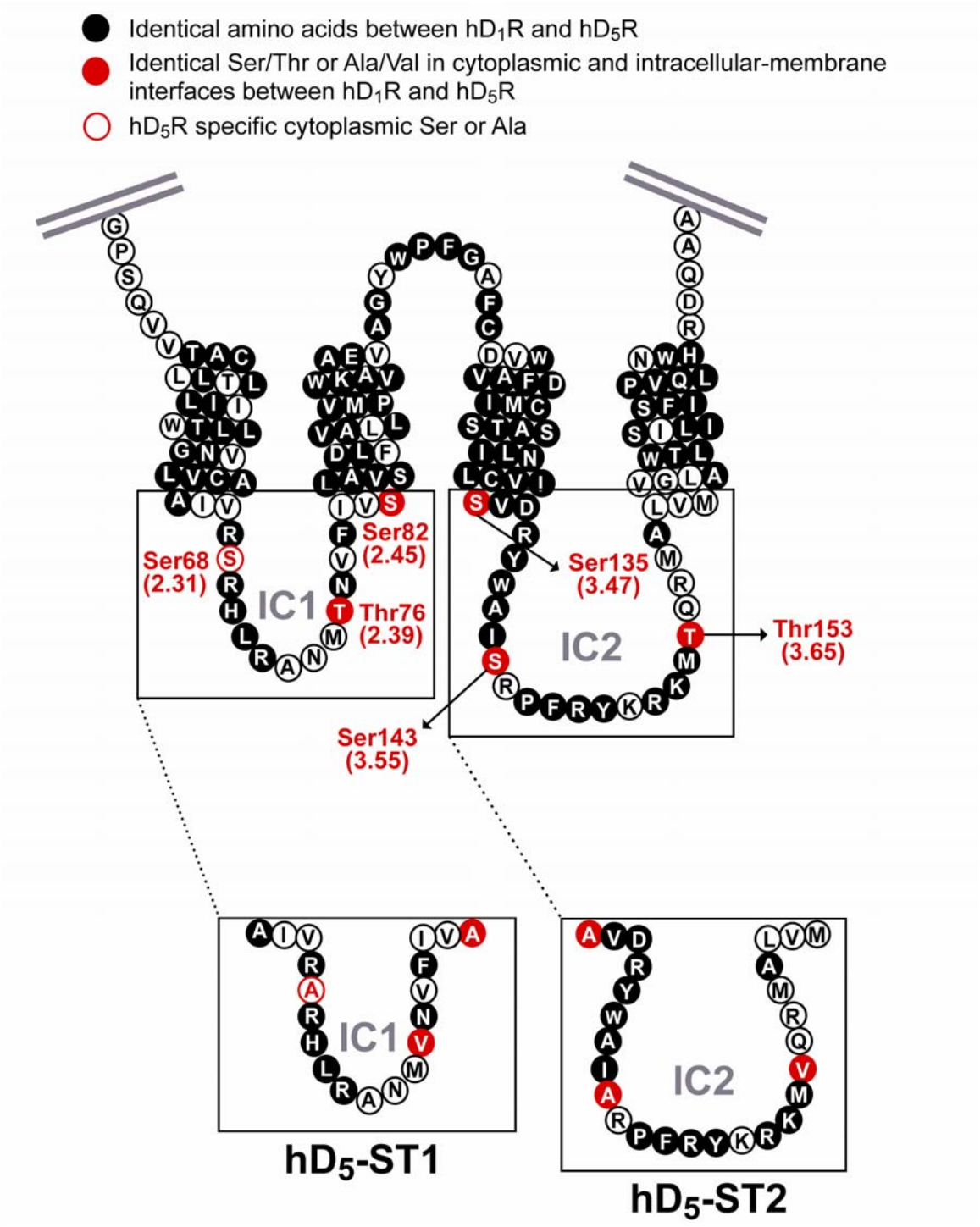

Figure 11. Amino acid sequence of the hD_5R and ST mutant receptors.
The hD_5-ST1 has $Ser^{2.31}$, $Thr^{2.39}$, and $Ser^{2.45}$ mutated to $Ala^{2.31}$, $Val^{2.39}$, and $Ala^{2.45}$, respectively. The hD_5-ST2 has $Ser^{3.47}$, $Ser^{3.55}$, and $Thr^{3.65}$ mutated to $Ala^{3.47}$, $Ala^{3.55}$, and $Val^{3.65}$, respectively.

Methods

1. Materials

N-[methyl-^{3}H]-SCH23390 and [^{3}H]-adenine were acquired from Perkin Elmer (Boston, MA, USA). [^{14}C]-cAMP was from Moravek Biochemicals (Brea, CA, USA). DA, *cis*-flupenthixol, thioridazine, thiothixene, 1-methyl-3-isobutylxanthine (IBMX), dimethyl sulfoxide (DMSO), bovine serum albumin (BSA) and ascorbic acid (AA) were obtained from Sigma-Aldrich (Oakville, ON, Canada). Dihydrexidine was from Tocris Bioscience (Ellisville, MO, USA). Trypsin-EDTA, HEPES buffer (4-(2-hydroxyethyl)-1-piperazineethanesulfonic acid), fetal bovine serum (FBS), and gentamicin were bought from Life Technologies (Burlington, ON, Canada). Minimal essential media (MEM) and phosphate buffered-saline (PBS) were purchased from Wisent Bioproducts (St-Bruno, QC, Canada). Paraformaldehyde was from Electron Microscopy Sciences (Hatfield, PA, USA). Bio-Rad Protein Dye, DC protein assay kit, and Triton-X were obtained from Bio-Rad (Bio-Rad Laboratories Inc, Mississauga, ON, Canada).

2. Construction of Receptors

2.1 – Human D_1-class ST1 and ST2 mutant receptors

Ser and Thr residues located in cytoplasmic regions and intracellular-membrane interfaces of hD_1R and hD_5R were all mutated using a custom gene synthesis into pUC57 plasmid vector (GenScript USA Inc., NJ, USA) to generate two constructs: cm-hD_1R and cm-hD_5R. The cm-hD_1R and cm-hD_5R in pUC57 vector were utilized to make D_1-class ST1 and ST2 mutants as follows. To create the hD_1-ST1 in pCMV5, cm-hD_1R pUC57 was digested with *EcoR*I and *Bgl*II to obtain a cassette (~ 220 bp) that was subcloned into hD_1R pCMV5 expression plasmid DNA, which had been linearized with *EcoR*I and

*Bgl*II. The hD_5-ST1 in pCMV5 was created by digesting cm-hD_5R pUC57 with *Kpn*I-*Hae*II (~290 bp) and *Hae*II-*Hind*III (~1160 bp), and ligating the fragments in empty pCMV5 digested with *EcoR*I and *Hind*III. A *Bgl*II-*Hind*III DNA cassette derived from cm-hD_1R pUC57 construct (~400 bp) was subcloned into hD_1R-pCMV5 linearized with *Bgl*II and *Hind*III to obtain hD_1-ST2 in pCMV5. To generate hD_5-ST2 into pCMV5, the *Hae*II-*Hind*III (~1330 bp) fragment of cm-hD_5R and the *Kpn*I-*Hae*II (~310 bp) fragment of hD_5R-pCMV5 were ligated to empty pCMV5 vector digested with *Kpn*I and *Hind*III.

2.2 – Single point mutant receptors of hD_1R

Single point mutant receptors were created by PCR (polymerase chain reaction) using overlap extension strategy (Plouffe *et al.*, 2010). In the first step, primer pairs P1-P2 and P3-P4 (**Table 1**) amplified hD_1R-pCMV5 to produce two products or "megaprimers" that contained the single point mutations as well as silent mutations. The purpose for silent mutations was to incorporate novel restriction sites for diagnostic testing. In the second step, primer pairs P5-P6 (**Table 1**) extended the overlap region of the two megaprimers. Overlap product (~1200 bp) was digested with *EcoR*I and *Hind*III to generate an approximately 600 bp fragment that was subcloned into hD_1R-pCMV5 linearized with *EcoR*I and *Hind*III. DNA sequences from synthesized mutant receptors were confirmed by automated DNA sequencing from StemCore Laboratories of the Ottawa Hospital Research Institute (Ottawa, ON, Canada) Custom-designed primers were from Sigma-Aldrich (Oakville, ON, Canada).

Table 1. Primer sequences used to create mutant receptors of hD_1R.

Receptor	Primer Sequences (5'→ 3')
hD_1-S56A	P1: CCATGGTGATGCGGTTTT
	P2: CACCTTGGCCCGCAGGTGTCGGAACCTGATAACTGCAGCA CAGACCAGCGTGTTCCC
	P3: CTGGTCTGTGCTGCAGTTATCAGGTTCCGACACCTGCGGG CCAAGGTGACCAACTTC
	P4: TTAGGACAAGGCTGGTGG
	P5: CAAAATGTCGTAATAACCCCG
	P6: GCAAAGTCTGTACCATCCTAAGAGGGT
hD_1-T59V	P1: CCATGGTGATGCGGTTTT
	P2: CAAGAGATCCGACACAGCCAAGGAGATGACAAAGAAGTT GACCACCTTGGACCGCAGGTGTCG
	P3: CGGTCCAAGGTGGTCAACTTCTTTGTCATCTCCTTGGCTGT GTCGGATCTCTTGGTGGCCGTC
	P4: TTAGGACAAGGCTGGTGG
	P5: CAAAATGTCGTAATAACCCCG
	P6: GCAAAGTCTGTACCATCCTAAGAGGGT
hD_1-S65A	P1: CCATGGTGATGCGGTTTT
	P2: AGCCAAGGCGATGACAAAGAAGTTGGTCACCTTGGACCG CAGGTGTCGGAACCTGATAACGGCCGCACAGACCAGCGTGTT CCCCAG
	P3: ACGCTGGTCTGTGCGGCCGTTATCAGGTTCCGACACCTGC GGTCCAAGGTGACCAACTTCTTTGTCATCGCCTTGGCTGTGTC AGAT
	P4: TTAGGACAAGGCTGGTGG
	P5: CAAAATGTCGTAATAACCCCG
	P6: GCAAAGTCTGTACCATCCTAAGAGGGT
hD_1-D120A	P1: CCATGGTGATGCGGTTTT
	P2: GATAGCCCAATACCTGGCCACGCTGATCACACA
	P3: TGTGTGATCAGCGTGGCCAGGTATTGGGCTATC
	P4: TTAGGACAAGGCTGGTGG
	P5: CAAAATGTCGTAATAACCCCG
	P6: GCAAAGTCTGTACCATCCTAAGAGGGT
hD_1-R121A	P1: CCATGGTGATGCGGTTTT
	P2: GATAGCCCAATACGCGTCGACGCTGATCACACAGAG
	P3: ATCAGCGTCGACGCGTATTGGGCTATCTCCAGCCCT
	P4: TTAGGACAAGGCTGGTGG
	P5: CAAAATGTCGTAATAACCCCG
	P6: GCAAAGTCTGTACCATCCTAAGAGGGT

Table 1 (continued). Primer sequences used to create mutant receptors of hD_1R.

Receptor	Primer Sequences (5'→ 3')
hD_1-Y131A	P1: CCATGGTGATGCGGTTTT
	P2: TCTCTCAGCCCGGAAAGGGCTCGAGATAGCCCAATACCT GTC
	P3: GCTATCTCGAGCCCTTTCCGGGCTGAGAGAAAGATGACC CCC
	P4: TTAGGACAAGGCTGGTGG
	P5: CAAAATGTCGTAATAACCCCG
	P6: GCAAAGTCTGTACCATCCTAAGAGGGT
hD_1-N113A	P1: CCATGGTGATGCGGTTTT
	P2: CACACAGAGGGCGAGGATCGATGCAGTGGAGCACATGAT
	P3: TCCACTGCATCGATCCTCGCCCTCTGTGTGATCAGCGTG
	P4: TTAGGACAAGGCTGGTGG
	P5: CAAAATGTCGTAATAACCCCG
	P6: GCAAAGTCTGTACCATCCTAAGAGGGT
hD_1-W148A	P1: CCATGGTGATGCGGTTTT
	P2: CCAGCTGAGTTGCACTGGGATGAAGGAGATGAGTACAG ACAAGGTCGCTGCCACACTGATCAGGATGAA
	P3: ATCAGTGTGGCAGCGACCTTGTCTGTACTCATCTCCTTCA TCCCAGTGCAACTCAGCTGGCACAAGGCA
	P4: TTAGGACAAGGCTGGTGG
	P5: CAAAATGTCGTAATAACCCCG
	P6: GCAAAGTCTGTACCATCCTAAGAGGGT
hD_1-W148F	P1: CCATGGTGATGCGGTTTT
	P2: CCAGCTGAGTTGCACTGGGATGAAGGAGATGAGTACAG ACAAGGTGAATGCCACACTGATCAGGATGAA
	P3: ATCAGTGTGGCATTCACCTTGTCTGTACTCATCTCCTTCA TCCCAGTGCAACTCAGCTGGCACAAGGCA
	P4: TTAGGACAAGGCTGGTGG
	P5: CAAAATGTCGTAATAACCCCG
	P6: GCAAAGTCTGTACCATCCTAAGAGGGT
hD_1-W148Y	P1: CCATGGTGATGCGGTTTT
	P2: GATGAGTACAGACAACGTGTATGCCACACTGATCAG
	P3: CTGATCAGTGTGGCATACACGTTGTCTGTACTCATC
	P4: TTAGGACAAGGCTGGTGG
	P5: CAAAATGTCGTAATAACCCCG
	P6: GCAAAGTCTGTACCATCCTAAGAGGGT
HA-hD_1-ST1	P1: GAATTCGCCGCCACCATGTACCCATACGACGTCCCAGAC TACGCTAGGACTCTGAAC
	P2: CACAGCATGTGGGAT

Table 1 (continued). Primer sequences used to create mutant receptors of hD_1R.

Receptor	Primer Sequences (5'→ 3')
FLAG-hD_1-ST1	P1: GAATTCGCCGCCACCATGGACTACAAGGACGATGACGACAAGAGGACTCTGAAC
	P2: CACAGCATGTGGGAT

2.2 – Tagging the N-termini of Receptors with HA and Flag Epitopes

HA-hD_1-ST1 and FLAG-hD_1-ST1 were constructed using a single-step PCR with P1-P2 primer pair (**Table 1**) and hD_1-ST1 as template. The product was digested with *EcoR*I and *Hind*III and subcloned into hD_1R-pCMV5 linearized with *EcoR*I and *Hind*III. HA-hD_5-ST1 and FLAG-hD_5-ST2 were constructed through digesting hD_5-ST1-pCMV5 with *Sma*I and subcloning the fragments into existing HA-hD_5R-pCMV5 and FLAG-hD_5R-pCMV5 (Plouffe *et al.*, 2010) linearized with *Sma*I. FLAG-hD_1-ST2 was made by digesting hD_1-ST2 using *Bgl*II and *BamH*I and subcloning the fragment (~1200 bp) into existing FLAG-hD_1R-PCMV5 (Plouffe *et al.*, 2010) linearized with *Bgl*II and *BamH*I. FLAG-hD_1-N113A and FLAG-hD_1-W148Y were constructed by digesting hD_1-N113A and hD_1-W148Y with *Bgl*II and *Xba*I and subcloning the fragments (~1200 bp) into FLAG-hD_1-pCMV5 linearized with *Bgl*II and *Xba*1. Both HA-tagged and FLAG-tagged versions of hD_1-S56A, hD_1-T59V, and hD_1-S65A were created following the PCR approach described in Methods Section 2.1 and using HA-hD_1R-pCMV5 and FLAG-hD_1R-pCMV5 as template. The same corresponding primers listed in **Table 1** were used. DNA sequences from HA- and FLAG-tagged receptors were confirmed by automated DNA sequencing from StemCore Laboratories of the Ottawa Hospital Research Institute (Ottawa, ON, Canada).

3. Homology Modelling, Docking, and Molecular Dynamics

Homology models of hD_1R, hD_5R, hD_1-ST2, and hD_1-ST2 were built with YASARA Structure (version 15.11.18) using hm_build macro that was modified to select the top ranked crystal structures in their putative inactive states, which consisted: β_1AR

with cyanopindolol (PDB: 2VT4), β_2AR with carazolol (PDB: 2RH1), muscarinic M_2 receptor with 3-quinuclidinyl-benzilate (PDB: 3UON), and D_3R with eticlopride (PDB: 3PBL). Multiple sequence alignment was performed, followed by addition of side chains, loop optimization, and energy minimization in explicit solvent by simulated annealing and steepest descent. For all receptors, the final hybrid model, containing the best modelled parts from numerous generated models, was chosen for docking. The NT, IC3 loop, and CT were omitted. All models were validated and found to be in good quality as indicated by their Z scores and Ramachandran maps (**Table 2**).

Table 2. Structural quality scores for homology models of human D_1-class and ST2 mutant receptors.
The overall model quality Z-score evaluates normality of packing and dihedrals. The Chi1/Chi2 Z scores assess the side-chain dihedral angles Chi1 against Chi2. Z scores were calculated using WHATIF-YASARA twinset. Z scores above -1 are generally considered good. PROCHECK (Laskowski *et al.*, 1993) was used to generate Ramachandran scores, which evaluate backbone dihedral angles Phi against Psi.

	hD_1R	hD_5R	hD_1-ST2	hD_5-ST2
Overall model quality Z-score	0.371	-0.06	0.421	-0.212
Chi1/Chi2 Z-score	-0.281	0.189	-0.344	-0.404
% in most favoured Phi/Psi	95.6	95.4	95.6	95.7
% in additional allowed Phi/Psi	4.1	4.3	4.4	4.3

Hybrid models were docked with DA using induced-fit docking protocol (IFD) (Sherman *et al.*, 2006) from Glide (version 6.4, Schrodinger-2015 Maestro 10.1 interface). This scheme performs an initial docking using van der Waals scaling of 0.5 to increase flexibility of ligand and receptor. The docked receptor is then energy minimized to become an induced-fit receptor structure in which the ligand is re-docked more rigorously. DA ligand was retrieved from ZINC database (ZINC00033882). The centroid of workspace (i.e. binding site) was defined by $Asp^{3.32}$, $Ser^{5.42}$, and $Ser^{5.46}$. For hD_1R, and hD_1-ST2, the XP precision mode was chosen because it generated better docking scores than SP precision mode. Because Asp218 and Asp342 prevented DA from reaching the binding site of hD_5R and hD_5-ST2, the "trim side chain" function in Glide was used to mutate the two residues to alanines during the initial docking stage and then restore original side-chains during energy minimization. In these scenarios, the SP precision mode offered better docking scores compared to XP precision mode and was thus selected. Remaining settings in IFD were set to default. Top ranking poses were selected based on visual inspection.

Docked models of hD_1R and hD_1-ST2 were capped at Ile225 with *N*-methyl amide and Met263 with acetyl groups to avoid net charge from the internal chain break caused by removing the IC3 loop. Similarly, docked models of hD_5R and hD_5-ST2 were capped at Ile256 and Ala286 with *N*-methyl amide and acetyl groups, respectively. The docked model of hD_1R was also used to model the single point mutation in hD_1-W148Y by using the SwapRes command in YASARA to convert Trp148 to Tyr148. At the start of md_runmembrane macro, docked models were embedded in membranes composed of phosphatidyl-ethanolamine and then manually positioned to match the predicted

membrane boundaries from Orientation of Proteins in Membranes (Lomize *et al.*, 2012) of either hD_1R or hD_5R. Simulations in membrane (explicit solvent, periodic boundaries) then proceeded whereby the first 250 ps were a restrained equilibration phase to stabilize the membrane. The selected forcefield was YAMBER3, which is based from AMBER (Cornell *et al.*, 1994) and has been reported to be optimized in maintaining structural integrity (Krieger *et al.*, 2004). Default simulation and forcefield parameters were used, except the timestep was changed to calculate all intra/inter molecular forces every femtosecond.

4. Cell Culture and Transfection

HEK293 cells were housed in 5% CO_2, 37^{o}C incubator and grown between passages 41-52 in culture media comprised of MEM supplemented with 10% (v/v) FBS and gentamicin (20 μg/ml). Cells were transfected using a modified calcium phosphate method (Plouffe *et al.*, 2010) in 100-mm dishes at a density of 2.5 million/dish. The total amount of transfected DNA was consistently 5 μg. The amount of receptor DNA was adjusted to obtain the desired receptor B_{max}, and if less than 5 μg was used, the remaining transfected DNA was empty pCMV5 vector. For saturation studies, 5 μg of receptor DNA was consistently used regardless of the receptor condition. The following day, transfected cells were washed with PBS, trypsinized, resuspended in culture media, and then pooled per condition before reseeding.

5. Radioligand Binding Assays

Crude membranes were prepared using previously detailed procedures (Plouffe *et al.*, 2010). They were used immediately for saturation studies or frozen in -80^{o}C to be re-thawed for competition studies. Binding assays for saturation studies were comprised of (final concentration): binding buffer (50 mM Tris–HCL, pH 7.4; 120 mM NaCl; 5 mM KCL;4 mM $MgCl_2$; 1.5 mM $CaCl_2$; 1 mM EDTA (Ethylenediaminetetraacetic acid), pH 8.0), water or 10 µM of *cis*-flupenthixol (i.e. unlabelled drug, at concentrations around 100-1000 times its K_D to bind to essentially all dopamine receptors), and increasing concentrations (0.03 nM to 9 nM) of [^{3}H]-SCH23390—specific activity 81.9 Ci/mmol. The total mixture volume was 500 µl, which contained 300 µl binding buffer, 50 µl [^{3}H]-SCH23390, 50 µl (water or *cis*-flupenthixol), and 100 µl of membrane. Components for competition studies were (500 µl total mixture volume): 300 µl binding buffer, 50 µl [^{3}H]-SCH23390 at constant concentrations (0.5–1 nM), 50 µl of increasing concentrations of competing drugs, and 100 µl of membrane. To test the effects of Dyngo4a (**Figure 43**), assay constituents/volumes for competition studies were kept the same with the addition of 3 µl of 100% DMSO or 3 µl of 5 mM Dyngo4a (in 100% DMSO). All competing drugs were dissolved in water except for DA, which was dissolved in AA (0.1 mM final) to prevent oxidation of DA. After 90 min of incubation at room temperature, the assay underwent rapid filtration through glass fiber filters (GF/C, Whatman) followed by three times wash with cold buffer solution (50 mM Tris–HCL, pH 7.4; 100 mM NaCl). Filter disks were immersed in scintillation liquid from Bio-Safe II (Research Products International Corp, Mount Prospect, IL, USA). Beckman Counter (LS6500) was used to detect bound radioactivity. Membrane protein concentrations were

extrapolated from a standard curve using bovine serum albumin and detected using Bio-Rad Protein Dye.

6. Whole-Cell cAMP Assays

Cells were reseeded in 6-well dishes for basal activity and 12-well dishes for dose-response studies. The next day, culture media was replaced with labelling media that consisted of MEM with 5% (v/v) FBS, gentamicin (10 μg/mL) and [^{3}H]-adenine (1-2 μCi/ml). Experiments were performed the following day. Labelling media was replaced with incubation solution (MEM containing 20 mM HEPES and 1 mM IBMX—final concentration of 1 mM was obtained using a stock concentration of 200 mM IBMX in 100% DMSO). Subsequently, either AA (0.1 mM final) or DA (dissolved in 0.1 mM AA) was applied for 30 min at 37^{o}C unless stated otherwise. Stock concentrations of 25 mM for Pitstop2, Neg Pitstop2 and 30 mM for Dyngo4a were prepared in 100% DMSO and stored in aliquots at -20^{o}C. On the day of the experiment, desired final concentrations of Pitstop2, Neg Pitstop2, and Dyngo4a were achieved by diluting stock concentrations in incubation solution. Once labelling media was aspirated (from 12-well dishes), this solution was then applied to the cells for 10-15 mins incubation period at 37^{o}C. AA (0.1 mM final) or DA (dissolved in 0.1 mM AA) were subsequently added to the wells during 10 mins stimulation period at 37^{o}C. A control for Dyngo4a was 0.6% DMSO to account for DMSO vehicle of Dyngo4a (0.1%) and IBMX (0.5%) in the incubation solution.

To stop cAMP assays, media was removed, and each well was given 1 mL of lysis solution composed of 2.5% (v/v) perchloric acid, 0.1 mM cAMP, and [^{14}C]-cAMP (6000–8000 dpm) for 30 mins at 4^{o}C. The solution (containing cell lysates) from each

well was then transferred into test tubes containing 100 µL of 4.2M KOH and vortexed. After centrifugation at 15 000 rpm at 4°C, [^{3}H] cAMP of the supernatant was measured using sequential chromatography (Dowex and alumina columns) as detailed previously (Plouffe *et al.*, 2010). The relative AC activity was determined by dividing intracellular [^{3}H]-cAMP (CA) amount by the total intracellular [^{3}H]-adenine uptake (TU) and was expressed as CA/TU × 1000. In parallel to cAMP assays, B_{max} was measured from radioligand binding assays that were performed on crude membranes of transfected cells reseeded in 100-mm dishes. [^{3}H]-SCH23390 (8–10 nM) and 10 µM *cis*-flupenthixol (cold drug) was used.

To assess DA-induced desensitization, cells were reseeded in 6-well dishes. The next day, culture media was replaced with labelling media, and the experiment was performed the day after. Cells were pre-treated with either 0.1 mM AA or 10 µM DA for 5 mins in labelling media at 37°C. Media was aspirated, and each well was washed twice with room temperature PBS. Cells were then given incubation solution, and 10 µM DA (**Figure 18A**) or various doses of DA **(Figure 39)**, and incubated at 37°C for 10 mins. Assay was stopped as described above. To calculate the desensitizing response (% decrease in E_{max}) in **Figure 18A**, the following equation was used:

$$\text{Desensitization (\%)} = \frac{(DA_{AApretreat} - AA_{AApretreat}) - (DA_{DApretreat} - AA_{DApretreat})}{DA_{AApretreat} - AA_{AApretreat}} \times 100$$

,where the variables denoting cAMP responses were:

$DA_{AApretreat}$ (Pre-treatment with 0.1 mM AA and challenged with 10 µM DA)

$AA_{AApretreat}$ (Pre-treatment with 0.1 mM AA and challenged with 0.1 mM AA)

$DA_{DApretreat}$ (Pre-treatment with 10 μM DA and challenged with 10 μM DA)

$AA_{DApretreat}$ (Pre-treatment with 10 μM DA and challenged with 0.1 mM AA)

To generate dose-response curves in **Figure 39**, each raw data point from AA pre-treatment condition and DA pre-treatment condition was subtracted from the respective $AA_{AApretreat}$ and $AA_{DApretreat}$ and then plotting them as a function of DA concentrations. Every value was then divided by the best-fitted E_{max} of the curve from AA pre-treatment condition and pooled together corresponding to the dose to obtain average dose-response curves for each condition (AA pre-treatment and DA pre-treatment).

7. Western Blot

Cells were scraped and solubilized using 800-1000 μl of radioimmunoprecipitation assay (RIPA) buffer (Sedaghat & Tiberi, 2011) supplemented with protease inhibitors. Samples were centrifuged at 15,000 *g* for 15 mins at 4 ^{o}C. Protein concentrations in the supernatants (containing solubilized cell components) were quantified using Bio-Rad DC protein assay kit. Equivalent amounts of proteins (40 or 90 μg) for mock and receptor conditions were loaded onto 10% (v/v) acrylamide gels for SDS-PAGE. Trans-Blot SD semidry transfer cell (Bio-Rad) was used to transfer proteins onto PVDF (polyvinylidene difluoride) membranes at 15 V for 18 mins. Membranes were blocked overnight and then incubated overnight with either monoclonal rabbit anti-D_1R (ab81296, lot# GR106881-8; Abcam) or polyclonal rabbit anti-D_5R (ab32620, lot # GR2654-2; Abcam) diluted 1:1000 in Tris-buffered saline and Tween-20 (TBS-T: 20

mM Tris-HCL, pH 7.4; 137 mM NaCl; 0.2% (v/v) Tween-20). This was followed by 1 hr incubation with secondary anti-rabbit conjugated to horseradish peroxidase (NA934V; GE Healthcare) diluted 1:10 000 in TBS-T. Proteins were visualized using Amersham ECL Prime detection kit (RPN2232; GE Healthcare).

8. Enzyme-Linked Immunosorbent Assays (ELISA)

Cells transfected with mock (empty pCMV5 vector) and either FLAG-tagged or HA-tagged receptor DNA were reseeded in 12-well plates pre-coated with poly-D-lysine. ELISA was conducted approximately 48 hrs post transfection. For internalization assay, culture media was aspirated and was replaced with MEM containing 20 mM HEPES and 1 mM IBMX. Cells were then treated with either 0.1 mM AA (control) or DA for 5 or 10 mins at 37^{o}C. Afterwards, plates were immediately placed on ice whereby the media was replaced with 3.7% (v/v) paraformaldehyde in PBS and incubated on ice for 10 mins. If ELISA was used to measure normal (non-treated) cell surface expression, culture media was removed from transfected cells followed by incubation with 3.7% (v/v) paraformaldehyde in PBS at room temperature. In both assays, after cell fixation, plates were washed three times with 0.02% (w/v) BSA for 10 mins each and then blocked with 1% (w/v) BSA for 15 mins prior to incubating for 45 mins with anti-FLAG M2 monoclonal (F-3165; lot# 121K9185; Sigma-Aldrich) diluted 1:10 000 in 1% (w/v) BSA (containing NaN_3) or mouse anti-HA (32-6700, lot# 1389267; Zymed Laboratories) diluted 1:2000 in 1% (w/v) BSA (containing NaN_3). Plates were subsequently washed with 0.02% (w/v) BSA for 10 mins each, blocked with 1% (w/v) BSA for 15 mins, and then incubated for 45 mins with goat anti-mouse conjugated with horseradish peroxidase

(115-053-003; Jackson ImmunoResearch) diluted between 1:2000 and 1:5000 in 1% (w/v) BSA if receptors were FLAG-tagged. If receptors were HA-tagged, the secondary antibody used was sheep anti-mouse linked to horseradish peroxidase (NA9310V; GE Healthcare) that was diluted 1:1000 in 1% (w/v) BSA. Another washing step was performed, involving three times with 0.02% (w/v) BSA for 10 mins each. All washing, blocking, and antibody incubation steps were performed at room temperature on a gentle rocker. After aspirating, each well was given 400 µl o-phenylenediamine dihydrochloride (OPD) solution (0.4 mg/ml OPD, 0.4 mg/ml urea hydrogen peroxide and 0.05 M phosphate-citrate pH 5.0; SIGMAFAST OPD, P9187). Plates were covered with aluminium foil and placed on rocker for 12 mins. The reaction was stopped with 100 µl of 3M HCL. Solution in each well was transferred to 96 well plates. SpectraMaxM5 (Molecular Devices) was used to read the optical density at 490 nm.

To measure total receptor expression, after cell fixation with 3.7% (v/v) paraformaldehyde in PBS at room temperature, 0.1% (v/v) Triton-X in PBS was applied to all subsequent ELISA steps (washes, blockade, antibody incubation) until the addition of OPD (12 mins incubation) and 3M HCL. Total receptor or cell surface receptor levels relative to wild-type were calculated using the following equation, where OD represents the ELISA optical density at 490 nm corresponding to the condition denoted in subscript:

$$\text{Total/Cell Surface Expression (\%)} = \frac{\text{OD}_{Receptor} - \text{OD}_{Mock}}{\text{OD}_{Wild-type} - \text{OD}_{Mock}} \times 100$$

DA-induced internalization was assessed by the % decrease of the ELISA OD at 490 nm of DA-treated condition from AA-treated condition. This was corrected from mock condition and followed the equation:

$$\text{Internalization (\%)} = \frac{(\text{OD}_{AA} - \text{OD}_{Mock}) - (\text{OD}_{DA} - \text{OD}_{Mock})}{\text{OD}_{AA} - \text{OD}_{Mock}} \times 100$$

9. Statistical Analysis

Statistical analyses and curve fitting were performed using GraphPad Prism (version 6.02). Equilibrium dissociation constants (K_D, K_I) and B_{max} were calculated using non-linear regression curve fitting derived from one-binding site algorithm. Individual dose-response curves containing raw data (CA/TU x 1000) were fitted by a four-parameter logistic equation. Unless stated otherwise, average dose-response curves for each receptor condition were generated by expressing the amount of intracellular cAMP for each dose (raw data) as a percentage of best-fitted wild-type E_{max} value and pooling the transformed values together corresponding to the dose. Best-fitted EC_{50} and E_{max} from averaged curves were compared using unconstrained, shared, and constrained global curve fitting. Results were deemed statistically significant at $p < 0.05$ using statistical tests (one sample *t*-test, unpaired two-tailed *t*-test, or multiple *t*-tests with Holm Sidak correction method) as mentioned in text.

Results

1. Functional Screening Studies

1.1 - Binding properties of D_1-class IC2 mutant receptors

Saturation studies revealed that ST2 mutant receptors were able to bind to the selective D_1-class benzazepine compound, [^{3}H]-SCH23390 (See **Figure 12** for ligand structures and **Figure 13** for an example of a saturation curve) with high affinity as parent receptors. This indicated that for all ST2 mutants, the ligand binding pocket was able to fold properly to the extent where it remained functional **(Table 3)**. Although SCH23390 is generally considered to be a selective D_1-class antagonist, it has also been shown to also exert partial agonism at D_1-class receptors expressed in heterologous cells (Sugamori *et al.*, 1998, Tiberi & Caron, 1994). Meanwhile, the B_{max} of ST2 mutant receptors appeared to be lower compared to their wild-type counterparts when 5 μg of transfected receptor DNA was used—an amount previously shown to achieve the maximum B_{max} for hD_1R and hD_5R with our transfection protocol in HEK293 cells (Plouffe *et al.*, 2010). Derived from saturation curves, the B_{max} is a parameter that can be used to describe functional receptor expression.

Competition studies were performed with DA, dihydrexidine (DHX), and inverse agonists, thioridazine and thiothixene (D'Aoust & Tiberi, 2010), to probe whether ligand binding was altered in ST2 mutant receptors **(Table 3, Figure 14)**. Whereas the hD_5-ST2 exhibited a major loss of affinity for DA compared to hD_5R, the hD_1-ST2 displayed a small but statistically significant gain in affinity for DA compared to hD_1R. The affinity for the synthetic agonist DHX was also lowered in hD_5-ST2 by approximately the same order of magnitude as DA; meanwhile, DHX affinity for hD_1-ST2 was not statistically

different from hD_1R. The affinity changes for inverse agonists were minor with only hD_5-ST2 displaying a statistically lower affinity for thioridazine **(Table 3, Figure 14)**.

SCH23390 (LogP: 3.94)

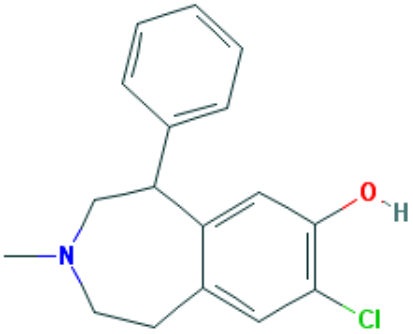

Dopamine (LogP: -0.4)

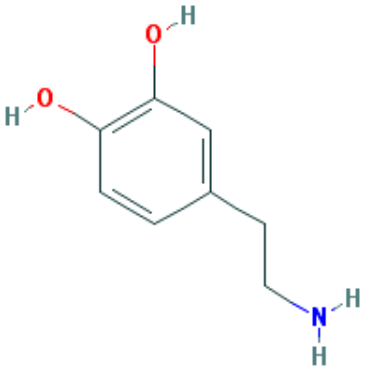

Dihydrexidine (LogP: 2.18)

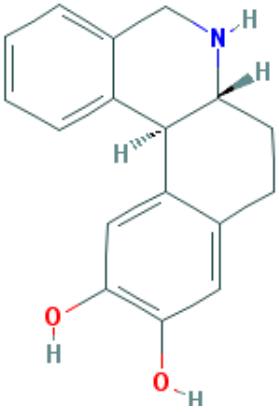

Thioridazine (LogP: 5.93)

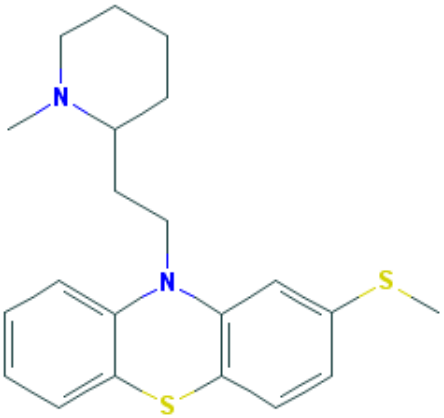

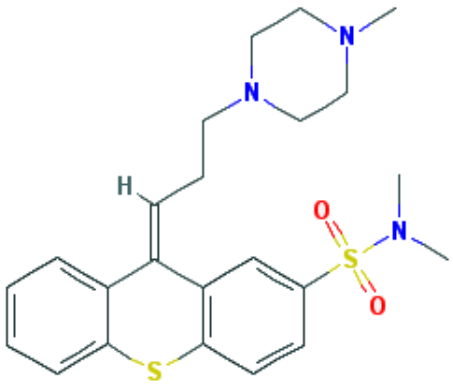

Thiothixene (LogP: 4.01)

Figure 12. Chemical structures of various ligands used in saturation and competition binding assays.
Structures were obtained from https://pubchem.ncbi.nlm.nih.gov/. They were then submitted (in .sdf format) to an online version of ALOGPS 2.1 for calculation of LogP values (Tetko *et al.*, 2005). In general, compounds with LogP values below 0.5 are highly water-soluble and may not cross the lipid membrane. Compounds with LogP values above 3 are considered highly lipid-soluble (Kenakin, 2012).

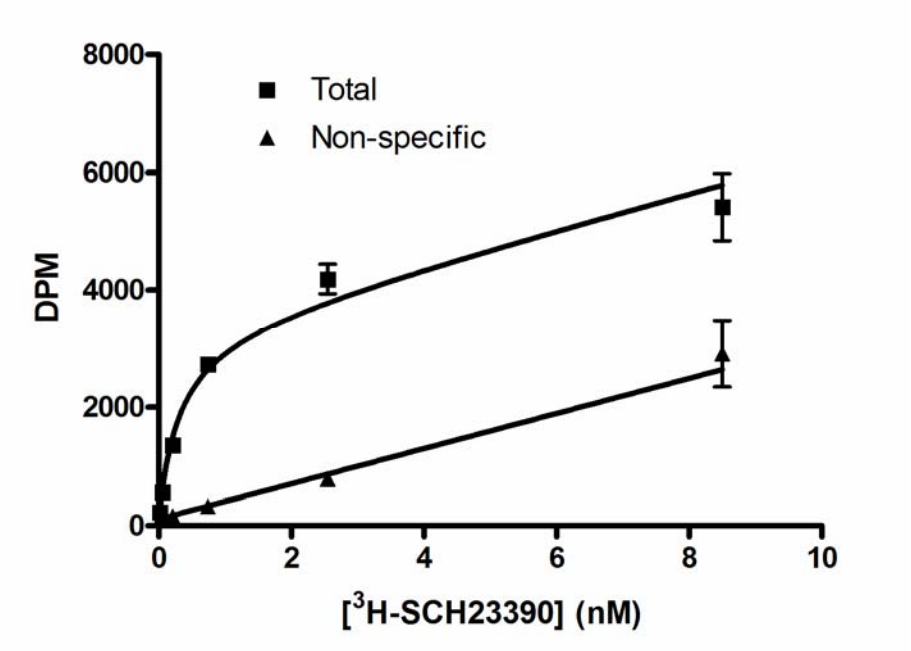

Figure 13. A representation of a saturation binding curve from radioligand binding assays performed on transfected HEK293 cells.
Receptor condition was the hD_1-ST2 using 5 μg of receptor DNA. Curve was fitted using the one-site model for saturation binding in GraphPad Prism. DPM, disintegrations per minute.

Table 3. Dissociation constants (K_D, K_I) and B_{max} values of [^{3}H]-SCH23390 for wild-type and ST2 mutant receptors.
pK_D and pK_I (negative logarithm of K_D and K_I in molar) are expressed as arithmetic means ± S.E. with the corresponding K_I and K_D (nM) shown in brackets. B_{max} values (pmol/mg of membrane proteins) are expressed as arithmetic means ± S.E.. See **Figure 14** for statistical comparisons of dissociation constants.

	Saturation Curves		**Competition Curves**			
	[^{3}H]-SCH23390 (n = 6-7)		Dopamine (n = 4-5)	Dihydrexidine (n = 5-6)	Thioridazine (n = 5-6)	Thiothixene (n = 4-6)
	pK_D (K_D, nM)	B_{max} (pmol/mg)	pK_I (K_I, nM)			
hD_1R	9.39 ± 0.04 (0.41)	8.77 ± 0.72	5.12 ± 0.03 (7520)	6.30 ± 0.05 (507)	7.02 ± 0.03 (96.0)	7.17 ± 0.01 (67.9)
hD_1-ST2	9.45 ± 0.05 (0.36)	2.78 ± 0.13	5.30 ± 0.05 (5006)	6.34 ± 0.06 (455)	7.04 ± 0.02 (91.1)	7.21 ± 0.03 (61.1)
hD_5R	9.12 ± 0.05 (0.76)	16.0 ± 2.3	6.00 ± 0.04 (994)	7.05 ± 0.04 (90.2)	6.24 ± 0.07 (571)	6.33 ± 0.09 (464)
hD_5-ST2	8.97 ± 0.05 (1.1)	13.1 ±1.7	5.16 ± 0.05 (6965)	6.29 ± 0.03 (508)	6.12 ± 0.05 (758)	6.22 ± 0.04 (604)

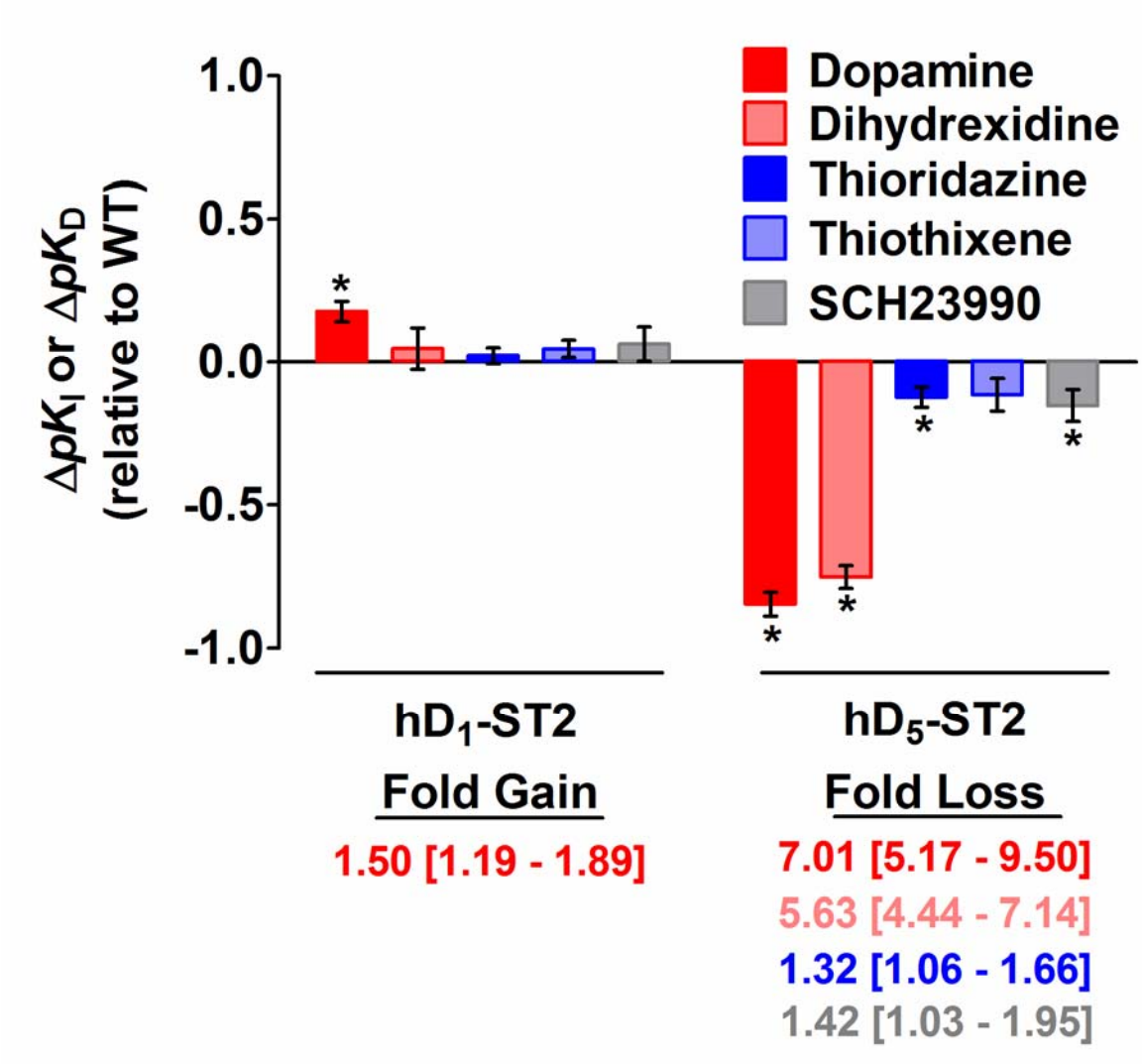

Figure 14. Changes in ligand affinities of ST2 mutant receptors compared to wild-type.
Bars represent the arithmetic mean ± S.E. of differences in calculated pK_D (SCH23390) and pK_I (dopamine, dihydrexidine, thioridazine, and thiothixene) values **(Table 3)** for each ST2 mutant relative to their respective wild-type receptor (hD_1R, left; hD_5R, right). Wild-type receptor value was subtracted from mutant receptor value. Positive ΔpK_D and ΔpK_I values indicate gains in ligand affinities. Negative ΔpK_D and ΔpK_I values indicate losses in ligand affinities. Statistically significant ΔpK_D and ΔpK_I relative to wild-type are further described by their corresponding fold change (using K_D and K_I values), which are reported below with the 95% lower and upper confidence interval. *, $p < 0.05$ when compared with wild-type (value of 0) using one sample *t*-test. WT, wild-type.

1.2 - Constitutive and DA-mediated activation of AC of D_1-class IC2 mutant receptors

At similar B_{max} values, introducing Ser/Thr mutations into IC2 did not alter the constitutive activity of hD_1R. In contrast, these mutations abolished hD_5R constitutive activity to levels of the mock condition **(Figure 15)**. In regards to agonist-dependent G protein coupling properties measured at matched B_{max} values (1-2 pmol/mg protein), there were once again subtype-specific differences. The hD_1-ST2 mutant exhibited an approximately 1.5-fold increase in DA-mediated maximal cAMP response (E_{max}). However, its increased affinity for DA, as previously mentioned, did not induce a statistically significant change in EC_{50} relative to hD_1R. In contrast, the hD_5-ST2 mutant receptor harboured a 15-fold rightward EC_{50} shift (i.e. a decreased potency) for DA with a small but statistically significant reduction in DA efficacy compared to hD_5R **(Figure 16, Table 4)**. This shift underscores its reduced affinity for DA but also suggests a loss in G protein coupling. Because the B_{max} value in our membrane binding assays can account for functional receptors on the surface and inside the cell, ELISA was performed on FLAG-tagged D_1-class and ST2 mutant receptors to assess their cell surface expression **(Figure 17)**. We found at matched B_{max} values—at levels comparable to those expressed in constitutive (basal) activity and dose-response curve (DRC) studies—cell surface expression of ST2 mutant receptors were similar compared to wild-type. Cell surface expression of hD_1-ST2 was found to be statistically higher than hD_1R, but this increase was only 11%. As such, the calculated B_{max} value correlates with cell-surface expression.

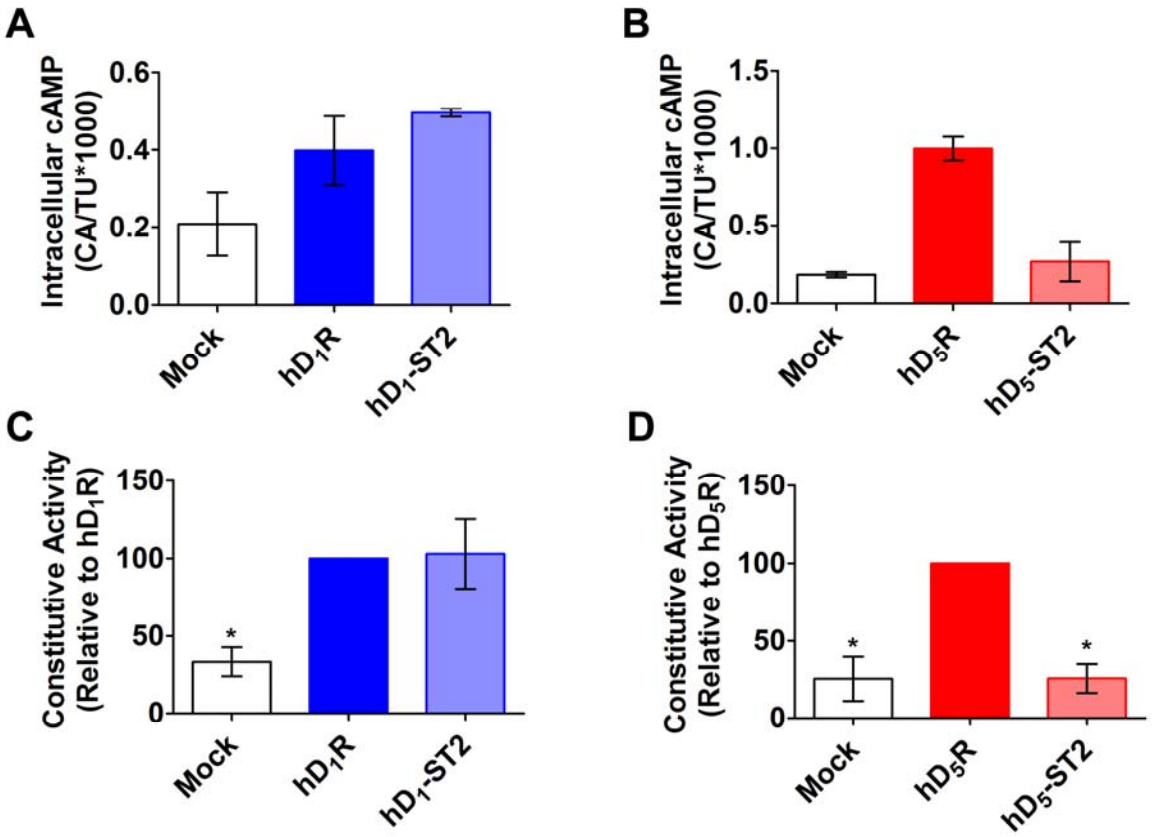

Figure 15. Agonist-independent activation of AC for D_1-class and ST2 mutant receptors.

(A) and (B) An example of raw data (done with triplicates) showing the constitutive activity ± S.E. of wild-type and mutant receptors expressed in [^{3}H]-cAMP formed (CA) over the total amount of [^{3}H]-adenine uptake (TU) x 1000. (C) and (D) Constitutive activity is normalized relative to wild-type. Each bar represents the arithmetic mean ± S.E. of normalized values from three to six experiments. The B_{max} values (pmol/mg of membrane proteins) in arithmetic means ± S.E. were as follows: 2.45 ± 0.24 (hD_1R), 2.57 ± 0.20 (hD_1-ST2), 6.10 ± 0.31 (hD_5R) and 5.17 ± 0.50 (hD_5-ST2). *, $p < 0.05$ when compared with wild-type (100%) using one sample *t*-test.

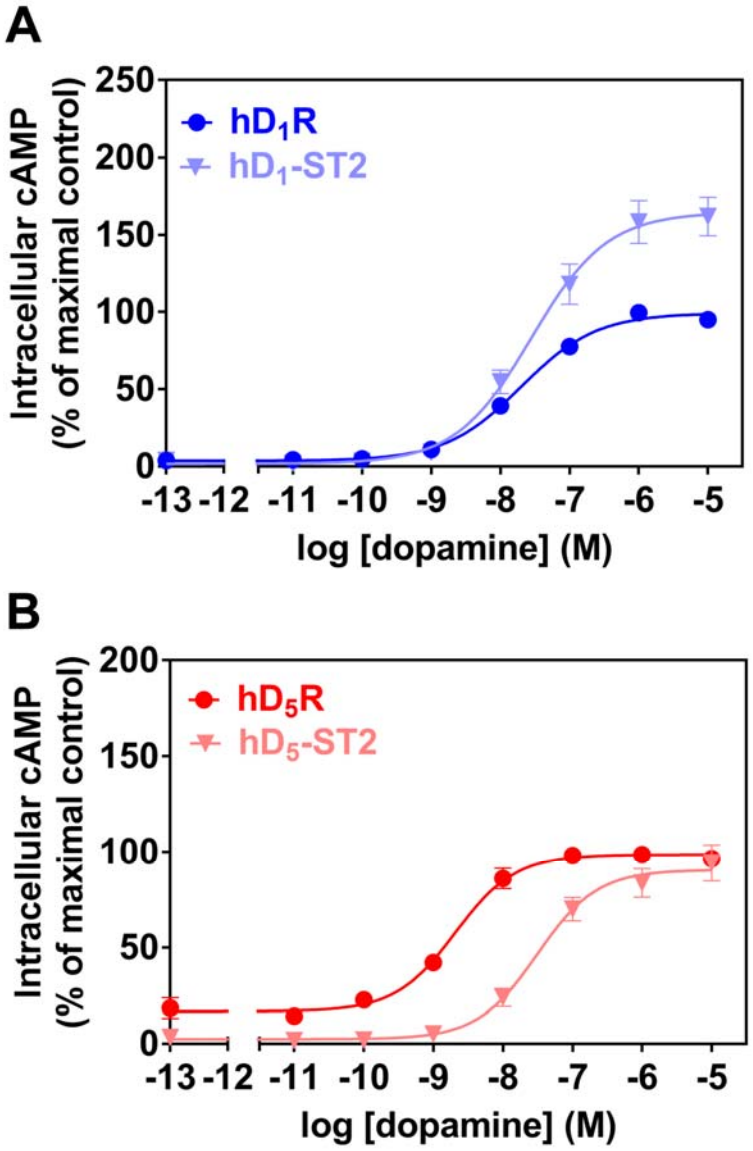

Figure 16. DA-mediated stimulation of AC for D_1-class and ST2 mutant receptors. (A) and (B) Dose-response curves were generated by expressing each point in relation to the best-fitted wild-type E_{max} value (100%) and then plotting them as a function of logarithmic DA concentrations. Each point represents the arithmetic mean ± S.E. from six experiments. B_{max} values (pmol/mg of membrane proteins) in arithmetic means ± S.E. were: 1.34 ± 0.23 (hD_1R), 1.23 ± 0.21 (hD_1-ST2), 1.03 ± 0.29 (hD_5R), and 1.04 ± 0.27 (hD_5-ST2).

Table 4. Best-fitted values of pEC_{50} (negative logarithm of EC_{50} in molar), EC_{50}, and E_{max} from Figure 16.
Statistical comparisons were performed using unconstrained and constrained global nonlinear regression curve fitting approach. *, $p < 0.05$ when compared with wild-type.

Panel	Condition	pEC_{50} ± S.E.	EC_{50} (nM)	E_{max} (%) ± S.E.
A	hD_1R	7.70 ± 0.15	19.8	99.1 ± 4.8
	hD_1-ST2	7.55 ± 0.09	28.1	165 ± 5.5*
B	hD_5R	8.69 ± 0.10	2.06	98.7 ± 2.5
	hD_5-ST2	7.51 ± 0.10*	31.1*	90.7 ± 3.3*

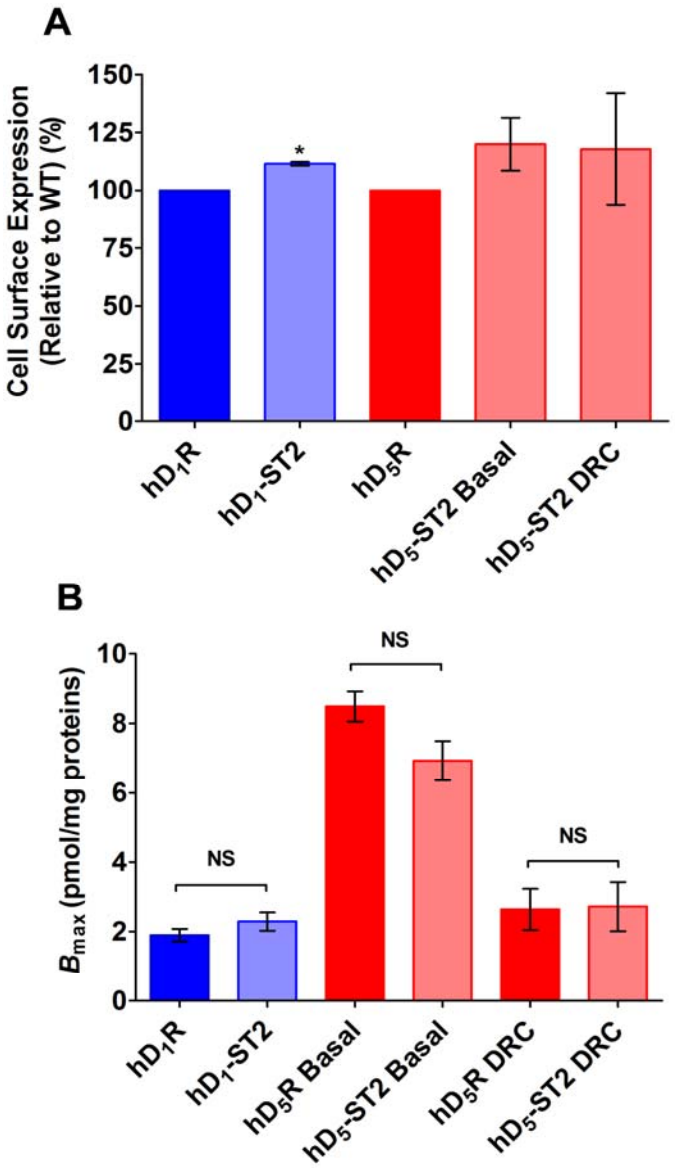

Figure 17. Cell surface values are balanced when receptors are expressed at matched B_{max} values previously reported in cAMP assays (Figures 15 and 16). (A) and (B) Each bar represents the arithmetic mean ± S.E. from four to five experiments. Basal and DRC labels denote cAMP studies measuring basal activity and DA dose-response curves, respectively, to distinguish the different matched B_{max} values used between hD_5R and hD_5-ST2. All receptors used in ELISA and binding assays were FLAG-tagged at their N-termini. (A) Cell surface expression values (%) were determined by dividing ELISA absorbance at 490 nm (subtracted from mock) over that of wild-type (hD_1R or hD_5R). *, $p < 0.05$ when compared with wild-type (100%) using one sample *t*-test (B) Corresponding receptor B_{max} values were determined from radioligand binding assays that were performed concurrently with ELISA in (A). Statistical comparisons of B_{max} were performed using multiple *t*-tests with Holm-Sidak correction method. NS, not significant ($p > 0.05$).

1.3 - Agonist-induced desensitization and internalization of D_1-class IC2 mutant receptors

Previous studies in the lab have demonstrated after 5 mins of DA pre-treatment and following 10 mins stimulation of DA (re-challenge), hD_1R exhibits a rightward shift in EC_{50} and reduction in E_{max} (Jackson *et al.*, 2002). Using the same experimental paradigm, I again observed a reduction in E_{max} (41%) for hD_1R in DA pre-treatment from control (Figure 11a). In addition, hD_5R demonstrated a 74% reduction in E_{max} relative to control and therefore indicated a stronger ability to desensitize in the presence of DA compared to hD_1R **(Figure 18A)**. On the other hand, DA-induced desensitization was almost abrogated in the hD_1-ST2 and significantly impaired in hD_5-ST2 **(Figure 18A)**. I also employed ELISA to measure differences in receptor cell surface expression between with and without DA treatment conditions as means to evaluate agonist-induced internalization. For both ST2 mutant receptors, the extent of internalization following 5 mins stimulation with DA was not found to be statistically different from those of their parent receptors **(Figure 18B)**.

1.4 - MD simulations of D_1-class and IC2 mutant receptors

To predict the structural positions of Ser/Thr of IC2 and IC2/TM3 membrane juncture, homology models of D_1-class and ST2 mutant receptors were created using only templates of crystallized GPCRs in their inactive states. DA was then docked onto these homology models, followed by simulation in membrane for 10 ns (see **Figure 19** for docked poses before simulation). Root-mean-square deviation (RMSD) trajectories for hD_1R, hD_1-ST2, and hD_5-ST2 eventually plateaued, and RMSD trajectory for hD_5R in

time began to slowly increase at a very slow rate. This indicated that an equilibrium (i.e. conformational stability) had been reached for all models (**Figure 20**).

Figure 21 shows the predicted positions of $Ser^{3.47}$, $Ser^{3.55}$, and $Thr^{3.65}$ that are well-conserved among D_1-class and biogenic amine receptors. Ser3.47 is located at the IC2/TM3 membrane juncture with its carbonyl backbone below the membrane (not shown) and its hydroxyl side-chain above the membrane **(Figure 21A, 21C)**. Throughout the simulations with both hD_1R and hD_5R, the hydroxyl side-chain of $Ser^{3.47}$ consistently hydrogen bonded with the carbonyl backbone of $Leu^{3.43}$. Furthermore, $Ser^{3.55}$ and $Thr^{3.65}$ are located at the ends of cytoplasmic extensions of TM3 and TM4, respectively, and therefore mark the beginning and finish of the loop region of IC2. For D_1-class receptors, the hydroxyl side-chain of $Ser^{3.55}$ consistently interacted with the carbonyl backbone of $Tyr^{3.51}$. Also, the hydroxyl side-chain of $Thr^{3.65}$ consistently interacted with the amide backbone of $Ala/Met^{3.68}$ **(Figure 21A, 21C)**. These hydrogen bonds were not possible in hD_1-ST2 and hD5-ST2 models due to the hydrophobic side-chains of $Ala^{3.47}$, $Ala^{3.55}$, and $Val^{3.65}$ **(Figure 21B, 21D)**. Furthermore, the isopropyl side-chain of $Val^{3.65}$ in hD_1-ST2 moved closer to central IC2, and this subsequently allowed its amide backbone to form new hydrogen bonds with carbonyl backbone of $Lys^{3.63}$, which did not occur in hD_1R during simulation **(Figure 21B, 21D)**.

As mentioned previously, hD_1R possesses an additional $Ser^{3.56}$ that is not conserved among biogenic amine receptors. During simulation of hD_1R, the hydroxyl side-chain of $Ser^{3.56}$ sampled interactions with nearby residues, but did not consistently form any stable interactions **(Figure 22)**. Therefore, unlike the other Ser/Thr of IC2, the hydroxyl side-chain of $Ser^{3.56}$ may not have any structural roles within the receptor.

Interestingly, in hD_5R where $Ser^{3.56}$ is replaced with arginine, the longer side-chain of $Arg^{3.56}$ allowed it to consistently hydrogen bond with the hydroxyl side-chain of $Ser^{3.55}$. In the hD_5-ST2, this interaction was not possible, and the side-chain of $Arg^{3.56}$ did not form any interactions with any residues during the simulation **(Figure 22)**.

Although 10 ns of simulation may be too short to provide any reliable indications as to how IC2 Ser/Thr mutations structurally impact IC2, distinct IC2 loop changes between wild-type and ST2 mutant receptors were observed during this simulation period. The time-averaged structures of hD_1R and hD_5R both showed an outward movement of IC2 loop relative to their starting models **(Figure 23)**. In contrast, outward movement of IC2 loop was entirely absent among time-averaged structures of ST2 mutant receptors. The IC2 loop of hD_1-ST2 remained mostly static, while the IC2 loop of hD_5-ST2 demonstrated a lateral shift towards TM4 when compared to their initial positions **(Figure 23)**.

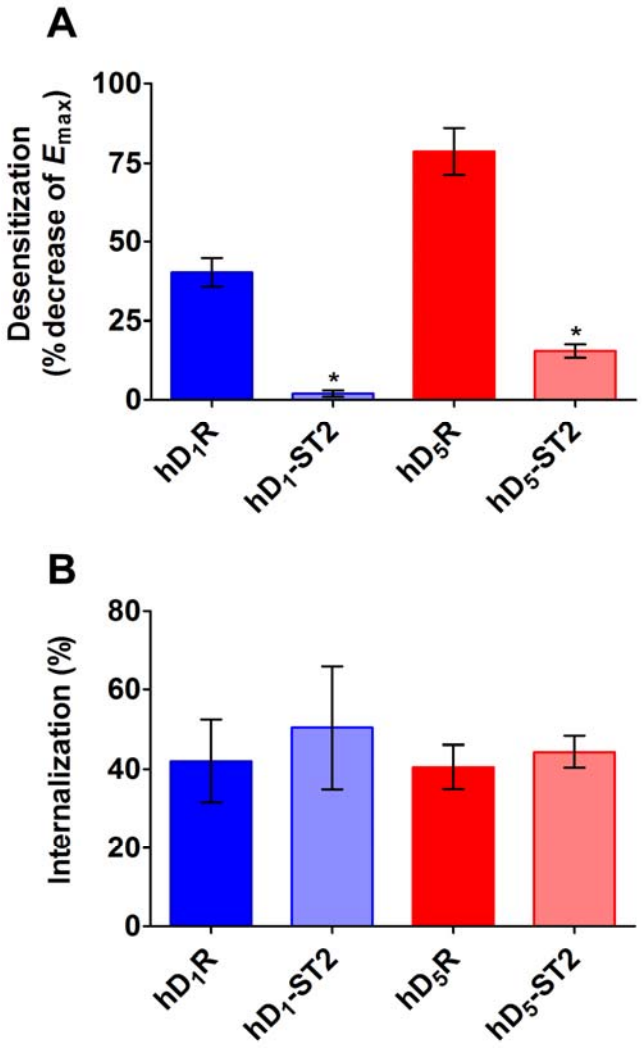

Figure 18. Agonist-induced desensitization and internalization of D_1-class and ST2 mutant receptors.

(A) Transfected cells were pre-treated with either 0.1 mM AA or 10 μM DA for 5 mins, washed twice with PBS, and then re-challenged with 10 μM DA for 10 mins. Desensitizing responses represent the % decrease in E_{max} of DA pre-treatment condition from the AA pre-treatment condition. Each bar represents the arithmetic mean ± S.E. from four to five experiments. B_{max} values (pmol/mg of membrane proteins) in arithmetic means ± S.E. were: 3.48 ± 0.66 (hD_1R), 3.63 ± 0.76 (hD_1-ST2), 2.80 ± 0.32 (hD_5R), and 1.97 ± 0.41 (hD_5-ST2). (B) Internalization was assessed by the % decrease in cell surface expression following 5 mins treatment with 10 μM DA relative to that of AA (vehicle). All receptors used in internalization assay were FLAG-tagged at their N-termini. Each bar represents the arithmetic mean ± S.E. from four experiments. No statistically detectable differences were observed between wild-type and mutant receptors. B_{max} values (pmol/mg of membrane proteins) in arithmetic means ± S.E. were: 0.95 ± 0.19 (hD_1R), 2.80 ± 1.4 (hD_1-ST2), 1.08 ± 0.38 (hD_5R), and 1.01 ± 0.30 (hD_5-ST2). *, $p <$ 0.05 when compared with wild-type using unpaired two-tailed *t*-test.

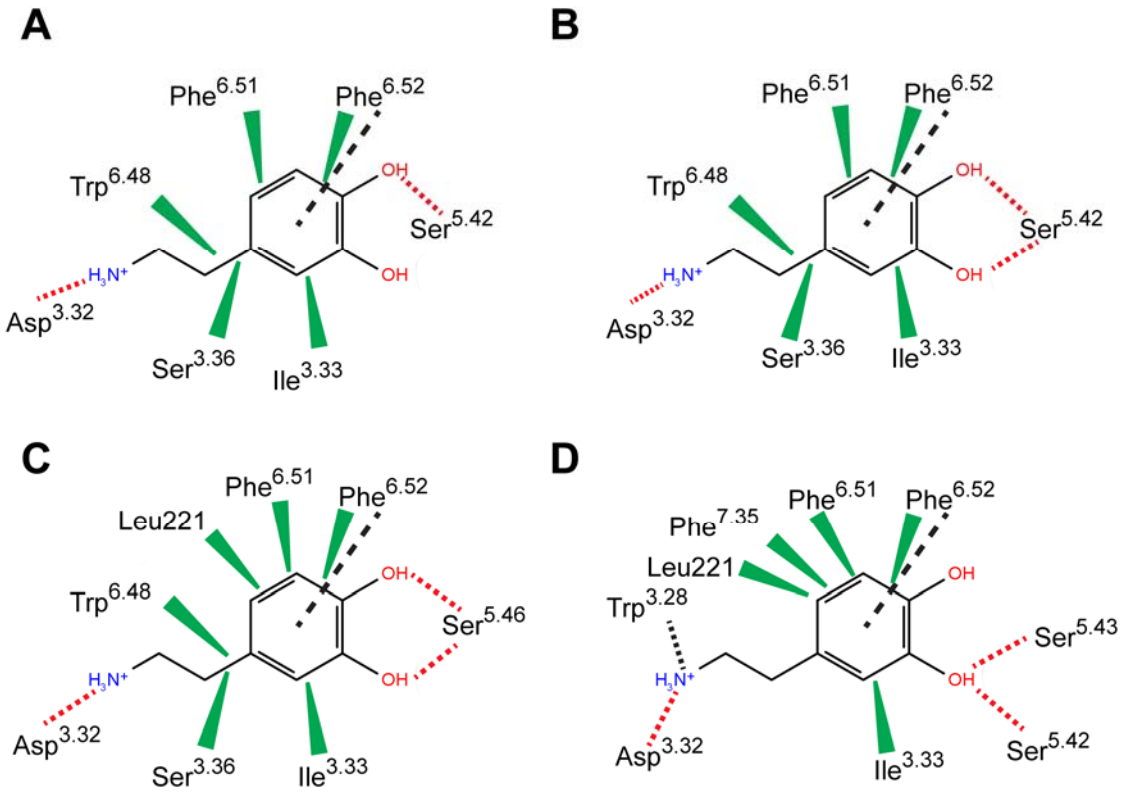

Figure 19. DA docking poses prior to simulation for homology models of D_1-class and ST2 mutant receptors.
(A) hD_1R (B) hD_1-ST2 (C) hD_5R (D) hD_5-ST2. Red dashed lines represent hydrogen bonds. Black dashed lines represent either π-π or cation-π interactions. Green rays represent hydrophobic interactions. In agreement with previous mutagenesis and ligand docking studies of D_1R, DA docks to all four receptors using its catechol moiety to hydrogen bond to either $Ser^{5.42}$ or $^{5.46}$ and its amine group to interact with $Asp^{3.32}$ (Malo *et al.*, 2012, Mente *et al.*, 2015, Pollock *et al.*, 1992). Previous studies have also predicted π-π stacking between $Phe^{6.52}$ and the aromatic ring of DA (Cho *et al.*, 1995, Malo *et al.*, 2012).

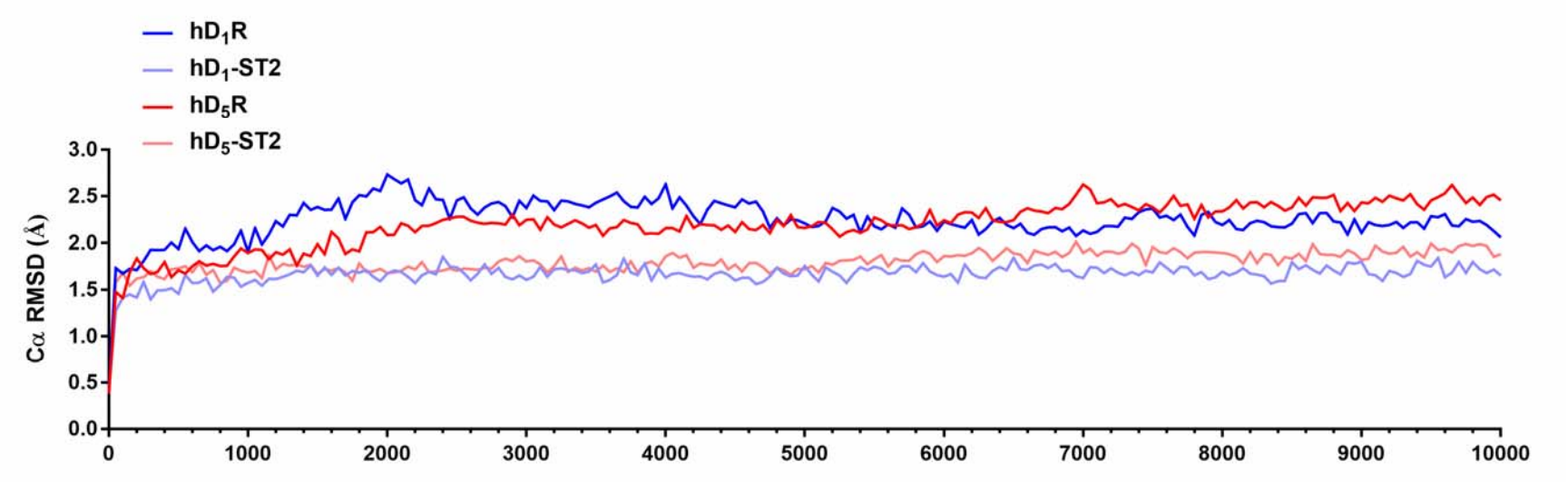

Figure 20. RMSD trajectories of alpha carbons for D_1-class and ST2 mutant receptors from their corresponding starting conformations.

Toward the second half of simulation, the RMSD trajectories of hD_1R, hD_1-ST2, and hD_5-ST2 plateaued, and the RMSD trajectories of hD_5R increased at a very slow pace. In all, this implies that an equilibrium had been reached. The trajectories did not produce large spikings indicating that the simulations were stable.

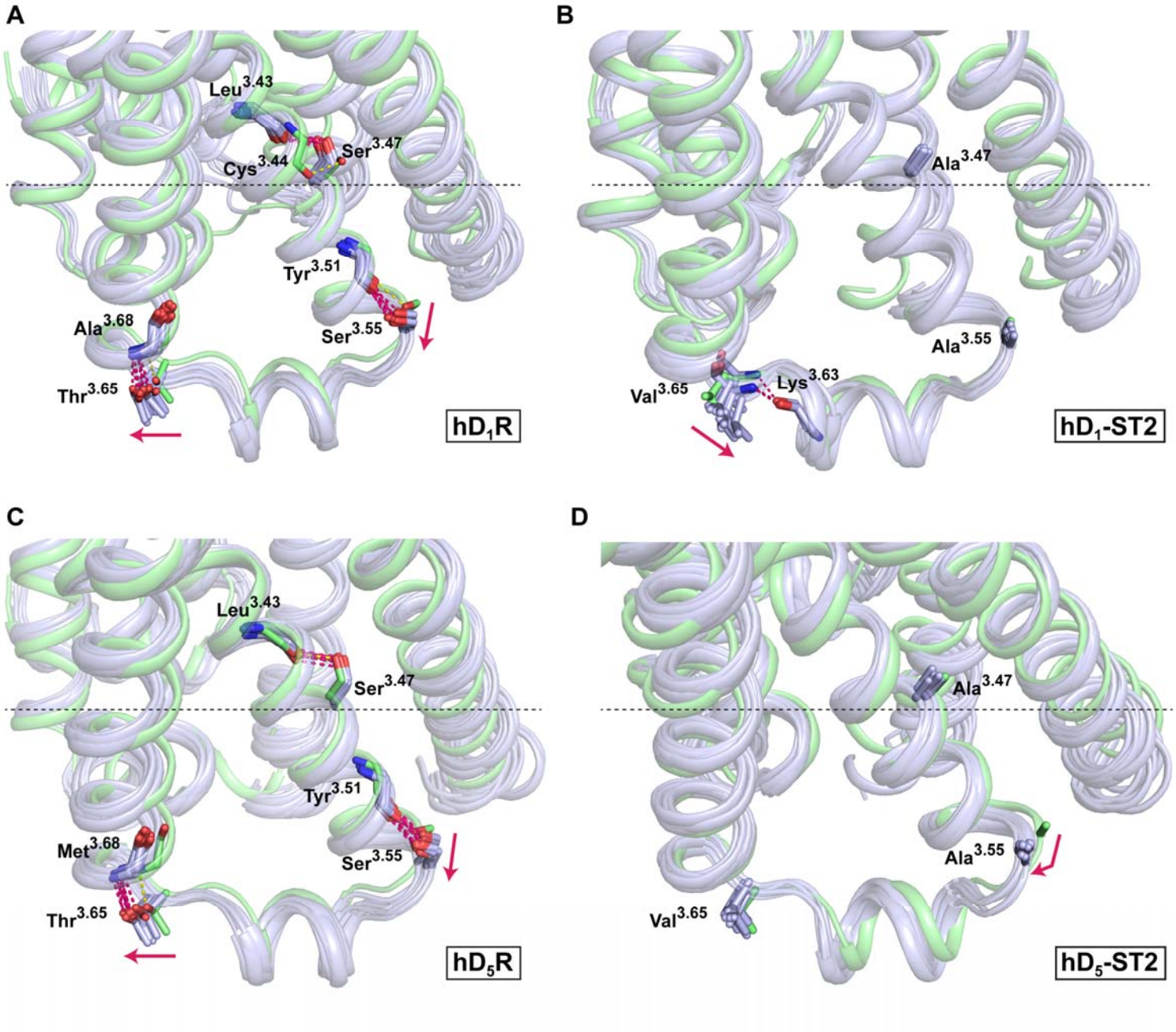
A
Leu3.43
Cys3.44
Ser3.47
Tyr3.51
Ala3.68
Ser3.55
Thr3.65
hD1R
B
Ala3.47
Ala3.55
Val3.65
Lys3.63
hD1-ST2
C
Leu3.43
Ser3.47
Tyr3.51
Met3.68
Ser3.55
Thr3.65
hD5R
D
Ala3.47
Ala3.55
Val3.65
hD5-ST2

Figure 21. Comparing the positioning of $Ser^{3.47}$, $Ser^{3.55}$, and $Thr^{3.65}$ of D_1-class receptors with $Ala^{3.47}$, $Ala^{3.55}$, and $Val^{3.65}$ of ST2 mutant receptors.
Green cartoons/sticks represent receptors before simulation. Grey cartoons/sticks represent simulation snapshots during every ns within the 10 ns simulation time frame. For ease of viewing and unless stated otherwise, only the side-chains of $Ser^{3.47}$, $Ser^{3.55}$, and $Thr^{3.65}$ are shown for D_1-class receptors; and only the side-chains of $Ala^{3.47}$, $Ala^{3.55}$, and $Val^{3.65}$ are shown for ST2 mutant receptors. Similarly, only the peptide backbone (amide and carbonyl groups) are shown for residues that hydrogen bonded with the aforementioned Ser/Thr/Ala/Val residues because their side-chains did not. Yellow and red dashed lines represent hydrogen bonds before and during simulation, respectively. Black dashed lines represent membrane boundaries predicted from Orientation of Proteins in Membranes (Lomize *et al.*, 2012). (A) Prior to simulation, the hydroxyl side-chain of $Ser^{3.47}$ hydrogen bonded with the carbonyl backbone of $Cys^{3.44}$. This was energetically unfavourable during simulation, as $Ser^{3.47}$ quickly switched to the carbonyl backbone of $Leu^{3.43}$ and remained there for the entire time. Arrows indicate the outward movement of the side-chain of $Ser^{3.55}$ and the lateral movement of the side-chain of $Thr^{3.65}$ during stimulation. $Ser^{3.55}$ and $Thr^{3.65}$ consistently hydrogen bonded with $Tyr^{3.51}$ and $Ala^{3.68}$, respectively. (B) In hD_1-ST2, the side-chain of $Val^{3.65}$ shifted towards central IC2 upon simulation. The amide backbone of $Val^{3.65}$ is shown because it hydrogen bonded with the carbonyl backbone of $Lys^{3.63}$ in some simulation snapshots. (C) In hD_5R, the side-chain of $Ser^{3.55}$ moved outward, and the side-chain of $Thr^{3.65}$ moved laterally. Hydrogen bonds were still maintained with $Tyr^{3.51}$ and $Met^{3.68}$. $Ser^{3.47}$ consistently hydrogen bonded with $Leu^{3.43}$. (D) In hD_5-ST2, the side-chain of $Val^{3.65}$ remained clustered around its initial position, and the side-chain of $Ala^{3.55}$ moved inward towards central IC2 upon simulation.

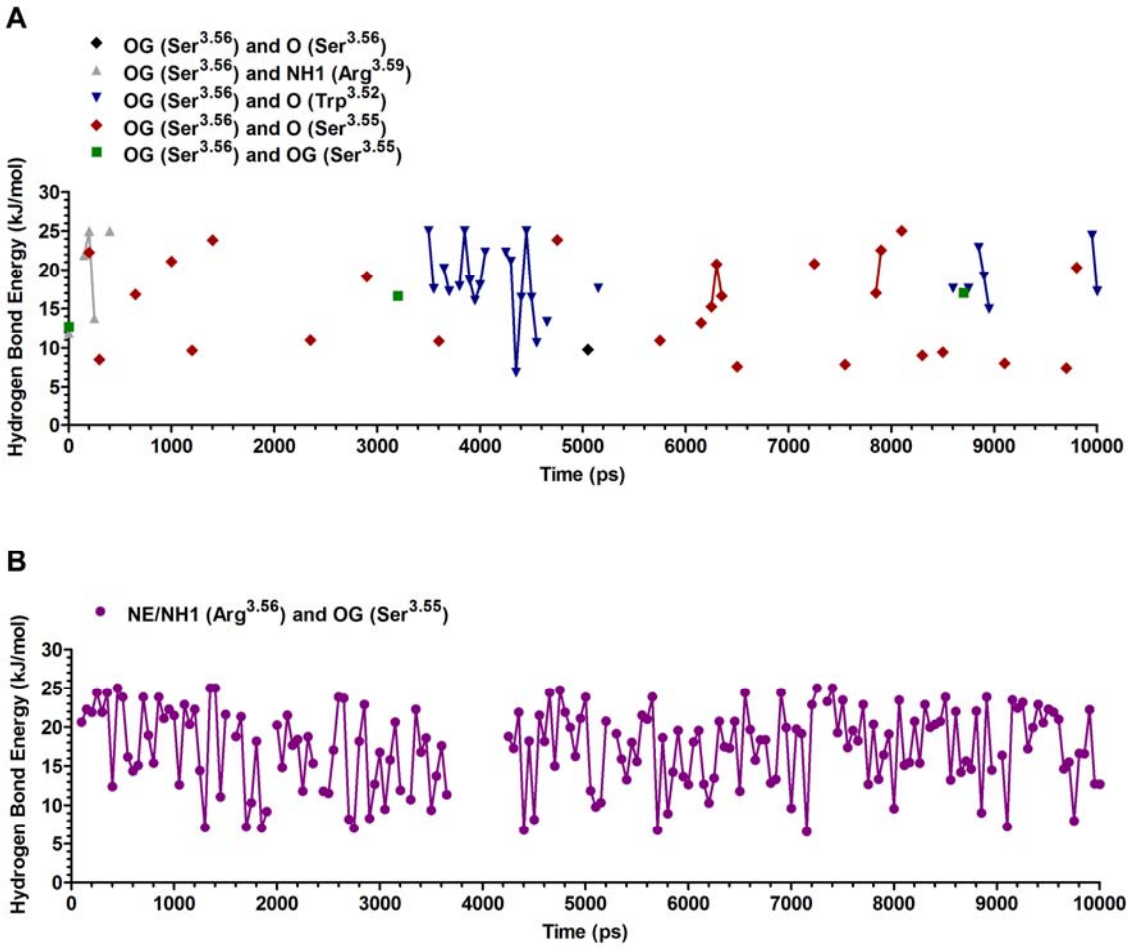

Figure 22. The hydroxyl side-chain of Ser$^{3.56}$ in hD$_1$R does not form any consistent hydrogen bonds during simulation (A), unlike the side-chain of Arg$^{3.56}$ in hD$_5$R (B). Lines between points represent consecutive hydrogen bonds. OG, O, NE/NH1 refers to the hydroxyl side-chain of Ser, the carbonyl oxygen in the peptide backbone, and the guanidinium side-chain of Arg, respectively.

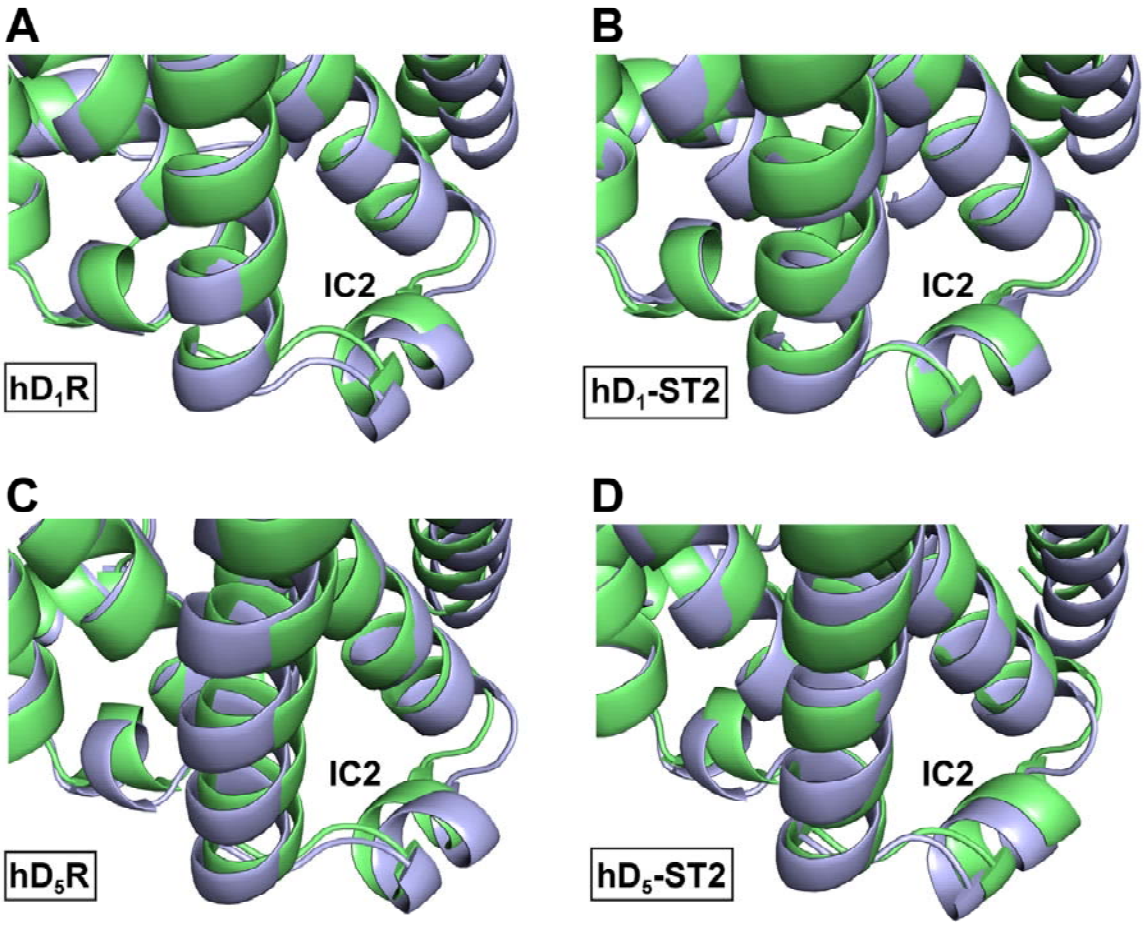

Figure 23. Simulations show IC2 loop for hD_1R and hD_5R move outward but not for hD_1-ST2 and hD_5-ST2.
DA-docked D_1-class and ST2 mutant receptors before (in green) and after simulation (averaged, in grey) for (A) hD_1R (B) hD_1-ST2 (C) hD_5R (D) hD_5-ST2.

After collectively examining the functional roles of Ser/Thr of IC2 and IC2/TM3 membrane juncture, I then employed the same holistic approach for Ser/Thr of IC1 and IC1/TM2 membrane juncture. I probed for any functional changes of ST1 mutant receptors among D_1-class receptors using pharmacological assays previously performed on ST2 mutant receptor.

1.5 - Binding properties of D_1-class IC1 mutant receptors

Saturation studies showed the K_D values for [^{3}H]-SCH23390 of both ST1 mutant receptors remained statistically unchanged compared to wild-type. However, the B_{max} value was greatly lowered in hD_1-ST1 (85% decrease) and hD_5-ST2 (95% decrease) relative to hD_1R and hD_5R, respectively **(Table 5)**. In competition studies, the hD_1-ST1 exhibited an approximately 2-fold loss in DA affinity, while the hD_5-ST1 demonstrated about 4-fold losses in affinity for both DA and DHX **(Table 5, Figure 24)**. Binding changes towards thioridazine and thiothixene were minor for both ST1 mutant receptors compared to wild-type, with only thiothixene showing a statistically gain in affinity for hD_1-ST1.

1.6 - Western blot and ELISA analysis of D_1-class IC1 mutant receptors

To investigate further the low B_{max} of ST1 mutant receptors, immunoblots and ELISA (both using 5 μg of receptor DNA as in saturation studies) were performed to assess receptor protein expression and cell surface localization. The immunoblot profile of hD_1R **(Figure 25A)** displayed a broad and prominent band (~75-85 kDa), which could represent glycosylated forms of hD_1R (theoretical mass of hD_1R is 49 kDa). Similar band

sizes have been previously been found in HEK293 cells and rat striatum (Sedaghat & Tiberi, 2011) and has also been demonstrated using *N*-glycosidase in membranes of the monkey caudate to be glycosylated D_1R (Bergson *et al.*, 1995b). The hD_1-ST1 condition showed diminished intensity of this 75-85 kDa band, concomitant with a diminished cell-surface expression (59% decrease relative to hD_1R) **(Figure 25A, 25C)**. Furthermore, under brief exposure periods, an approximately 65 kDa band found in the hD_1R condition was absent in the hD_1-ST1 condition **(Figure 25A)**. Immunoblots of hD_5R produced broad and prominent stainings (~60-65 kDa) that was higher than its theoretical mass (53 kDa) and may indicate glycosylated species of hD_5R. In contrast, the hD_5-ST1 condition displayed reductions of such band sizes, in conjuncture with a reduced cell surface expression (54% decrease relative to hD_5R) (**Figure 25B, 25D)**. Both conditions displayed an approximately 130 kDa band, which could represent SDS-resistant dimeric forms. Higher molecular weights (>100 kDa) of D_5R have been previously identified in membranes from rat and monkey brains (Bergson *et al.*, 1995a, Ciliax *et al.*, 2000). Because the hD_5-ST1 exhibited reduced cell-surface expressions in ELISA assays, it is possible for the 130 kDa molecular species of hD_5-ST1 to be localized differently (e.g. more 130 kDa forms of hD_5-ST1 inside the cell) compared to hD_5R.

1.7 - Constitutive and DA-mediated activation of AC of D_1-class IC1 mutant receptors

At matched B_{max} values between wild-type and corresponding ST1 mutant receptor, mutating all Ser/Thr residues of IC1 and IC1/TM2 membrane juncture abolished the constitutive activity of hD_1R and hD_5R to levels of the mock condition **(Figure 26A, 26B)**. Furthermore, using matched B_{max} conditions, the hD_1-ST1 and hD_5-

ST1, relative to wild-type, exhibited a 260-fold and 56-fold change in DA potency, respectively **(Figure 26C, 26D, Table 6).** Such drastic changes in DA potency cannot be solely described by the 2-4 fold losses of DA affinity experienced by both ST1 mutant receptors, but instead suggest losses in agonist-induced G protein coupling. Intriguingly, despite losing DA potency, both ST1 mutant receptors displayed an elevated E_{max} that was over 2-fold higher compared to parent receptors.

Summary

Results in this section demonstrate that Ser/Thr spanning IC1 and IC2 play important functional roles among D_1-class receptors. Subtype-specific changes to agonist binding and cAMP signalling were observed among hD_1-ST2 and hD_5-ST2 suggesting that Ser/Thr of IC2 and IC2/TM3 membrane juncture are further structural determinants underlying the unique pharmacological profiles of D_1-class receptors. Moreover, these residues can contribute towards agonist-induced desensitization of D_1-class receptors. In regards to the IC1 and IC1/TM2 membrane juncture, mutating Ser/Thr in this region for both hD_1R and hD_5R brought upon similar functional changes, which included diminished DA affinity, loss of basal activity, drastic reductions in DA potency, and interestingly, an over 2-fold elevation in E_{max} despite at lower B_{max} and cell surface levels relative to wild-type. It should be noted that the degree of some of these changes (e.g. decreased DA potency) relative to wild-type were different between the ST1 mutant receptors.

For the rest of my PhD thesis, I have decided to focus on the importance of Ser/Thr spanning IC1, because given the ST1 phenotype is shared among D_1-class

receptors, my screening study may have identified conserved functional and structural motifs among Family A GPCRs. Specifically, I have devoted my efforts in understanding the roles of Ser/Thr of IC1 and IC1/TM2 membrane juncture for hD_1R. In the following section, I examine individually the roles of these residues for hD_1R—two of which (Thr59 and Ser65) are conserved among many Family A GPCRs and another (Ser56) unique to hD_1R.

Table 5. Dissociation constants (K_D, K_I) and B_{max} values of [^{3}H]-SCH23390 for wild-type and ST1 mutant receptors.
pK_D and pK_I (negative logarithm of K_D and K_I in molar) are expressed as arithmetic means ± S.E. with the corresponding K_I and K_D (nM) shown in brackets. Taken from (Zhang *et al.*, 2015). See **Figure 24** for statistical comparisons of dissociation constants.

	Saturation Curves		**Competition Curves**			
	[^{3}H]-SCH23390 (n = 6-8)		Dopamine (n = 5-6)	Dihydrexidine (n = 6-8)	Thioridazine (n = 4-5)	Thiothixene (n = 4-5)
	pK_D (K_D, nM)	B_{max} (pmol/mg)	pK_I (K_I, nM)			
hD_1R	9.35 ± 0.03 (0.45)	8.14 ± 0.90	5.09 ± 0.05 (8214)	6.27 ± 0.05 (544)	7.04 ± 0.03 (91.4)	7.17 ± 0.01 (68.2)
hD_1-ST1	9.46 ± 0.07 (0.35)	1.22 ± 0.10	4.73 ± 0.04 (18490)	6.30 ± 0.08 (506)	7.15 ± 0.08 (71.0)	7.39 ± 0.05 (41.1)
hD_5R	9.15 ± 0.05 (0.71)	16.2 ± 2.0	6.02 ± 0.03 (966)	7.08 ± 0.04 (83.5)	6.17 ± 0.02 (674)	6.24 ± 0.01 (576)
hD_5-ST1	9.11 ± 0.08 (0.77)	0.79 ± 0.12	5.45 ± 0.07 (3557)	6.53 ± 0.09 (294)	6.06 ± 0.10 (866)	6.19 ± 0.04 (649)

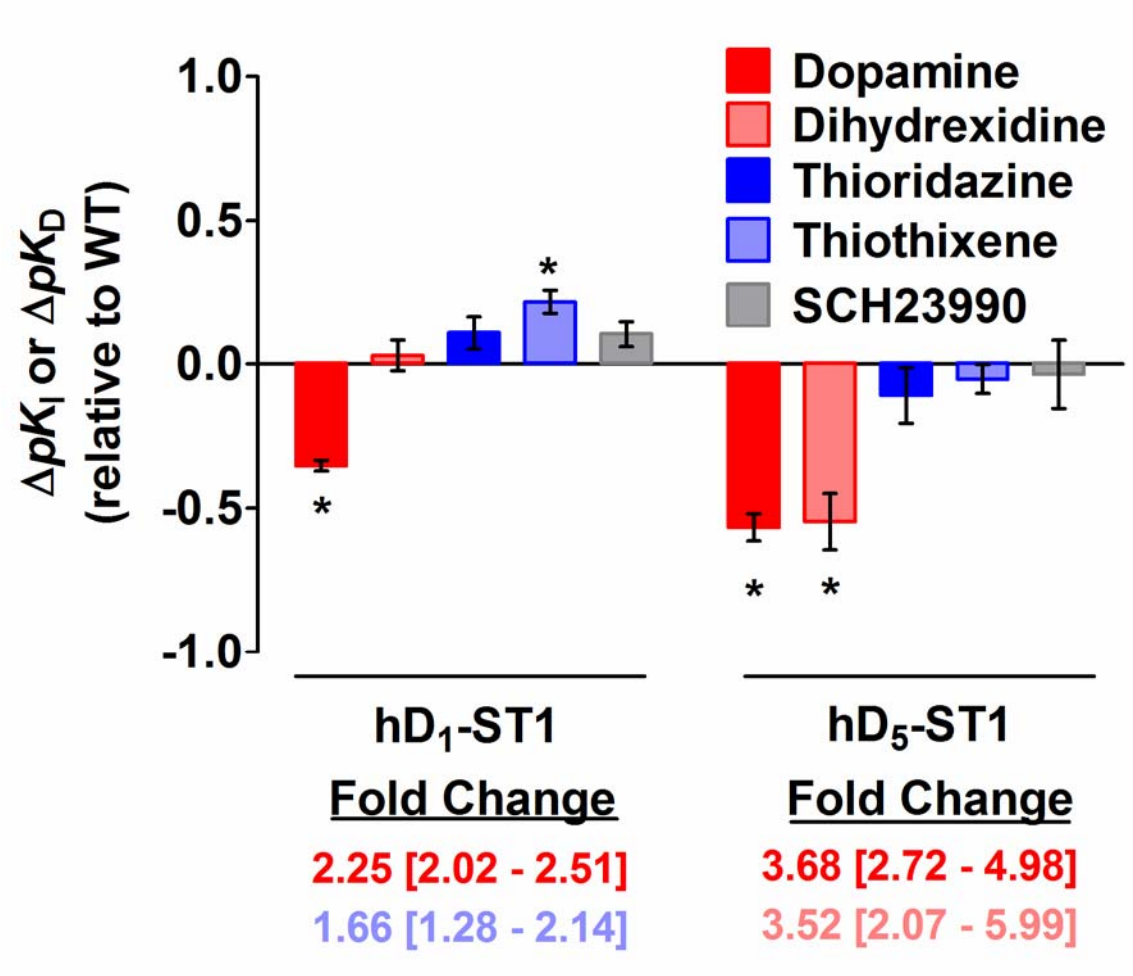

Figure 24. Changes in ligand affinities of ST1 mutant receptors compared to wild-type.
Bars represent the arithmetic mean ± S.E. of differences in calculated pK_D (SCH23390) and pK_I (dopamine, dihydrexidine, thioridazine, and thiothixene) values **(Table 5)** for each ST1 mutant relative to their respective wild-type receptor (hD_1R, left; hD_5R, right). Wild-type receptor value was subtracted from mutant receptor value. Positive ΔpK_D and ΔpK_I values indicate gains in ligand affinities. Negative ΔpK_D and ΔpK_I values indicate losses in ligand affinities. Statistically significant ΔpK_D and ΔpK_I relative to wild-type are further described by their corresponding fold change (using K_D and K_I values), which are reported below with the 95% lower and upper confidence interval. *, $p < 0.05$ when compared with wild-type (value of 0) using one sample *t*-test. WT, wild-type.

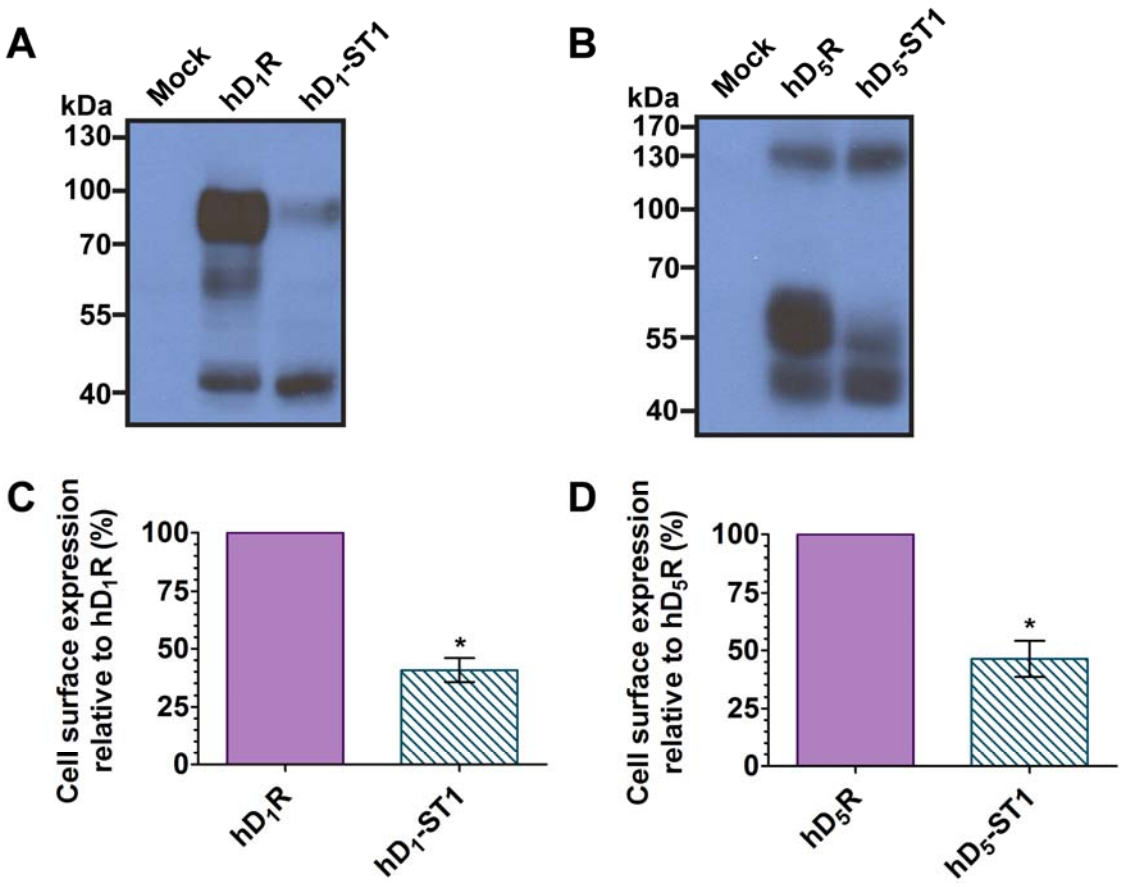

Figure 25. Changes to receptor expressions for ST1 mutant receptors compared to wild-type.

(A) and (B) Representative Western blots for mock and receptor conditions. B_{max} values (pmol/mg of membrane proteins) for representative Western blots were: 15.2 (hD_1R), 1.59 (hD_1-ST1), 16.1 (hD_5R), and 0.293 (hD_5-ST1). Western blots were repeated four times using 40 µg of total proteins for each condition. (C) and (D) Cell surface expression values (%) were determined by normalizing ELISA absorbance at 490 nm (subtracted from mock) over that of corresponding wild-type. All receptors used in ELISA were HA-tagged at their N-termini. Each bar represents the arithmetic mean ± S.E. from four experiments. B_{max} values (pmol/mg of membrane proteins) in arithmetic means ± S.E. were: 10.6 ± 0.32 (hD_1R), 1.28 ± 0.10 (hD_1-ST1), 14.6 ± 1.5 (hD_5R), and 0.24 ± 0.02 (hD_5-ST1). *, $p < 0.05$ when compared with wild-type (100%) using one sample *t*-test. Figure was taken from (Zhang *et al.*, 2015).

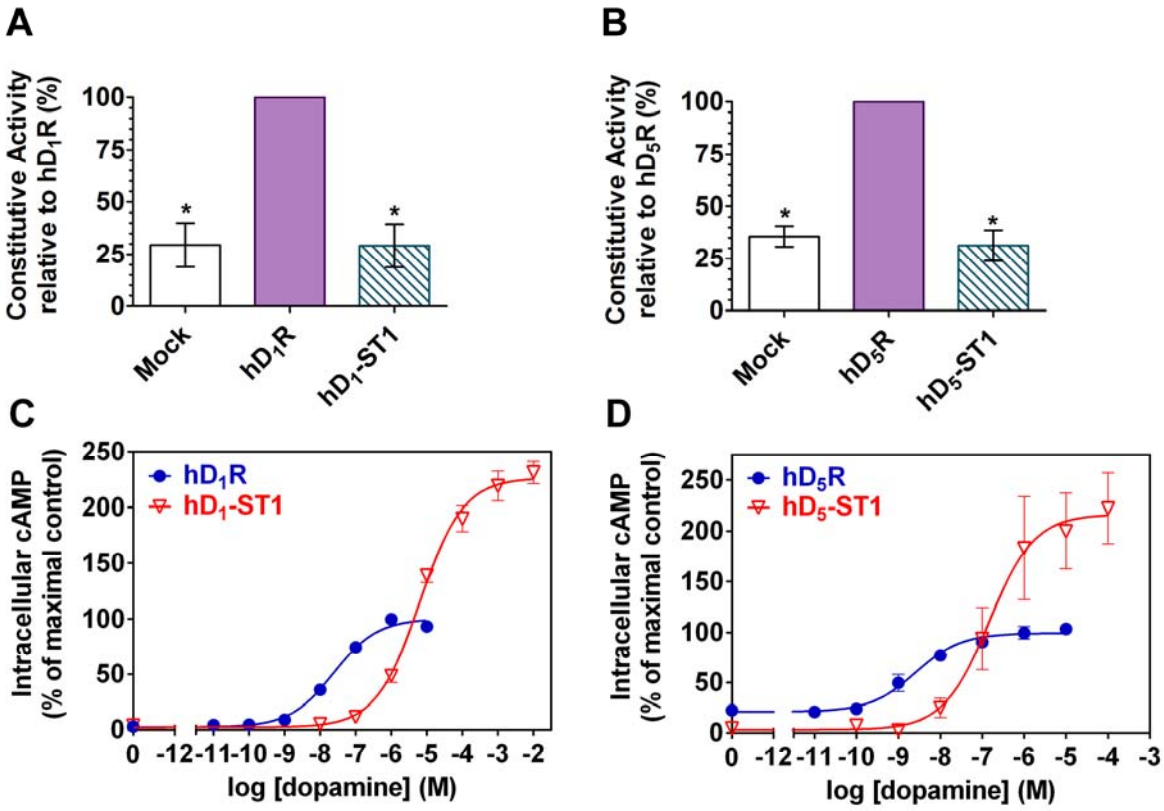

Figure 26. Agonist-independent and agonist-dependent activation of AC for D_1-class and ST1 mutant receptors.
(A) and (B) Constitutive activity (CA/TU × 1000) is normalized relative to wild-type. Each bar represents the arithmetic mean ± S.E. of normalized values from three to five experiments. The B_{max} values (pmol/mg of membrane proteins) in arithmetic means ± S.E. were as follows: 2.30 ± 0.24 (hD_1R), 1.77 ± 0.38 (hD_1-ST1), 0.40 ± 0.13 (hD_5R) and 0.37 ± 0.10 (hD_5-ST1). *, $p < 0.05$ when compared with wild-type (100%) using one sample *t*-test. (C) and (D) Each point represents the arithmetic mean ± S.E. (relative to best-fitted wild-type E_{max} value (100%)) from four to five experiments. B_{max} values (pmol/mg of membrane proteins) in arithmetic means ± S.E. were: 1.14 ± 0.15 (hD_1R), 1.05 ± 0.039 (hD_1-ST1), 0.27 ± 0.06 (hD_5R), and 0.23 ± 0.04 (hD_5-ST1). Figure was taken from (Zhang *et al.*, 2015).

Table 6. Best-fitted values of pEC_{50} (negative logarithm of EC_{50} in molar), EC_{50}, and E_{max} from Figure 26.
Statistical comparisons were performed using unconstrained and constrained global nonlinear regression curve fitting approach. *, $p < 0.05$ when compared with wild-type.

Panel	Condition	pEC_{50} ± S.E.	EC_{50} (nM)	E_{max} (%) ± S.E.
C	hD_1R	7.62 ± 0.16	23.9	100 ± 4.8
	hD_1-ST1	5.21 ± 0.07*	6216*	227 ± 4.6*
D	hD_5R	8.59 ± 0.56	2.58	99.3 ± 11.6
	hD_5-ST1	6.84 ± 0.21*	144*	217 ± 15.9*

2. Dissecting the hD_1-ST1

2.1 - Mutations at Thr59$^{2.39}$ and Ser65$^{2.45}$ dictate binding properties of hD_1-ST1

To pinpoint the specific residues that contribute towards the receptor properties of hD_1-ST1, three point mutants, hD_1-S56A, hD_1-T59V, and hD_1-S65A, were constructed and characterized. All three point mutants retained high affinities for [^{3}H]-SCH23390 as hD_1-ST1 and hD_1R. In addition, the hD_1-S56A mutant presented similar B_{max} and binding affinities for DA and DHX relative to hD_1R **(Table 7, Figure 27)**. This coincides with a previous study that showed mutating Ser56 to Leu56 in hD_1R (expressed in Chinese Hamster Ovarian (CHO) cells) did not alter ligand binding or G protein coupling (Jin *et al.*, 1998). Unexpectedly, underlying the 2-fold decrease in DA affinity of hD_1-ST1 was an interplay of opposing influences imposed by T59V and S65A mutations. Whereas the hD_1-T59V displayed a 5-fold and 2-fold decrease in affinity for DA and DHX, respectively, the hD_1-S65A mutant exhibited a 4-fold increase in affinity for both agonists **(Table 7, Figure 27)**. The S65A mutation lowered the B_{max} of hD_1R to an even greater extent previously reported with the triple mutant receptor. The T59V mutation once again played an opposing role in shaping the B_{max} of hD_1-ST1 because its B_{max} was 1.5-fold greater than hD_1R **(Table 7)**.

2.2 - Ser65$^{2.45}$ controls hD_1R expression

Using the transfection receptor conditions leading to highest achievable B_{max} (**Table 7**), immunostaining of whole cell lysates revealed the prominent bands within 75-85 kDa in hD_1-S56A and hD_1-T59V that were previously observed with hD_1R **(Figure 28A)**. In contrast, this particular band was only detectable for hD_1-S65A if the total

amount of protein loaded was increased to 90 µg from the original 40 µg designated for all receptor conditions. Another distinguishing feature of the hD_1-S65A immunoblot profile was increased immunostaining below 55 kDa, which could possibly signify elevated amounts of unglycosylated receptors compared to wild-type **(Figure 28A)**. At similar high B_{max} values as hD_1R, the hD_1-S56A and hD_1-T59V both showed cell surface expression levels that were statistically unchanged from hD_1R. The hD_1-ST1 and hD_1-S65A exhibited 60% and 79% decrease in cell surface levels from hD_1R, respectively **(Figure 28B)**. This was associated with their decreased B_{max} values (1.3 pmol/mg protein for hD_1-ST1 and 0.36 pmol/mg protein for hD_1-S65A).

Table 7. Dissociation constants (K_D, K_I) and B_{max} values of [^{3}H]-SCH23390 for hD$_1$R, hD$_1$-ST1, and single point mutant receptors.

pK_D and pK_I (negative logarithm of K_D and K_I in molar) are expressed as arithmetic means ± S.E. with the corresponding K_I and K_D (nM) shown in brackets. B_{max} values (pmol/mg of membrane protein) are expressed as arithmetic means ± S.E.. See **Figure 27** for statistical comparisons of dissociation constants.

	Saturation Curves		**Competition Curves**	
	[^{3}H]-SCH23390 (n = 4-5)		Dopamine (n =4-5)	Dihydrexidine (n =4-5)
	pK_D (K_D, nM)	B_{max} (pmol/mg)	pK_I (K_I, nM)	
hD$_1$R	9.32 ± 0.07 (0.48)	13.0 ± 1.8	5.09 ± 0.06 (8171)	6.31 ± 0.05 (490)
hD$_1$-ST1	9.48 ± 0.07 (0.34)	1.57 ± 0.24	4.82 ± 0.06 (15230)	6.27 ± 0.06 (533)
hD$_1$-S56A	9.30 ± 0.04 (0.50)	14.7 ± 1.6	5.12 ± 0.07 (7667)	6.33 ± 0.07 (472)
hD$_1$-T59V	9.21 ± 0.09 (0.62)	19.5 ± 2.0	4.38 ± 0.06 (41330)	5.93 ± 0.07 (1183)
hD$_1$-S65A	9.37 ± 0.19 (0.42)	0.41 ± 0.08	5.65 ± 0.15 (2234)	6.92 ± 0.2 (121)

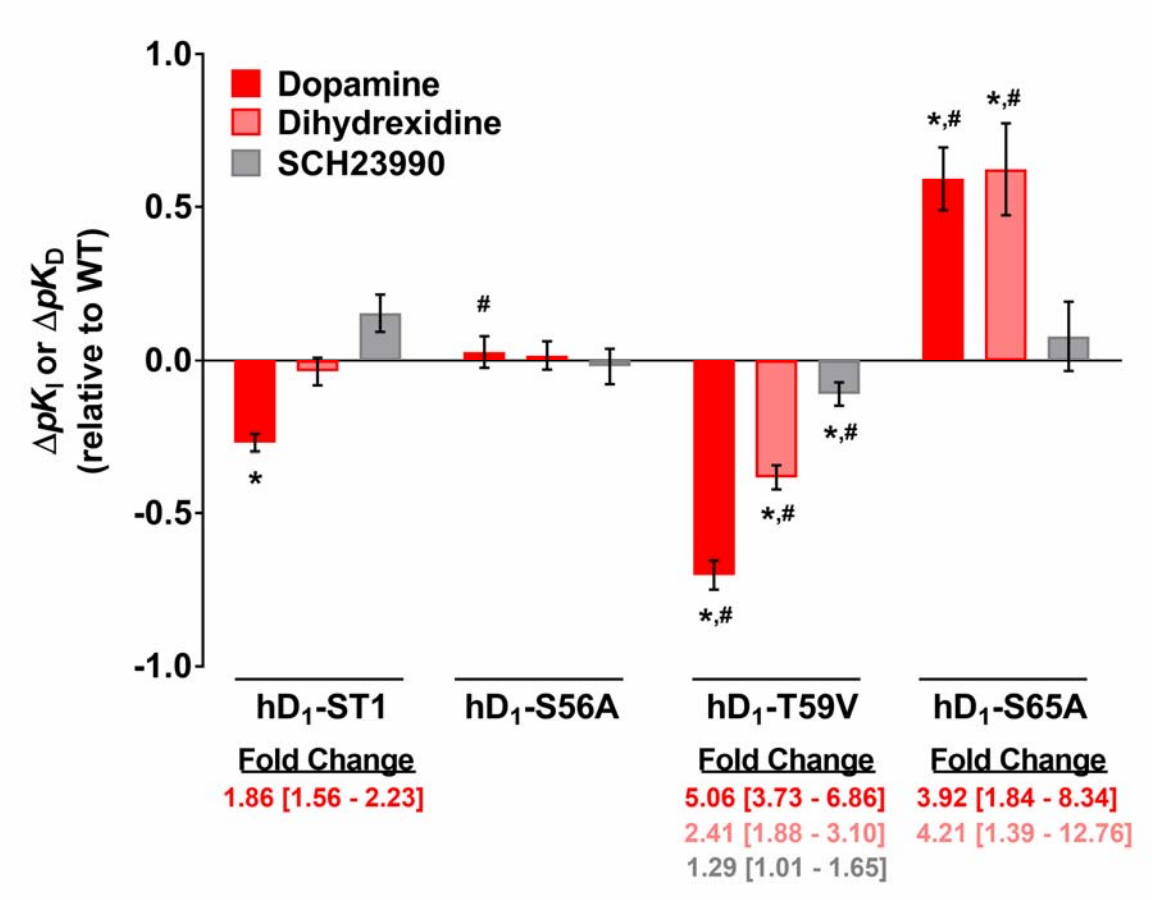

Figure 27. Changes in ligand affinities of hD_1-ST1 and single point mutant receptors compared to wild-type.
Bars represent the arithmetic mean ± S.E. of differences in calculated pK_D (SCH23390) and pK_I (dopamine and dihydrexidine) values **(Table 7)** for each mutant receptor relative to hD_1R. Wild-type receptor value was subtracted from mutant receptor value. Positive ΔpK_D and ΔpK_I values indicate gains in ligand affinities. Negative ΔpK_D and ΔpK_I values indicate losses in ligand affinities. Statistically significant ΔpK_D and ΔpK_I relative to wild-type are further described by their corresponding fold change (using K_D and K_I values), which are reported below with the 95% lower and upper confidence interval. *, $p < 0.05$ when compared with wild-type (value of 0) using one sample *t*-test. $^{\#}$, $p < 0.05$ when compared with hD_1-ST1 using two-tailed multiple *t*-tests with Holm-Sidak correction method. WT, wild-type.

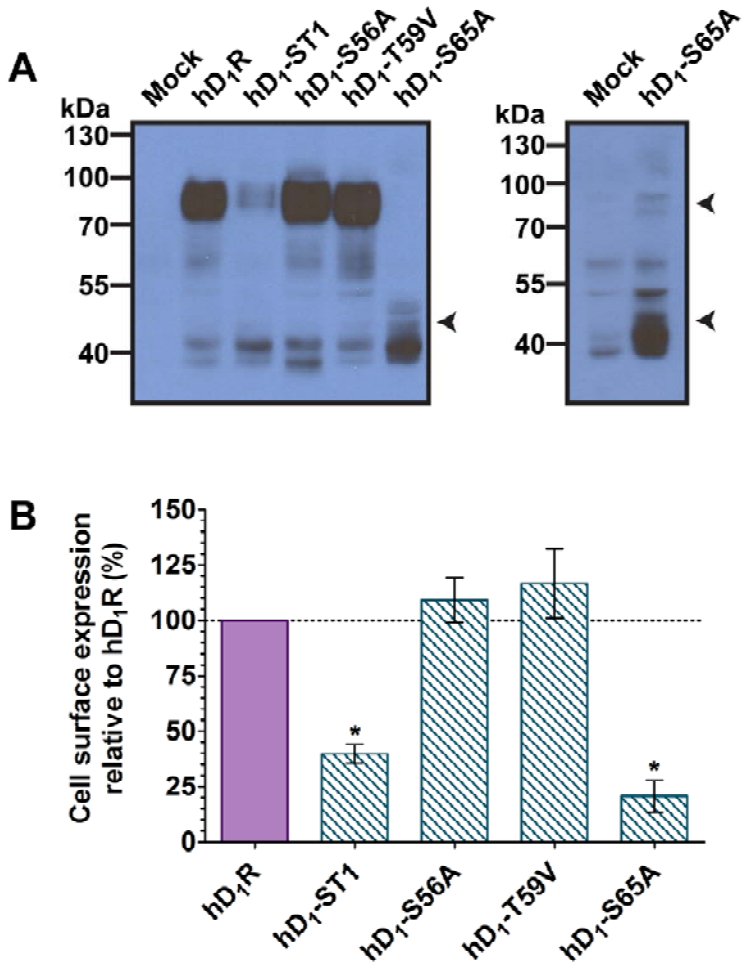

Figure 28. The S65A mutation is responsible for the reduced B_{max} of hD_1-ST1.
(A) *Left*, representative Western blot (from four independent experiments) for mock and receptor conditions using 40 μg of total proteins for each condition. B_{max} values (pmol/mg of membrane proteins) for representative Western blot were: 12.9 (hD_1R), 2.90 (hD_1-ST1), 14.3 (hD_1-S56A), 18.0 (hD_1-T59V), and 0.580 (hD1-S65A). *Right*, Western blot using 90 μg of total proteins for mock and hD_1-S65A (B_{max} = 0.37 pmol/mg of membrane proteins). Arrows indicate the 75-85 kDa band in hD_1-S65A (much more prominent compared to mock) as well as prominent band stainings below 55 kDa for hD_1-S65A. (B) Cell surface expression values (%) were determined by normalizing ELISA absorbance at 490 nm (subtracted from mock) over that of hD_1R. All receptors used in ELISA were HA-tagged at their N-termini. Each bar represents the arithmetic mean ± S.E. from five experiments. B_{max} values (pmol/mg of membrane proteins) in arithmetic means ± S.E. were: 10.7 ± 0.3 (hD_1R), 1.31 ± 0.08 (hD_1-ST1), 13.9 ± 1.3 (hD_1-S56A), 12.7 ± 1.5 (hD_1-T59V), and 0.36 ± 1.5 (hD_1-S65A). *, $p < 0.05$ when compared with wild-type (100%) using one sample *t*-test. Figure was taken from (Zhang *et al.*, 2015).

2.3 - Mutations at Thr59$^{2.39}$ and Ser65$^{2.45}$ primarily influence the activation of AC by hD$_1$-ST1

To further investigate the unique signalling properties of hD$_1$-ST1, cAMP assays were performed on the single point mutant receptors. The hD$_1$-T59V mutant showed the ablated basal activity of hD$_1$-ST1 even when it was expressed at a higher B_{max} value than wild-type **(Figure 29A)**. Whether the S65A mutation affected constitutive activation of hD$_1$R was undetermined because the constitutive activity of hD$_1$R was not detectable above mock condition at expression levels matched to hD$_1$-S65A. In the presence of DA, the T59V mutation exhibited a potency change not statistically different from that of hD$_1$-ST1 relative to hD$_1$R. On the other hand, only the S65A mutation produced the elevated E_{max} of hD$_1$-ST1 **(Figure 29B, Table 8)**. These findings thus demonstrate that drug potency and efficacy of a receptor can be dissociated. In addition, the hD$_1$-S56A did not drastically deviate from the hD$_1$R phenotype; however, it did show a significantly higher basal activity and a 2-fold increase in DA potency (i.e. leftward EC_{50} shift). When expressed at similar B_{max} values as **Figure 29B**, ELISA indicated that the cell surface expression of hD$_1$-ST1, hD$_1$-S56A, and hD$_1$-T59V were statistically unchanged from hD$_1$R **(Figure 29C)**. The cell surface expression of hD$_1$-S65A, congruent with its reduced B_{max}, was found to be lower than hD$_1$R. Nevertheless, when the B_{max} of hD$_1$R was lowered to similar levels as hD$_1$-S65A, cell surface expressions were found to be statistically indistinguishable between the two receptors **(Figure 29C)**. These results thus demonstrate that matching B_{max} values is appropriate for balancing cell surface levels among hD$_1$R, hD$_1$-ST1, and single point mutant receptors of hD$_1$-ST1.

To analyze how the elevated E_{max} of hD_1-ST1 and hD_1-S65A developed during the 30 min stimulation period, cAMP responses were collected at various time frames of stimulation (1 min, 3 mins, 5 mins, 10 mins, 20 mins, and 30 mins). In these time-course assays, both hD_1-ST1 and hD_1-S65A already exhibited 2-fold higher cAMP responses compared to hD_1R within 1 min of DA treatment, and this gap either persisted or increased during the time-course **(Figure 30A)**. The observed rate constant (k_{obs}) of hD_1R was not statistically different from hD_1-ST1 and hD_1-S65A **(Figure 30B)**. This indicated that hD_1-ST1 and hD_1-S65A were able to obtain their plateau (Y_{max}) at the same time as hD_1R. On the other hand, hD_1-S56A and hD_1-T59V displayed analogous time course curves as hD_1R, showing Y_{max} and k_{obs} values statistically resembling to wild-type.

2.4 - Thr$^{2.39}$ and Ser$^{2.45}$ display recurrent interactions among crystallized GPCR structures

As shown in **Figure 9B**, Thr59$^{2.39}$ and Ser65$^{2.45}$ are well-conserved among Family A GPCRs that have been crystallized. In these receptors, there exists recurring molecular patterns played by Thr$^{2.39}$ and Ser$^{2.45}$ **(Table 9)** and therefore suggests a generalized structural role for these two residues among Family A GPCRs. For example, the hydroxyl side-chain of Thr$^{2.39}$ hydrogen bonds with either Asp$^{3.49}$ or Arg$^{3.50}$ of the (E)DRY motif in the inactive R states of receptors (PDB accession code in brackets): adenosine A_{2A} (3EML), β_1-adrenergic (2VT4), dopamine D_3 (3PBL), δ opioid (4N6H), and κ opioid (4DJH). Upon receptor activation, the side-chain of Thr$^{2.39}$ breaks free from the (E)DRY motif and interacts with the side-chain of Tyr$^{3.60}$ of IC2, as observed in the R* states of $A_{2A}R$ and β_2AR **(Table 9,** see **Figure 31A, 31B** for examples**)**. In the case of Ser$^{2.45}$, in

both R and R* states, its hydroxyl side-chain almost always interacts with either $Trp^{4.50}$ and/or a polar residue at position 3.42 **(Table 9,** see **Figure 31C** for example**)**. Furthermore, for opioid receptors listed in **Table 9**, $Ser^{2.45}$ is replaced with $Asn^{2.45}$, which makes the same molecular network through $Trp^{4.50}$ and $Thr^{3.42}$.

Summary

In this section, I have shown that the functional phenotype of hD_1-ST1 is primarily caused by mutations at Thr59 and Ser65. The decreased DA affinity of hD_1-ST1 is attributed by T59V mutation but is also influenced to some extent by the increased DA affinity imposed by S65A mutation. The ablated basal activity and decreased DA potency of hD_1-ST1 is fully recapitulated by the T59V mutation. Meanwhile, the reduced B_{max} and elevated E_{max} of hD_1-ST1 is solely caused by the S65A mutation. The side-chain of $Thr59^{2.39}$ and $Ser65^{2.45}$ display conserved molecular interactions, which are reiterated among the current repertoire of crystallized Family A GPCRs. In the following sections, I attempt to validate these molecular interactions of $Thr^{2.39}$ and $Ser^{2.45}$ in hD_1R by utilizing single point mutant receptors.

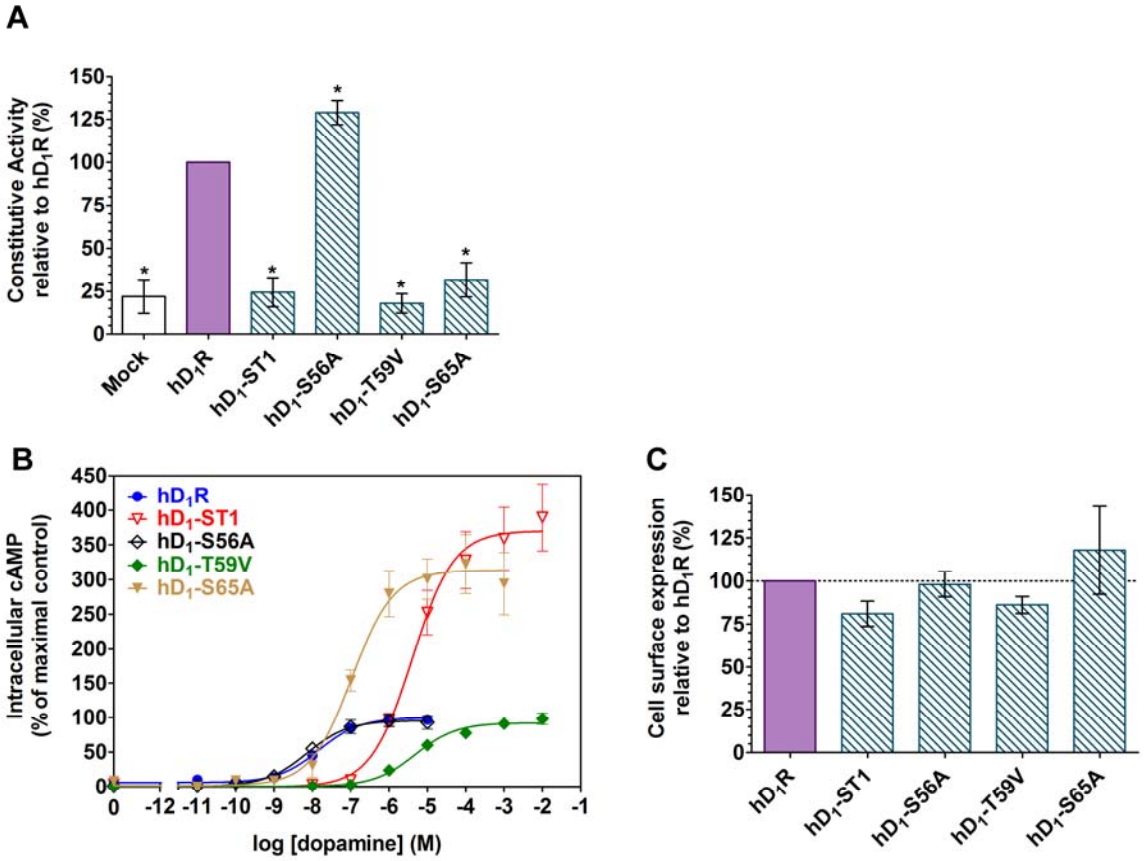

Figure 29. The T59V and S65A mutations primarily govern AC activation properties of hD_1-ST1.

(A) Each bar represents the arithmetic mean ± S.E. of normalized constitutive activity relative to hD_1R from three to four experiments. 5 μg of receptor DNA was used to achieve the following B_{max} values (pmol/mg of membrane proteins) in arithmetic means ± S.E.: 13.0 ± 1.0 (hD_1R), 1.41 ± 0.16 (hD_1-ST1), 12.2 ± 0.7 (hD_1-S56A), 18.5 ± 1.7 (hD_1-T59V), and 0.33 ± 0.04 (hD_1-S65A). *, $p < 0.05$ when compared with hD_1R (100%) using one sample *t*-test. (B) Each point represents the arithmetic mean ± S.E. (relative to best-fitted hD_1R E_{max} (100%)) from three to four experiments. B_{max} values (pmol/mg of membrane proteins) in arithmetic means ± S.E. were: 1.35 ± 0.18 (hD_1R), 1.75 ± 0.24 (hD_1-ST1), 1.46 ± 0.33 (hD_1-S56A), 1.37 ± 0.17 (hD_1-T59V), and 0.26 ± 0.09 (hD_1-S65A). (C) Cell surface levels of hD_1-ST1, hD_1-S56A, and hD_1-T59V were not statistically different from hD_1R under similar wild-type and mutant receptor B_{max} values in (B). Under similar B_{max} value of hD_1-S65A in (B), cell surface level of hD_1-S65A was compared with a "hD_1-low" condition (also represented by the purple bar labeled "hD_1R") whose B_{max} was 0.36 ± 0.13 (in pmol/mg of membrane proteins and expressed as mean ± S.E.). Each bar represents the arithmetic mean ± S.E. from four to six experiments. All receptors used in ELISA were HA-tagged at their N-termini. Figure was taken from (Zhang *et al.*, 2015).

Table 8. Best-fitted values of pEC_{50} (negative logarithm of EC_{50} in molar), EC_{50}, and E_{max} from Figure 29.
Statistical comparisons were performed using unconstrained and constrained global nonlinear regression curve fitting approach. *, $p < 0.05$ when compared with hD_1R. #, $p < 0.05$ when compared with hD_1-ST1

Condition	pEC_{50} ± S.E.	EC_{50} (nM)	E_{max} (%) ± S.E.
hD_1R	7.83 ± 0.38	14.7	99.5 ± 11.0
hD_1-ST1	5.40 ± 0.10*	4010*	370 ± 10.5*
hD_1-S56A	8.15 ± 0.38*,#	7.17*,#	95.5 ± 10.2#
hD_1-T59V	5.32 ± 0.39*	4770*	92.2 ± 9.84*,#
hD_1-S65A	6.97 ± 0.13*,#	107*,#	313 ± 11.1*,#

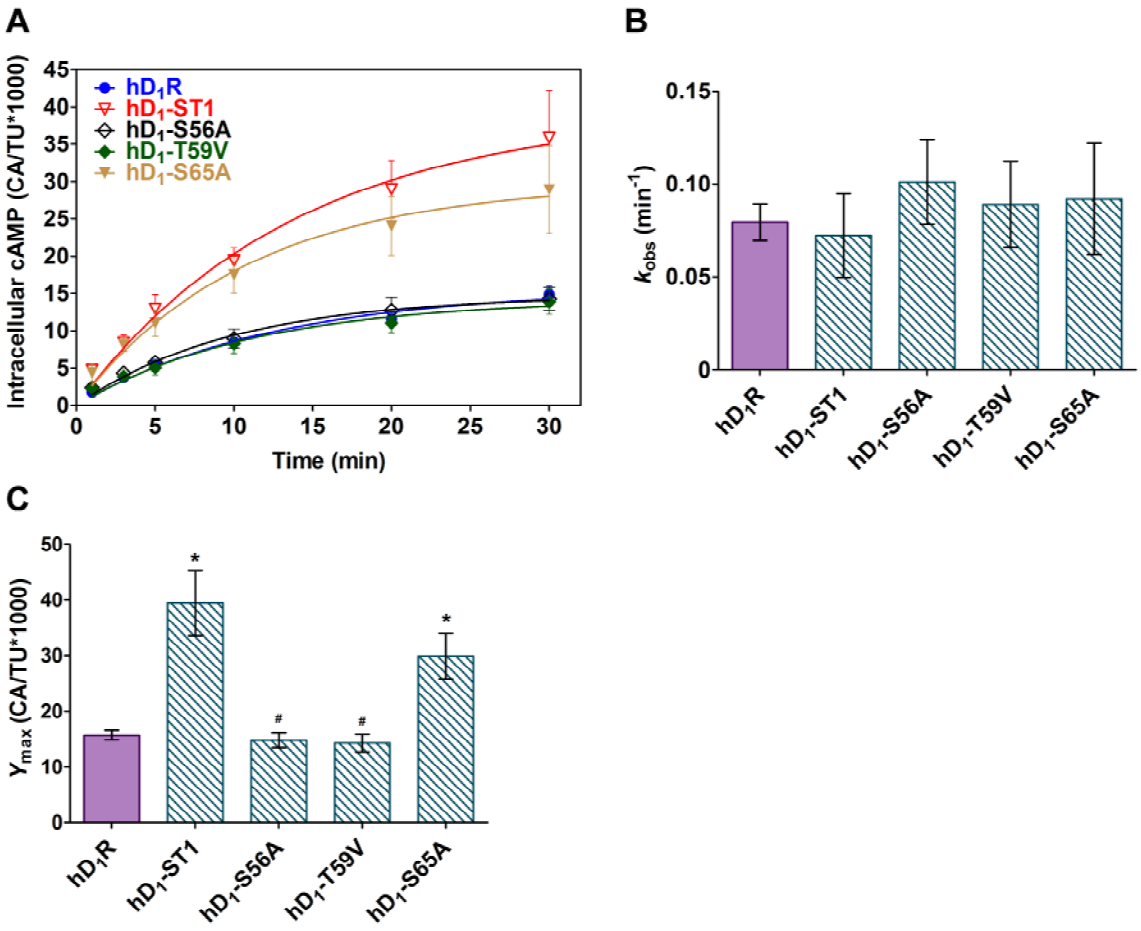

Figure 30. DA-mediated activation of AC observed in a time-course fashion.
(A) Each point represents the arithmetic mean ± S.E from four experiments of intracellular cAMP accumulated during various time periods of DA simulation. hD_1R, hD_1-S56A, and hD1-S65A were treated with 10^{-5} M of DA. hD1-ST1 and hD1-T59V were treated with 10^{-2} M of DA. Time-course curves were fitted by $Y = Y_{max} \bullet (1\text{-}e^{-kX})$. B_{max} values (pmol/mg of membrane proteins) in arithmetic means ± S.E. were: 1.23 ± 0.07 (hD_1R), 1.04 ± 0.1 (hD_1-ST1), 1.40 ± 0.2 (hD_1-S56A), 1.36 ± 0.2 (hD_1-T59V), and 0.23 ± 0.01 (hD_1-S65A). (B) and (C) Best-fitted k_{obs} and Y_{max} ± approximate S.E. derived from time-course curves. *, $p < 0.05$ compared to hD_1R; $^{\#}$, $p < 0.05$ compared to hD_1-ST1 using unconstrained and constrained global nonlinear regression curve fitting approach. Figure was taken from (Zhang *et al.*, 2015).

Table 9. Potential hydrogen bonds of Thr$^{2.39}$ and Ser$^{2.45}$ in solved structures of Family A GPCRs.
Letters (A, B, C, etc.) denote the multiple monomers in each solved structure. The nomenclature for describing specific side-chain atoms follows the PDB format. Hydrogen bonding partners and donor-acceptor distances were predicted using HBPLUS (McDonald & Thornton, 1994). N/A, Thr$^{2.39}$ or Ser$^{2.45}$ was not found to be conserved. -, no hydrogen bonding partner or side-chain side-chain hydrogen bonds were found for Thr$^{2.39}$ or Ser$^{2.45}$.

Solved GPCR structure	PDB accession code	Thr$^{2.39}$ OG1 contacts	Donor-acceptor distance (Å) from specific monomer	Ser$^{2.45}$ OG contacts	Donor-acceptor distance (Å) from specific monomer
Antagonist or Inverse Agonist Bound to R					
Adenosine A_{2A} receptor with ZM241385	3EML	Asp$^{3.49}$ OD2	2.62 (A)	Trp$^{4.50}$ NE1	3.09 (A)
β_1-adrenoceptor with cyanopindolol	2VT4	Asp$^{3.49}$ OD2	3.43 (A); 3.43 (D)	Trp$^{4.50}$ NE1	2.97 (A); 3.11 (B); 3.13 (C); 2.97 (D)
β_2-adrenoceptor with carazolol	2RH1	-	-	Trp$^{4.50}$ NE1	2.97 (A)
Dopamine D_3 receptor with eticlopride	3PBL	Asp$^{3.49}$ OD2	2.78 (A); 2.83 (B)	Asn$^{3.42}$ OD1/ND2	2.72/2.84 (A); 3.21/3.16 (B)
		Arg$^{3.50}$ NH1	2.70 (B)	Trp$^{4.50}$ NE1	2.86 (B)
Histamine H_1 receptor with doxepin	3RZE	N/A	N/A	Ser$^{3.42}$ OG	2.66 (A)
				Trp$^{4.50}$ NE1	2.84 (A)
Muscarinic M_2 receptor with 3-quinuclidinyl-benzilate	3UON	N/A	N/A	Asn$^{3.42}$ OD1	2.93 (A)
				Trp$^{4.50}$ NE1	2.84 (A)
Muscarinic M_3 receptor with tiotropium	4DAJ	N/A	N/A	Asn$^{3.42}$ ND2/OD1	2.63 (A)/2.68 (B)
				Trp$^{4.50}$ NE1	3.30 (B)
δ opioid receptor with naltrindole	4N6H	Arg$^{3.50}$ NH2	3.17 (A)	N/A	N/A
κ opioid receptor with JDTic	4DJH	Arg$^{3.50}$ NH1	3.20 (B)	N/A	N/A
μ opioid receptor with β-funaltrexamine	4DKL	-	-	N/A	N/A
*Agonist Bound to Intermediate or Full R**					
Adenosine A_{2A} receptor with truncated G_s	5G53	Tyr$^{3.60}$ OH	2.83 (A)	-	-
β_2-adrenoceptor with BI-167 107 and in complex with G_s	3SN6	Tyr$^{3.60}$ OH	2.69 (R)	Trp$^{4.50}$ NE1	3.08 (R)
Muscarinic M_2 receptor with iperoxo	4MQS	N/A	N/A	Asn$^{3.42}$ ND2	3.10 (A)
				Trp$^{4.50}$ NE1	3.05 (A)
Serotonin 1B receptor with ergotamine	4IAR	N/A	N/A	-	-
Serotonin 2B receptor with ergotamine	4IB4	-	-	His$^{3.42}$ NE2	2.94 (A)
				Trp$^{4.50}$ NE1	2.86 (A)

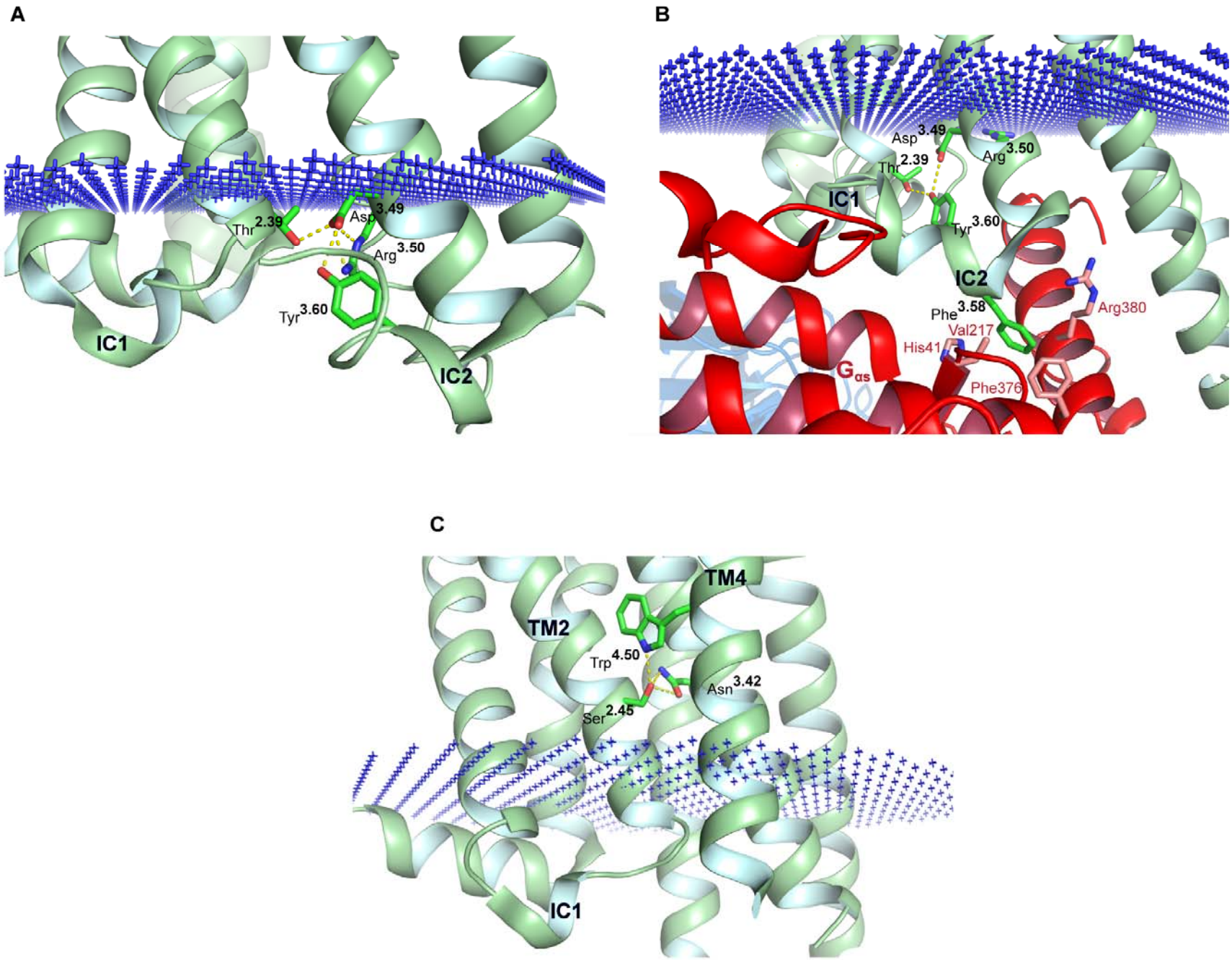
A
Thr2.39
Asp3.49
Arg3.50
Tyr3.60
IC1
IC2
B
Asp3.49
Arg3.50
Thr2.39
IC1
Tyr3.60
IC2
Phe3.58
Arg380
Val217
His41
Gαs
Phe376
C
TM4
TM2
Trp4.50
Asn3.42
Ser2.45
IC1

Figure 31. Examples of recurring molecular interactions by Thr$^{2.39}$ and Ser$^{2.45}$ in solved Family A GPCRs.
(A) In the inactive R state, Thr$^{2.39}$ interacts with the (E)DRY motif. Example shown is the $A_{2A}R$ bound to ZM241385 (3EML). (B) In active R* state, Thr$^{2.39}$ breaks from the (E)DRY motif and interacts with Tyr$^{3.60}$ of IC2. This can help stabilize the insertion of Phe$^{3.58}$ into the hydrophobic pocket of $G\alpha_s$ as observed in G protein-bound structures of A_2AR and β_2AR. Example shown is the β_2AR in complex with G_s (3SN6). Here, the hydrophobic pocket for Phe$^{3.58}$ is created by His41, Val217, Phe376, and Arg380 of $G\alpha_s$. (A) and (B) For better visualization of IC1, TM4 has been made transparent. (C) Ser$^{2.45}$ by the IC1/TM2 membrane juncture interacts with Trp$^{4.50}$ and/or Asn$^{3.42}$ in numerous GPCRs regardless of R or R* states. Example shown is the D_3R bound to eticlopride (3PBL). Blue asterisks represent membrane boundaries that were predicted from Orientation of Proteins in Membranes (Lomize *et al.*, 2012). Yellow dashed lines represent hydrogen bonds. Figure was adapted and taken from (Zhang *et al.*, 2015)

3. Investigating the Potential Molecular Network of Thr59 in hD_1R

3.1 - Distinct functional phenotypes of DRY mutant and $Tyr^{3.60}$ mutant receptors compared to hD_1-T59V

Based on crystallized Family A GPCRs, the potential molecular contacts for the hydroxyl side-chain of $Thr59^{2.49}$ in hD_1R consist of $Asp120^{3.49}$ and $Arg121^{3.50}$ in the R state and $Tyr131^{3.60}$ of IC2 in the R* state (**Table 9**). To probe if these potential molecular networks are important towards the functional deficits of hD_1-T59V, further single point mutagenesis were undertaken to construct hD_1-D120A, hD_1-R121A, and hD_1-Y131A. Binding studies revealed a drastic decrease in receptor expression for hD_1-D120A and hD_1-R121A, and this may reflect nature's mechanism to preserve the stabilizing selection for the (E)DRY motif **(Table 10)**. Mutating Tyr131 in the middle of IC2 also decreased the B_{max} of hD_1R, but this decrease was less compared to those produced by Asp120 and Arg121 mutations. Whereas the hD_1-D120A and hD_1-Y131A showed affinities for [^{3}H]-SCH23390 close to hD_1R, the hD_1-R121A demonstrated a 5-fold loss compared to hD_1R **(Table 10, Figure 32)**. Competition studies with unlabelled SCH23390 resulted in K_I value (1.5 nM) that was reminiscent to the K_D value obtained with the radioligand (2.5 nM) **(Figure 33A)**. Interestingly, despite potential disruptions to its binding pocket, the hD_1-R121A maintained a DA affinity that was close to hD_1R **(Figure 33B)**. The hD_1-D120A displayed a 114-fold increase in affinity for DA, while the hD_1-Y131A showed a 4-fold increase in affinity for both DA and DHX **(Table 10, Figure 32)**. Such trends were opposite to hD_1-T59V, which demonstrated losses in affinity for both agonists.

The hD_1-T59V was previously shown to exhibit negligible basal activity and a pronounced rightward shift (over 200-fold) in EC_{50} for DA. In striking contrast, the hD_1-D120A displayed a robust increase in basal activity, despite its much lower receptor expression compared to hD_1R **(Figure 34)**. Also in opposing fashion, the hD_1-D120A displayed a 27-fold leftward shift in EC_{50} for DA and a 3-fold increase in E_{max} relative to hD_1R at matched B_{max} levels **(Figure 35A, Table 11)**. Although the basal activity of hD_1-R121A was at mock conditions levels, meaningful conclusions could not be made because the constitutive activity of hD_1R, when expressed at B_{max} levels of hD_1-R121A, would also be at mock condition levels. Nevertheless, under matched B_{max} levels, the hD_1-R121A displayed a statistically unchanged EC_{50} for DA and approximately 3-fold elevation in E_{max} compared to hD_1R **(Figure 35A, Table 11)**. The hD_1-Y131A mimicked the ablated basal activity of the hD_1-T59V **(Figure 34)**, but its rightward shift in EC_{50} for DA was only 10-fold relative to hD_1R **(Figure 35B, Table 11)**. This could have been partially offset by the increased DA affinity of hD_1-Y131A.

Summary

Among the three residues observed to interact with $Thr59^{2.39}$ in crystal structures, only mutating Tyr131 in IC2 produced functional deficits, which partially reflected the hD_1-T59V phenotype. In contrast, replacing $Asp120^{3.49}$ with Ala in the (E)DRY motif produced a more active hD_1R displaying enhanced DA affinity, basal activity, DA potency, and E_{max}. This behaviour further supports the role of $Asp^{3.49}$ in constraining the receptor in the inactive R state. Intriguingly, mutating $Arg121^{3.50}$ in the (E)DRY motif caused little changes to DA affinity or potency for hD_1R, but did produce a noticeable

loss of affinity to SCH23390 along with an elevated E_{max}. In the next section, I employ further single point mutagenesis to disrupt potential molecular contacts with the side-chain of Ser65$^{2.45}$ in hD_1R.

Table 10. Dissociation constants (K_D, K_I) and B_{max} values of [^{3}H]-SCH23390 for hD$_1$-T59V and its potentially related mutant receptors compared to wild-type.
pK_D and pK_I (negative logarithm of K_D and K_I in molar) are expressed as arithmetic means ± S.E. with the corresponding K_I and K_D (nM) shown in brackets. B_{max} values (pmol/mg of membrane proteins) are expressed as arithmetic means ± S.E.. See **Figure 32** for statistical comparisons of dissociation constants.

	Saturation Curves		**Competition Curves**	
	[^{3}H]-SCH23390 (n = 3-7)		Dopamine (n =4-6)	Dihydrexidine (n =5-6)
	pK_D (K_D, nM)	B_{max} (pmol/mg)	pK_I (K_I, nM)	
hD$_1$R	9.33 ± 0.02 (0.47)	11.7 ± 0.80	5.16 ± 0.06 (6948)	6.11 ± 0.05 (769.9)
hD$_1$-T59V	9.35 ± 0.02 (0.44)	12.2 ± 0.91	4.58 ± 0.02 (26450)	5.95 ± 0.02 (1126)
hD$_1$-D120A	9.16 ± 0.08 (0.70)	0.140 ± 0.022	7.13 ± 0.2 (73.68)	ND
hD$_1$-R121A	8.60 ± 0.06 (2.5)	0.168 ± 0.029	5.48 (3346)*	ND
hD$_1$-Y131A	9.51 ± 0.04 (0.31)	1.85 ± 0.45	5.71 ± 0.03 (1939)	6.69 ± 0.1 (206.6)

*Exception: Dopamine competition study was performed once with hD1-R121A
ND, not determined

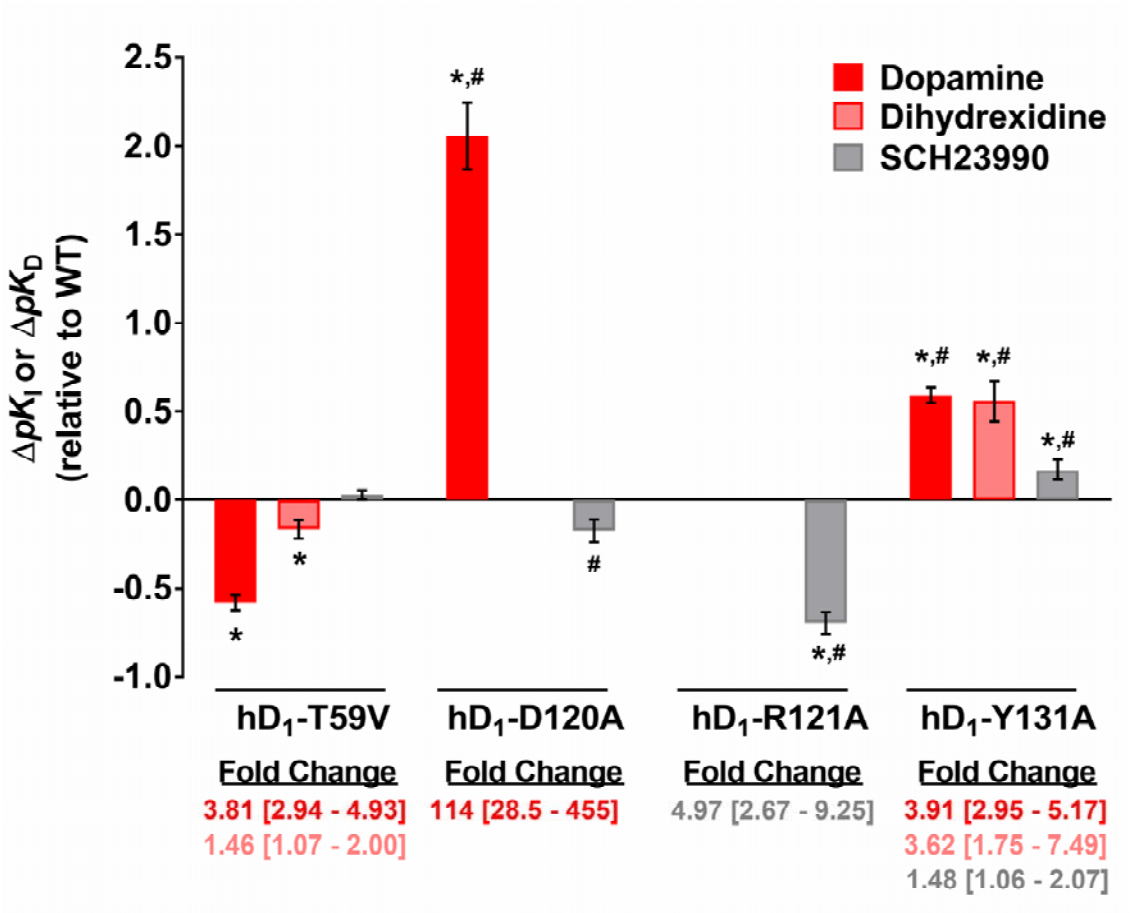

Figure 32. Changes in ligand affinities of hD_1-T59V and its potentially related mutant receptors compared to wild-type.
Bars represent the arithmetic mean ± S.E. of differences in calculated pK_D (SCH23390) and pK_I (dopamine and dihydrexidine) values **(Table 10)** for each mutant receptor relative to hD_1R. Wild-type receptor value was subtracted from mutant receptor value. Positive ΔpK_D and ΔpK_I values indicate gains in ligand affinities. Negative ΔpK_D and ΔpK_I values indicate losses in ligand affinities. Statistically significant ΔpK_D and ΔpK_I relative to wild-type are further described by their corresponding fold change (using K_D and K_I values), which are reported below with the 95% lower and upper confidence interval. *, $p < 0.05$ when compared with wild-type (value of 0) using one sample *t*-test. $^{\#}$, $p < 0.05$ when compared with hD_1-T59V using either two-tailed unpaired *t*-test or two-tailed multiple *t*-tests with Holm-Sidak correction method. WT, wild-type.

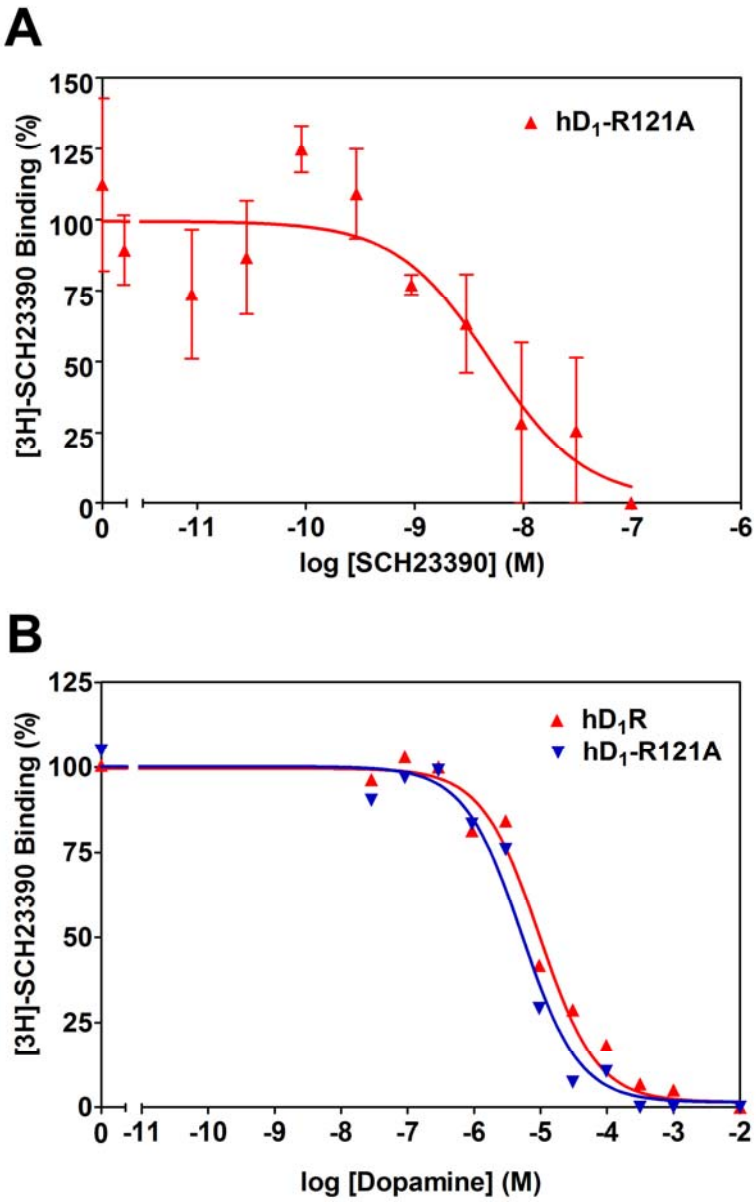

Figure 33. Competition curves of [^{3}H]-SCH23390 binding to hD_1R and hD_1-R121A using (A) SCH23390 and (B) dopamine.
Each point represents the arithmetic mean ± S.E. from two experiments (A) and one experiment (B), all performed using duplicates. Curve points for each condition were generated by taking the average of duplicates and then subtracting the "baseline", which was set as the value (dpm) corresponding to the highest concentration of competing drug. These values were then normalized relative to the best-fitted Top value (100%). Inhibition constants (K_I, nM) were: (A) for SCH23390, 1.5 (hD1-R121A); (B) for dopamine, 4498 (hD_1R) and 3346 (hD_1-R121A).

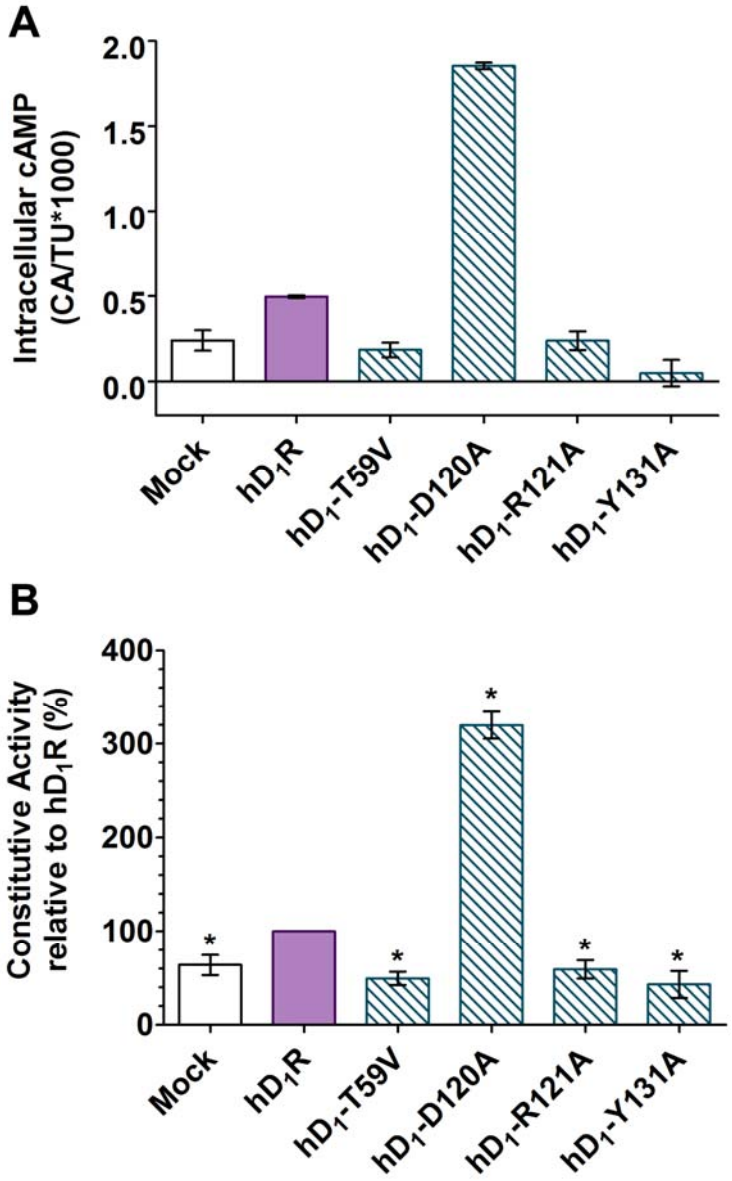

Figure 34. Agonist-independent activation of AC for hD$_1$-T59V and its potentially related mutant receptors compared to wild-type.
(A) An example of raw data (done with triplicates) showing the constitutive activity ± S.E of wild-type and mutant receptors expressed in [^{3}H]-cAMP formed (CA) over the total amount of [^{3}H]-adenine uptake (TU) x 1000. (B) Constitutive activity is normalized relative to wild-type. Each bar represents the arithmetic mean ± S.E. from five experiments. B_{max} values (pmol/mg of membrane proteins) in arithmetic means ± S.E.: 2.22 ± 0.30 (hD$_1$R), 12.4 ± 1.3 (hD$_1$-T59V), 0.212 ± 0.030 (hD$_1$-D120A), 0.146 ± 0.026 (hD$_1$-R121A), and 2.53 ± 0.24 (hD$_1$-Y131A). *, $p < 0.05$ when compared with hD$_1$R (100%) using one sample *t*-test.

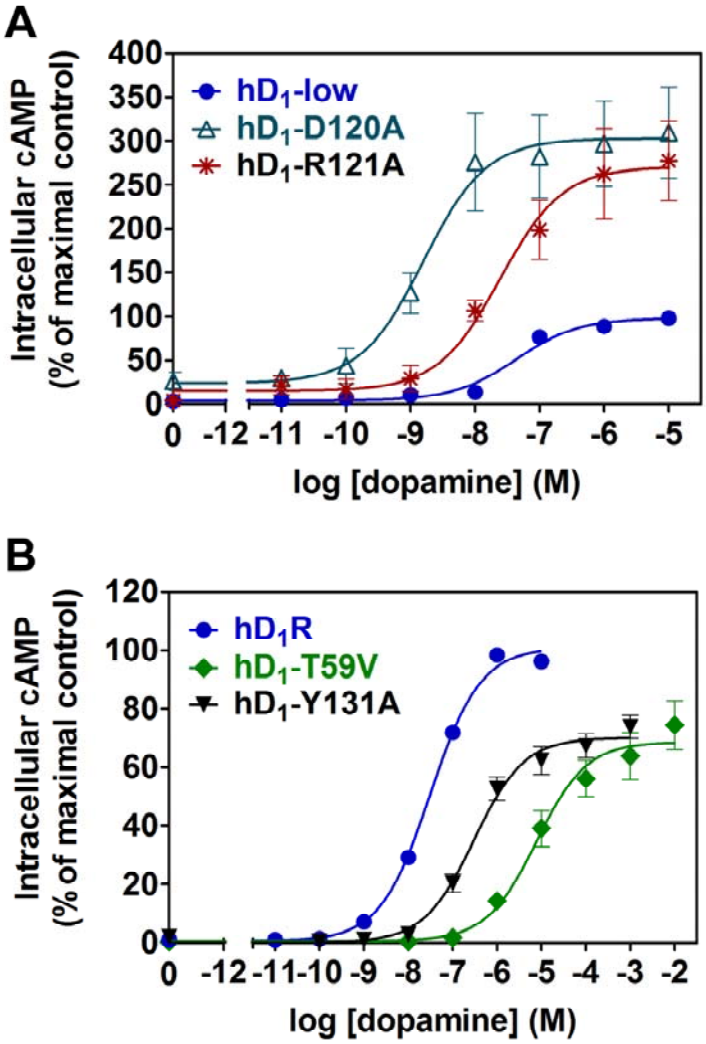

Figure 35. DA-mediated stimulation of AC for hD_1-T59V and its potentially related mutant receptors compared to wild-type.

(A) and (B) Dose-response curves were generated by expressing each point in relation to the best-fitted wild-type E_{max} value (100%) and then plotting them as a function of logarithmic DA concentrations. Each point represents the arithmetic mean ± S.E. from three to five experiments. "hD1-low" refers to hD_1R condition at a lower B_{max} to match those of hD_1-D120A and hD_1-R121A. B_{max} values (pmol/mg of membrane proteins) in arithmetic means ± S.E. were: 0.193 ± 0.096 (hD_1R), 0.133 ± 0.015 (hD_1-D120A), 0.177 ± 0.043 (hD_1-R121A), 1.04 ± 0.11 (hD_1R), 0.952 ± 0.23 (hD_1-T59V), and 0.988 ± 0.19 (hD_1-Y131A).

Table 11. Best-fitted values of pEC_{50} (negative logarithm of EC_{50} in molar), EC_{50}, and E_{max} from Figure 35.
Statistical comparisons were performed using unconstrained and constrained global nonlinear regression curve fitting approach. *, $p < 0.05$ when compared with wild-type (hD_1-low or hD_1R). #, $p < 0.05$ when compared with hD_1-T59V.

Panel	Condition	pEC_{50} ± S.E.	EC_{50} (nM)	E_{max} (%) ± S.E.
A	hD_1-low	7.36 ± 0.60	43.5	98.6 ± 19
	hD_1-D120A	8.80 ± 0.19*	1.59*	303 ± 15*
	hD_1-R121A	7.61 ± 0.22	24.4	271 ± 19*
B	hD_1R	7.51 ± 0.091	30.9	101 ± 3.2
	hD_1-T59V	5.12 ± 0.13*	7652*	68.7 ± 2.5*
	hD_1-Y131A	6.53 ± 0.12*,#	299*,#	70.1 ± 2.3*

4. Investigating the Potential Molecular Interactions of Ser65 in hD_1R and their Underlying Functions.

4.1 - Matching functional phenotypes of $Trp^{4.50}$ and $Asn^{3.42}$ mutant receptors compared to hD_1-S65A

If Ser65 of hD_1R exhibits the molecular interactions of $Ser^{2.45}$ listed in **Table 9**, its hydroxyl side-chain will hydrogen bond with the side-chains of $Trp148^{4.50}$ and $Asn113^{3.42}$ of hD_1R. To validate the existence and importance of hydrogen bonding between Ser65 and Asn113/Trp148 in dictating hD_1R function, two single point mutant receptors were made: hD_1-N113A and hD_1-W148A. The hD_1-N113A mutation decreased the B_{max} of hD_1R to levels of hD_1-S65A **(Table 12)**. Because the B_{max} of hD_1-W148A was undetectable, two additional mutants hD_1-W148F and hD_1-W148Y, were constructed with hopes that an aromatic side-chain—akin to tryptophan's—may improve receptor B_{max}. Although hD_1-W148F displayed exceptionally low B_{max} (~0.03 pmol/mg of membrane proteins in one experiment) and weak specific binding, the B_{max} of hD_1-W148Y improved to approximately 1 pmol/mg of membrane proteins **(Table 12)**.

The K_D of hD_1-S65A in this section was found to be statistically different from hD_1R; nevertheless, this fold change was only 1.25-fold. Minor but statistically significant changes in K_D (relative to wild-type) were also observed in hD_1-N113A and hD_1-W148Y (**Table 12, Figure 36**). Further binding studies were not performed on hD_1-W148F because of its low specific binding signal. Competition studies showed both the hD_1-N113A and hD_1-W148Y emulated the increased agonist affinity of hD_1-S65A, as demonstrated by their calculated ΔpK_I. Although their ΔpK_I values appeared to be lower relative to those of hD_1-S65A—a possible sign of combinatorial effects—statistical

analyses indicated only those regarding DHX for hD_1-N113A and hD_1-W148Y were statistically different when compared with hD_1-S65A **(Table 12, Figure 36)**.

Given their hydrophobic nature, the side-chains of Ala113 and Phe148 cannot hydrogen bond with the side-chain of Ser65 in hD_1R. To understand how the hydroxyl side-chain of Tyr148 interacts with Ser65, MD simulations were conducted for 25 ns. As a reference, the side-chain of Trp148 was found to consistently hydrogen bond with the side-chain of Ser65 throughout the entire 25 ns of simulation (**Figure 37A, 37B**). During approximately the first 2 ns, the side-chain of Tyr148 sampled interactions with the side-chain of Ser65. Afterwards, it moved more than 4 Å away from the side-chain of Ser65 and remained there for the rest of the simulation, making hydrogen bonds with either the carbonyl backbone of Ser65 and/or the side-chain of Ser69 (**Figure 37C, 37D**). Since the phenol group of Tyr protrudes more horizontally compared to the side-chain of Trp at 148, it may pose more steric clashes and therefore moving upwards from Ser65 may be more energetically favourable. Consequently, these results indicate that a hydrogen bond between the side-chains of Ser65 and Tyr148 is likely to be predominately absent in the hD_1-W148Y mutant receptor.

Assessing the dose-response curves with DA revealed that EC_{50} and E_{max} parameters of the hD_1-N113A and hD_1-S65A were not statistically different **(Figure 38A, Table 13)**. The hD_1-W148Y also produced the elevated E_{max} characteristic of the hD_1-S65A, albeit to greater levels possibly due to its higher B_{max} than hD_1-S65A (~ 1 pmol/mg proteins and matching B_{max} of hD_1R). DA potency of hD_1-W148Y was found to be statistically indistinguishable to hD_1R. To assess hD_1-W148F (with a B_{max} of 0.08 pmol/mg proteins), the B_{max} of hD_1R was further titrated to low levels (0.1-0.2 pmol/mg

proteins). Under these circumstances, the E_{max} of hD_1-W148F was found to be significantly higher than hD_1R **(Figure 38B, Table 13)**. As a control, a mock condition was included to show the low B_{max} of hD_1R did produce a specific hD_1R-dependent cAMP response **(Figure 38B, Table 13)**. In addition, because more transfected HEK293 cells had to be pooled to detect specific binding from hD_1-W148F, this increased cell pooling was also performed for the mock condition. The B_{max} of [^{3}H]-SCH23390 in mock was consistently found to be lower than hD_1-W148F, indicating that the specific binding of hD_1-W148F was receptor specific. In all, these dose-response studies demonstrate that breaking either the Ser65-Asn113 interaction or the Ser65-Trp148 interaction is sufficient to produce an elevated E_{max}.

Table 12. Dissociation constants (K_D, K_I) and B_{max} values of [^{3}H]-SCH23390 for hD$_1$-S65A and its potentially related mutant receptors compared to wild-type.
pK_D and pK_I (negative logarithm of K_D and K_I in molar) are expressed as arithmetic means ± S.E. with the corresponding K_I and K_D (nM) shown in brackets. B_{max} values (pmol/mg of membrane proteins) are expressed as arithmetic means ± S.E.. See **Figure 36** for statistical comparisons of dissociation constants.

	Saturation Curves		**Competition Curves**	
	[^{3}H]-SCH23390 (n = 12-13)		Dopamine (n =6-7)	Dihydrexidine (n =7-8)
	pK_D (K_D, nM)	B_{max} (pmol/mg)	pK_I (K_I, nM)	
hD$_1$R	9.30 ± 0.02 (0.50)	14.0 ± 1.0	4.91 ± 0.02 (12290)	6.01 ± 0.04 (979)
hD$_1$-S65A	9.41 ± 0.03 (0.39)	0.409 ± 0.032	5.84 ± 0.06 (1437)	6.86 ± 0.05 (139)
hD$_1$-N113A	9.42 ± 0.04 (0.38)	0.561 ± 0.058	5.61 ± 0.09 (2452)	6.70 ± 0.05 (199)
hD$_1$-W148Y	9.56 ± 0.05 (0.28)	1.32 ± 0.091	5.70 ± 0.07 (2007)	6.62 ± 0.06 (238)
hD$_1$-W148F	9.27 (0.54)*	0.034*	ND	ND

*Exception: Saturation study was performed once with hD$_1$-W148F
ND, not determined

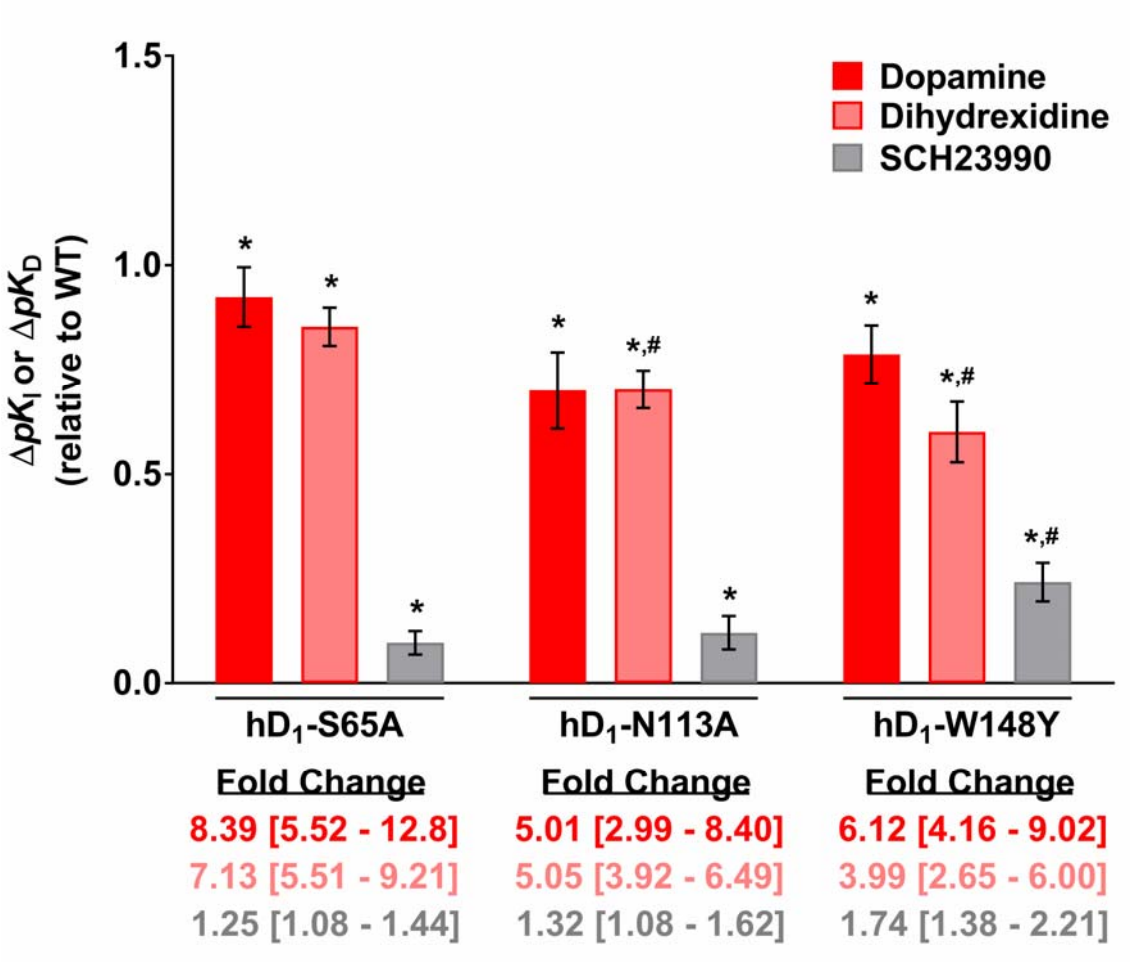

Figure 36. Changes in ligand affinities of hD_1-S65A and its potentially related mutant receptors compared to wild-type.
Bars represent the arithmetic mean ± S.E. of differences in calculated pK_D (SCH23390) and pK_I (dopamine and dihydrexidine) values **(Table 12)** for each mutant receptor relative to hD_1R. Wild-type receptor value was subtracted from mutant receptor value. Positive ΔpK_D and ΔpK_I values indicate gains in ligand affinities. Negative ΔpK_D and ΔpK_I values indicate losses in ligand affinities. Statistically significant ΔpK_D and ΔpK_I relative to wild-type are further described by their corresponding fold change (using K_D and K_I values), which are reported below with the 95% lower and upper confidence interval. *, $p < 0.05$ when compared with wild-type (value of 0) using one sample *t*-test. $^{\#}$, $p < 0.05$ when compared with hD_1-S65A using two-tailed multiple *t*-tests with Holm-Sidak correction method. WT, wild-type.

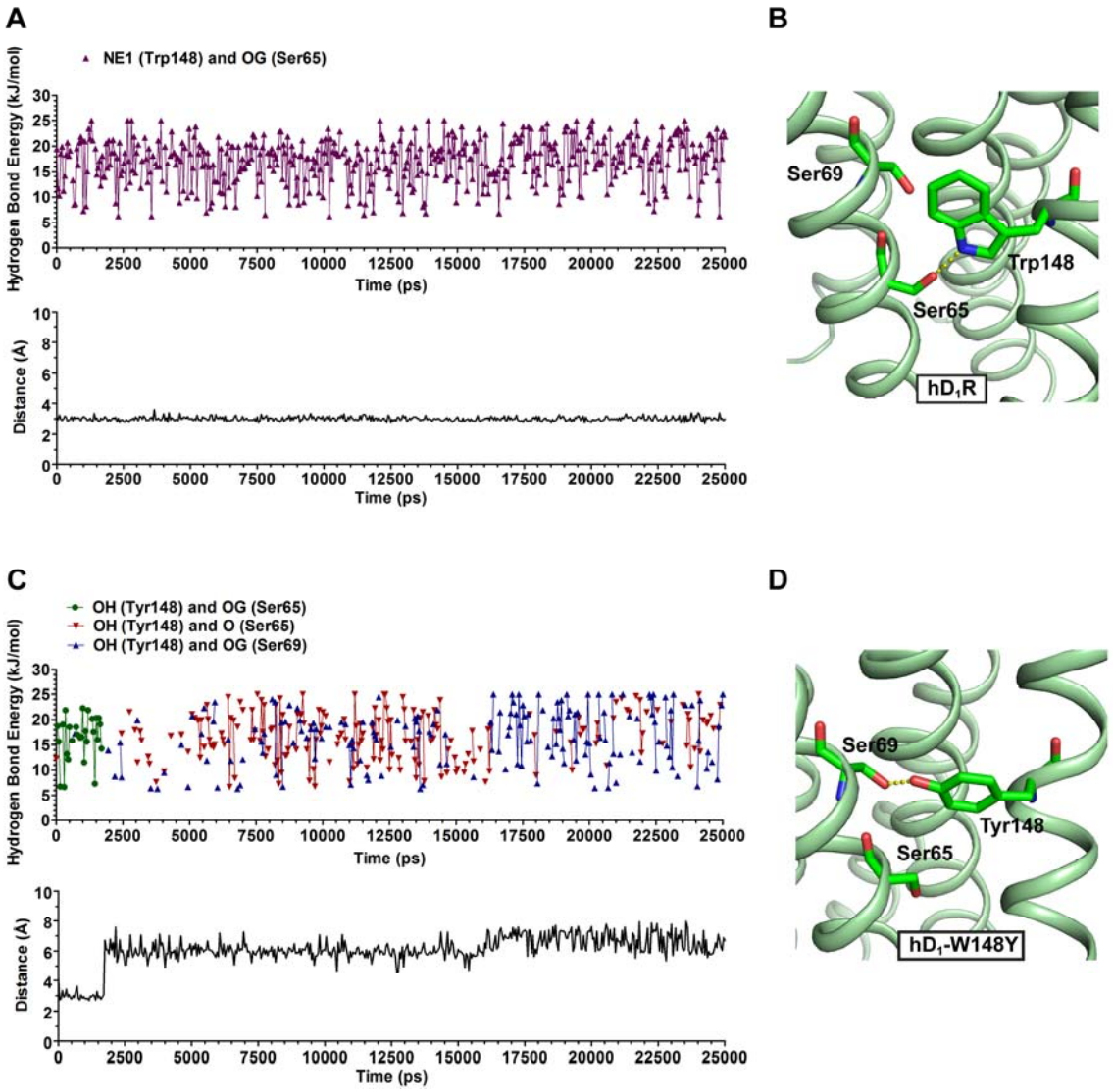

Figure 37. MD simulations (25 ns) of hD_1R and hD_1-W148Y.
(A) *Upper panel*, the nitrogen (NE1) within Trp148 side-chain consistently hydrogen bonded with the hydroxyl side-chain (OG) of Ser65 in hD_1R during simulation. *Lower panel*, distance in angstroms between NE1 of Trp148 and OG of Ser65 in hD_1R during simulation. (B) In the last simulation snapshot, NE1 of Trp148 hydrogen bonded with OG of Ser65 in hD_1R. (C) *Upper panel*, during the first ~2 ns, the hydroxyl group (OH) within Tyr148 side-chain sampled hydrogen bonds with OG of Ser65. Afterwards, OH of Tyr148 moved upward from OG of Ser65 and hydrogen bonded with OG of Ser69 and/or the carbonyl backbone (O) of Ser65 for the rest of simulation. This coincided with the increase in distance between OH of Tyr148 and OG of Ser65 (*lower panel*). (D) In the last simulation snapshot, OH of Tyr148 hydrogen bonded with OG of Ser69 in hD_1-W148Y. In both (A) and (C) *Upper panels*, lines between points indicate consecutive hydrogen bonds. In both (B) and (D), OG of Ser65 further hydrogen bonded with the side-chain of Asn113, which is not shown.

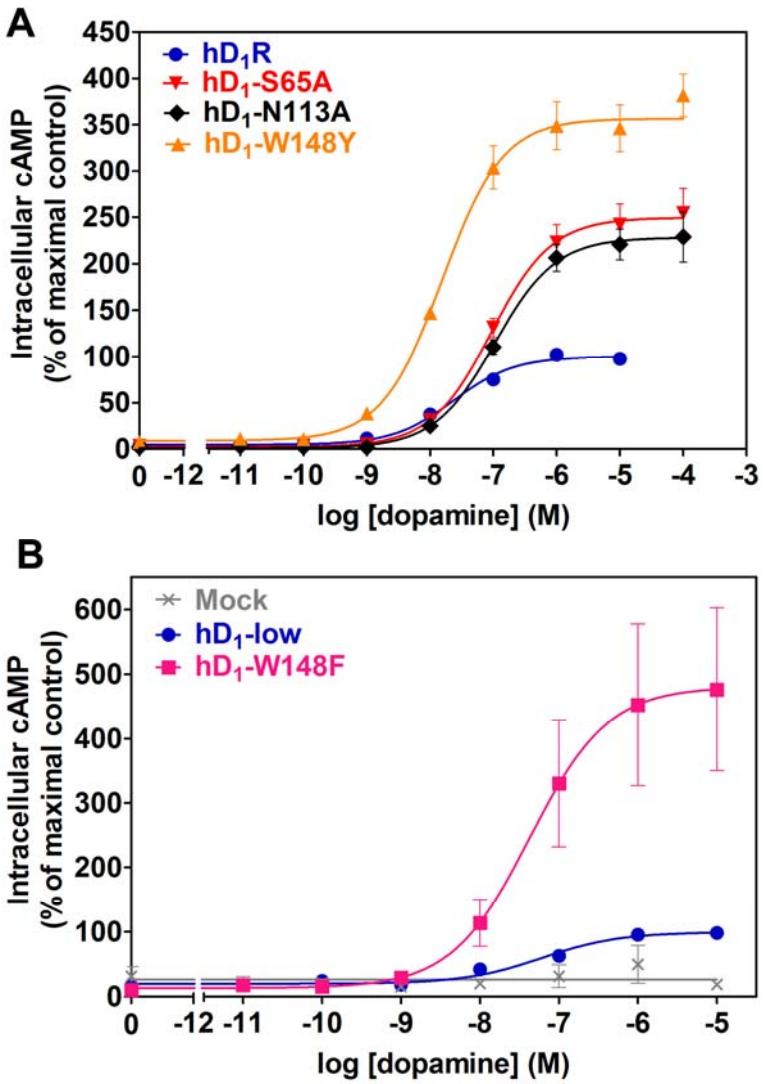

Figure 38. DA-mediated stimulation of AC for hD_1-S65A and its potentially related mutant receptors compared to wild-type.

(A) and (B) Dose-response curves were generated by expressing each point in relation to the best-fitted wild-type E_{max} value (100%) and then plotting them as a function of logarithmic DA concentrations. Each point represents the arithmetic mean ± S.E. from five to six experiments. "hD1-low" refers to hD_1R condition at a lower B_{max} in efforts to equate with the B_{max} of hD_1-W148F. B_{max} values (pmol/mg of membrane proteins) in arithmetic means ± S.E. were: 1.78 ± 0.43 (hD_1R), 0.413 ± 0.022 (hD_1-S65A), 0.558 ± 0.051 (hD_1-N113A), 1.25 ± 0.14 (hD_1-W148Y), 0.0146 ± 0.0055 (Mock), 0.198 ± 0.035 (hD_1-low), and 0.0840 ± 0.0060 (hD_1-W148F).

Table 13. Best-fitted values of pEC_{50} (negative logarithm of EC_{50} in molar), EC_{50}, and E_{max} from Figure 38.
Statistical comparisons were performed using unconstrained and constrained global nonlinear regression curve fitting approach. *, $p < 0.05$ when compared with wild-type (hD_1R or hD_1-low). #, $p < 0.05$ when compared with hD_1-S65A. -, ambiguous.

Panel	Condition	pEC_{50} ± S.E.	EC_{50} (nM)	E_{max} (%) ± S.E.
A	hD_1R	7.63 ± 0.26	23.5	100 ± 8.1
	hD_1-S65A	7.03 ± 0.094*	92.4*	250 ± 7.8*
	hD_1-N113A	6.98 ± 0.10*	106*	228 ± 8.3*
	hD_1-W148Y	7.81 ± 0.067#	15.6#	357 ± 7.7*,#
B	Mock	-	-	-
	hD_1-low	7.22 ± 1.4	61.0	100 ± 41
	hD_1-W148F	7.37 ± 0.24	43.0	480 ± 46*

4.2 - Evaluating the signalling regulation of hD$_1$-S65A and its intracellular pool

To delve deeper into the mechanisms contributing to the elevated E_{max} of hD$_1$-S65A, agonist-induced desensitization of hD$_1$-S65A was first assessed. Following DA pre-treatment for 5 mins and DA re-challenge for 10 mins, the hD$_1$-S65A displayed the same blunted response as hD$_1$R: 10% decrease in E_{max} and within 2 to 3-fold rightward EC_{50} shift compared to vehicle (AA) condition **(Figure 39, Table 14)**. This suggests that the elevated E_{max} of hD$_1$-S65A is not caused by an altered ability to desensitize in the presence of DA.

The steep time-course curves of hD$_1$-ST1 and hD$_1$-S65A **(Figure 30)** were reminiscent to that of a hD$_1$R mutant receptor with a truncated CT, which was shown to have impairments to its agonist-induced endocytosis (Jackson *et al.*, 2002). Thus, it could be possible for hD$_1$-ST1 and hD$_1$-S65A to have impaired abilities to internalize that enables them to prolong their activation of AC, culminating into an elevated cAMP response. To assess the agonist-induced endocytic pathway of hD$_1$-S65A, cAMP assays were performed with compounds marketed to block CME: Pitstop2, an inhibitor of clathrin and Dyngo4a, an inhibitor of dynamin. Pitstop2 have been tested in the lab to diminish the ability of hD$_1$R to internalize during 10 mins of DA stimulation (**Figure 40**). Upon pre-treatment with Pitstop2 (20 μM) for 10 mins and following stimulation with DA for 10 mins (in the presence of Pitstop2), hD$_1$R displayed a 20-fold rightward EC_{50} shift compared to control **(Figure 41A, Table 15)**. A higher dosage of Pitstop2 (25 μM) brought an additional decrease in E_{max} of AC for hD$_1$R **(Figure 41B, Table 15)**. For hD$_1$-S65A, Pitstop2 elicited a rightward EC_{50} shift in combination with a drop in E_{max} (over 30%) compared to control **(Figure 41, Table 15)**. With 30 μM of Dyngo4a, the same

effects were observed as Pitstop2—only with more pronounced changes relative to control **(Figure 42A, Table 16)**. Furthermore, removing Dyngo4a after pre-treatment and stimulating with DA (i.e. in the absence of Dyngo4a) also reproduced the trend of rightward EC_{50} shift and decreased E_{max} for hD_1R and hD_1-S65A **(Figure 42B, 42C, Table 16)**. The degree of such impairments to their signalling was lessened if lower dosages of Dyngo4a were applied.

Because **Figure 42** resembled the outcomes from applying a competitive antagonist, one experiment was performed to test whether Dyngo4a had any effects on DA binding to the receptor. Surprisingly, in a mixture composed of buffer ions, DA, 30 μm Dyngo4a, [^{3}H]-SCH23390, and crude membranes, Dyngo4a drastically impaired [^{3}H]-SCH-23390 binding to hD_1R and hD_1-S65A **(Figure 43)**. This also affected the ability of increasing doses of DA to lower the binding of [^{3}H]-SCH-23390, and consequently, K_I values of DA for hD_1R and hD_1-S65A could not be calculated. This experiment therefore adds towards the growing list of non-specific effects of Dyngo4a (and Pitstop2) that needs to be fully appreciated (Dutta *et al.*, 2012, Guo *et al.*, 2015, Liashkovich *et al.*, 2015, Park *et al.*, 2013, Preta *et al.*, 2015, Smith *et al.*, 2013, Willox *et al.*, 2014).

ELISA-based internalization assays later revealed that hD_1-ST1 did show impairments to undergoing DA-induced internalization; however, this was caused by the hD_1-T59V mutation **(Figure 44)**. In fact, hD_1-S56A, hD_1-S65A, hD_1-N113A, and hD_1-W148Y all displayed wild-type behaviour to internalize following 10 mins stimulation with DA. Interestingly, when Triton-X was used to permeablize the cell, total receptor expression for hD_1-ST1, hD_1-S65A, hD_1-N113A, and hD_1-W148Y were found to be over

2-fold greater than hD_1R **(Figure 45)**. By having less cell-surface expression compared to hD_1R, these mutant receptors should possess a larger intracellular population compared to hD_1R. On the other hand, the hD_1-S56A and hD_1-T59V displayed statistically unaltered cell surface and total receptor expressions as wild-type when B_{max} values were matched.

Summary

Results in this section indicate the existence of side-chain interactions of Ser65 with Asn113 and Trp148, which are functionally important to hD_1R. Both hD_1-N113A and hD_1-W148Y mimicked the hD_1-S65A phenotype in terms of reduced B_{max}, increased agonist affinity, and elevated E_{max}. In particular, the hD_1-N113A phenotype showed the closest resemblance to hD_1-S65A because it displayed identical DA potency and E_{max} as the hD_1-S65A. The hD_1-S65A exhibited wild-type abilities to undergo agonist-induced desensitization and internalization. However, agonist-induced internalization was impaired for hD_1-ST1 and hD_1-T59V. ELISA assays suggest that hD_1-S65A, hD_1-N113A, and hD_1-W148Y have more internalized receptors despite having lower cell-surface levels compared to hD_1R.

Applying Pitstop2 and Dyngo4a greatly hampered cAMP signalling of hD_1R and hD_1-S65A in a dose-dependent manner. Unexpectedly, competition studies revealed that Dyngo4a interfered with ligand binding towards hD_1R and hD_1-S65A. Such non-specific effects may account for the negative effects imposed by Dyngo4a (and potentially Pitstop2) on hD_1R and hD_1-S65A signalling. Therefore, caution must be taken when using these drugs in the future.

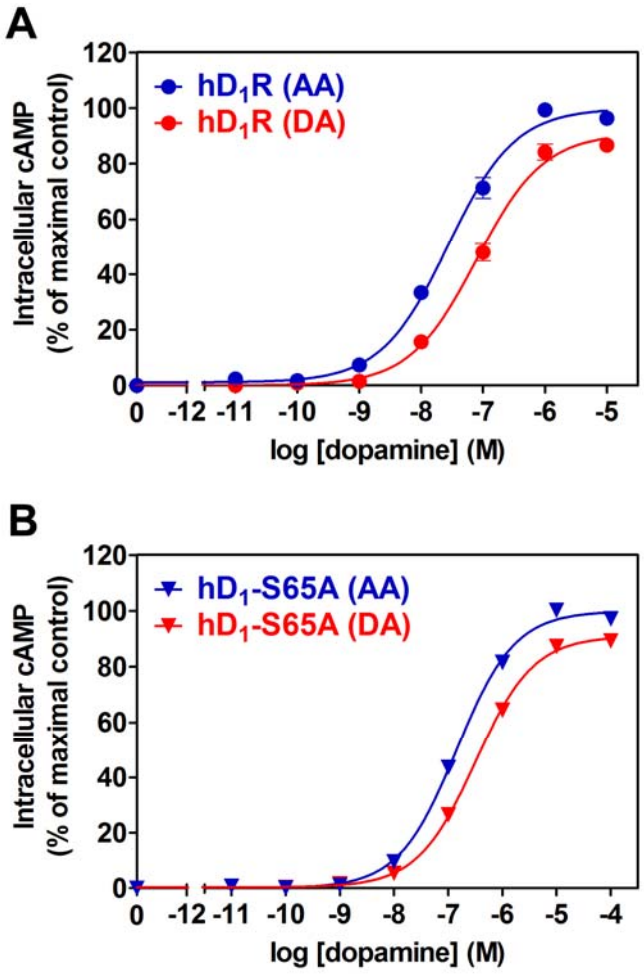

Figure 39. Agonist-induced desensitization is not altered in hD_1-S65A compared to wild-type.

(A) and (B) Cells were pre-treated with either 0.1 mM AA or 10 µM DA for 5 mins, washed twice with PBS, and then re-challenged with various doses of DA for 10 mins. For each receptor, dose-response curves were generated by expressing each point (after subtracted from basal) in relation to the best-fitted E_{max} value (100%) of AA condition and then plotting them as a function of logarithmic DA concentrations. Each point represents the arithmetic mean ± S.E. from five experiments. B_{max} values (pmol/mg of membrane proteins) in arithmetic means ± S.E. were: 2.02 ± 0.25 (hD_1R) and 0.312 ± 0.020 (hD_1-S65A).

Table 14. Best-fitted values of pEC_{50} (negative logarithm of EC_{50} in molar), EC_{50}, and E_{max} from Figure 39.

Panel	Condition	pEC_{50} ± S.E.	EC_{50} (nM)	E_{max} (%) ± S.E.
A	hD_1R (AA)	7.57 ± 0.051	27.2	100 ± 1.8
	hD_1R (DA)	7.10 ± 0.057	78.8	91 ± 2.1
B	hD_1-S65A (AA)	6.85 ± 0.033	142	100 ± 1.1
	hD_1-S65A (DA)	6.50 ± 0.038	317	91 ± 1.2

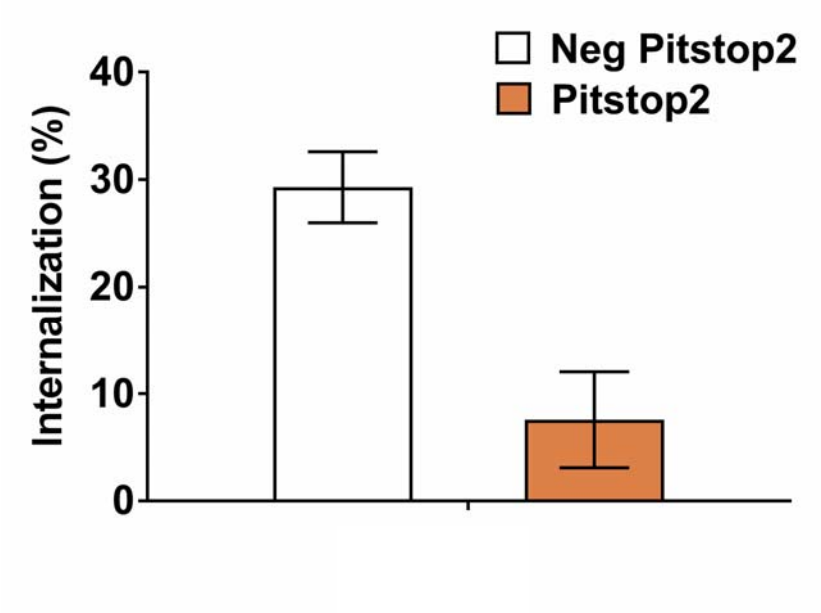

Figure 40. Internalization assay with Pitstop2 shows decreased DA-mediated internalization for FLAG-hD$_1$R.
Cells were incubated with either 20 μM Pitstop2 or the inactive Negative (Neg) Pitstop2 for 10 mins and then stimulated with 0.1 mM AA (vehicle) or 10 μM of DA for 10 mins without removing Pitstop2 or Neg Pitstop2. Internalization was assessed by the % decrease in cell surface expression following 10 mins treatment with DA relative to that of AA. Each bar represents the arithmetic mean ± S.E. from four experiments. B_{max} value (pmol/mg of membrane proteins) in arithmetic means ± S.E. obtained from untreated cells was 1.51 ± 0.14 for FLAG-hD$_1$R.

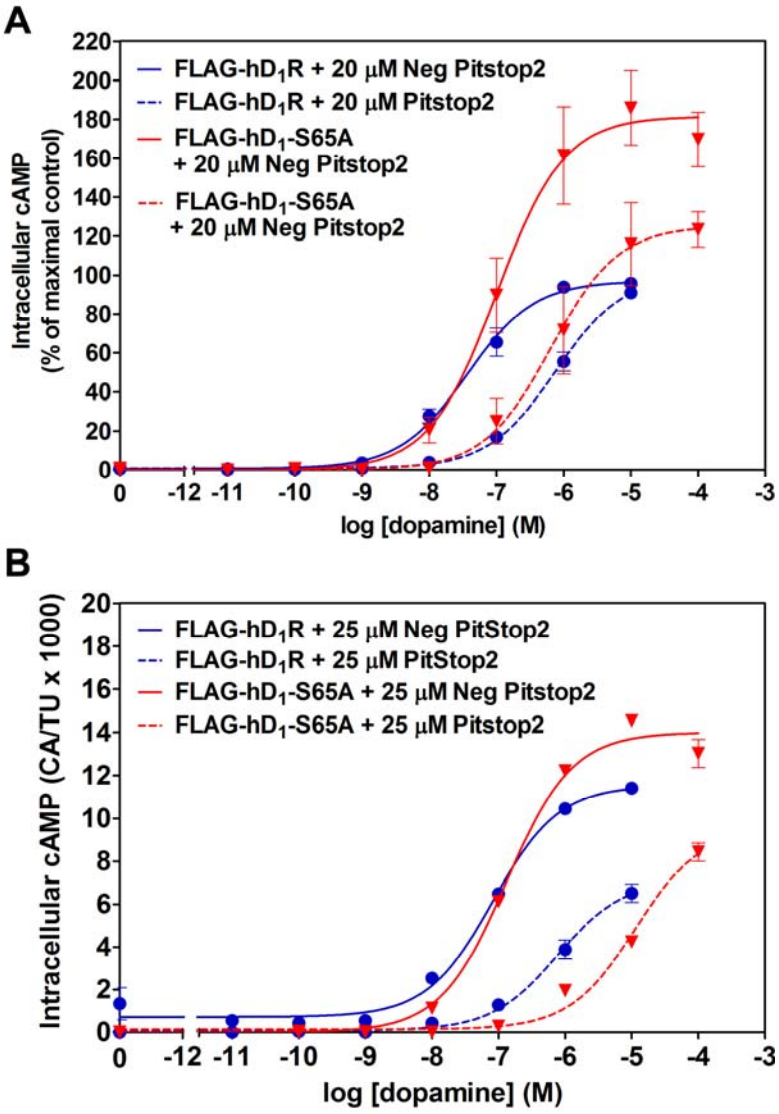

Figure 41. Pitstop2 effects on DA-mediated AC activation for hD$_1$R and hD$_1$-S65A. (A) Cells were incubated with either 20 µM Pitstop2 or the inactive Negative (Neg) Pitstop2 for 10 mins and then stimulated with DA for 10 mins in the presence of Pitstop2 or Neg Pitstop2. Dose-response curves were generated by expressing each point in relation to the best-fitted E_{max} value (100%) of FLAG-hD$_1$R + 20 µM Neg Pitstop2 condition and then plotting them as a function of logarithmic DA concentrations. Each point represents the arithmetic mean ± S.E. from four experiments. B_{max} values (pmol/mg of membrane proteins) were obtained from untreated cells and were, in arithmetic means ± S.E.: 1.71 ± 0.29 (FLAG-hD$_1$R) and 0.400 ± 0.050 (FLAG-hD$_1$-S65A). (B) Stimulation paradigm described in A) was used for 25 µM Pitstop2 and Neg Pitstop2 for one experiment done in triplicates. Each point represents the arithmetic mean ± S.E. of intracellular cAMP expressed in [^{3}H]-cAMP formed (CA) over the total amount of [^{3}H]-adenine uptake (TU) x 1000. B_{max} values (pmol/mg of membrane proteins) were obtained from untreated cells and were: 0.77 (FLAG-hD$_1$R) and 0.17 (FLAG-hD$_1$-S65A).

Table 15. Best-fitted values of pEC_{50} (negative logarithm of EC_{50} in molar), EC_{50}, and E_{max} from Figure 41.

Panel	Condition	pEC_{50} ± S.E.	EC_{50} (nM)	E_{max} (%) ± S.E.
A	FLAG-hD_1R + 20 µM Neg Pitstop2	7.44 ± 0.21	36.5	97.1 ± 7.0
	FLAG-hD_1R + 20 µM Pitstop2	6.12 ± 0.25	757	100 ± 13
	FLAG-hD_1-S65A + 20 µM Neg Pitstop2	7.00 ± 0.10	101	182 ± 6.8
	FLAG-hD_1-S65A + 20 µM Pitstop2	6.19 ± 0.16	652	125 ± 8.4
Panel	**Condition**	**pEC_{50} ± S.E.**	**EC_{50} (nM)**	**E_{max} (CA/TU*1000) ± S.E.**
B	FLAG-hD_1R + 25 µM Neg Pitstop2	7.10 ± 0.090	81.4	11.5 ± 0.40
	FLAG-hD_1R + 25 µM Pitstop2	6.11 ± 0.17	770	7.14 ± 0.65
	FLAG-hD_1-S65A + 25 µM Neg Pitstop2	6.89 ± 0.066	130	14.0 ± 0.32
	FLAG-hD_1-S65A + 25 µM Pitstop2	4.95 ± 0.14	11280	9.55 ± 0.77

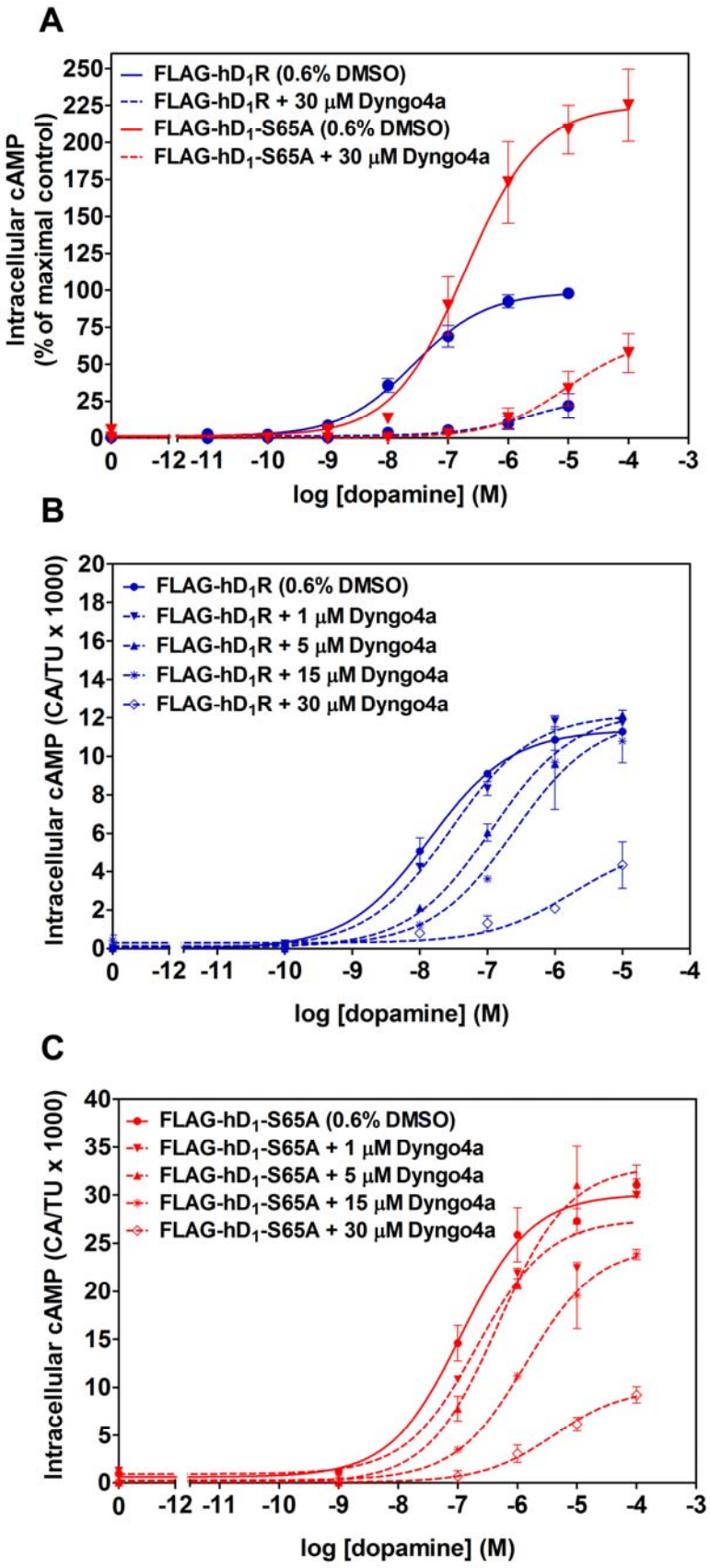
A
FLAG-hD1R (0.6% DMSO)
FLAG-hD1R + 30 µM Dyngo4a
FLAG-hD1-S65A (0.6% DMSO)
FLAG-hD1-S65A + 30 µM Dyngo4a
Intracellular cAMP (% of maximal control)
log [dopamine] (M)
B
FLAG-hD1R (0.6% DMSO)
FLAG-hD1R + 1 µM Dyngo4a
FLAG-hD1R + 5 µM Dyngo4a
FLAG-hD1R + 15 µM Dyngo4a
FLAG-hD1R + 30 µM Dyngo4a
Intracellular cAMP (CA/TU x 1000)
log [dopamine] (M)
C
FLAG-hD1-S65A (0.6% DMSO)
FLAG-hD1-S65A + 1 µM Dyngo4a
FLAG-hD1-S65A + 5 µM Dyngo4a
FLAG-hD1-S65A + 15 µM Dyngo4a
FLAG-hD1-S65A + 30 µM Dyngo4a
Intracellular cAMP (CA/TU x 1000)
log [dopamine] (M)

Figure 42. Dyngo4a effects on DA-mediated AC activation for hD_1R and hD_1-S65A. (A) Cells were incubated with either 30 μM Dyngo4a or in 0.6% DMSO (vehicle) for 15 mins and then stimulated with DA in the presence of Dyngo4a or 0.6% DMSO for 10 mins. Dose-response curves were generated by expressing each point in relation to the best-fitted E_{max} value (100%) of FLAG-hD_1R (0.6% DMSO) condition and then plotting them as a function of logarithmic DA concentrations. Each point represents the arithmetic mean ± S.E. from three experiments. B_{max} values (pmol/mg of membrane proteins) were obtained from untreated cells and were, in arithmetic means ± S.E.: 2.31 ± 0.33 (FLAG-hD_1R) and 0.493 ± 0.13 (FLAG-hD_1-S65A). (B and C) In one experiment, done in triplicates, cells were incubated with various dosages of Dyngo4a or 0.6% DMSO for 15 mins for FLAG-hD_1R and FLAG-hD_1-S65A conditions. The media was aspirated and replaced with fresh media. Appropriate amounts of DA were then added. Each point represents the arithmetic mean ± S.E. of intracellular cAMP expressed in [^{3}H]-cAMP formed (CA) over the total amount of [^{3}H]-adenine uptake (TU) x 1000. B_{max} values (pmol/mg of membrane proteins) were obtained from untreated cells and were: 1.97 (FLAG-hD_1R) and 0.45 (FLAG-hD_1-S65A).

Table 16. Best-fitted values of pEC_{50} (negative logarithm of EC_{50} in molar), EC_{50}, and E_{max} from Figure 42.

Panel	Condition	pEC_{50} ± S.E.	EC_{50} (nM)	E_{max} (%) ± S.E.
A	FLAG-hD$_1$R (0.6% DMSO)	7.57 ± 0.25	26.7	98.6 ± 7.6
	FLAG-hD$_1$R + 30 µM Dyngo4a	5.62 ± 1.6	2399	29.1 ± 26
	FLAG-hD$_1$-S65A (0.6% DMSO)	6.72 ± 0.11	192	225 ± 8.6
	FLAG-hD$_1$-S65A + 30 µM Dyngo4a	5.03 ± 0.51	9360	68 ± 17
Panel	**Condition**	**pEC_{50} ± S.E.**	**EC_{50} (nM)**	**E_{max} (CA/TU*1000) ± S.E.**
B	FLAG-hD$_1$R (0.6% DMSO)	7.86 ± 0.11	13.8	11.4 ± 0.38
	FLAG-hD$_1$R + 1 µM Dyngo4a	7.56 ± 0.11	27.8	12.2 ± 0.42
	FLAG-hD$_1$R + 5 µM Dyngo4a	6.94 ± 0.12	115	12.3 ± 0.55
	FLAG-hD$_1$R + 15 µM Dyngo4a	6.61 ± 0.13	247	12.0 ± 0.66
	FLAG-hD$_1$R + 30 µM Dyngo4a	5.74 ± 0.43	1820	5.47 ± 1.2
C	FLAG-hD$_1$-S65A (0.6% DMSO)	6.95 ± 0.13	112	30.1 ± 1.1
	FLAG-hD$_1$-S65A + 1 µM Dyngo4a	6.68 ± 0.15	208	27.5 ± 1.2
	FLAG-hD$_1$-S65A + 5 µM Dyngo4a	6.32 ± 0.12	474	33.1 ± 1.4
	FLAG-hD$_1$-S65A + 15 µM Dyngo4a	5.86 ± 0.18	1382	24.6 ± 1.7
	FLAG-hD$_1$-S65A + 30 µM Dyngo4a	5.40 ± 0.49	4027	9.91 ± 2.0

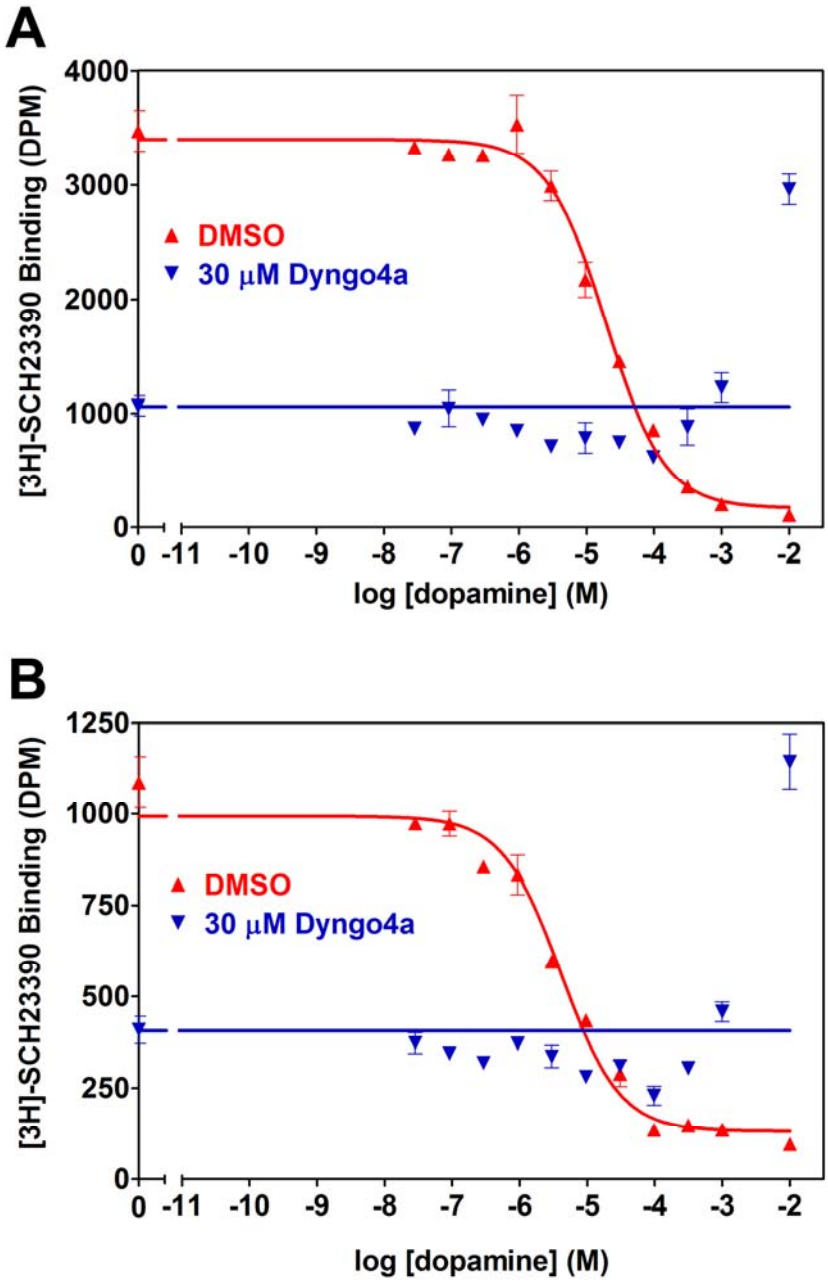

Figure 43. Dyngo4a alters ligand binding to hD_1R and hD_1-S65A.
Competition curves of [^{3}H]-SCH23390 binding to A) FLAG-hD_1R and B) FLAG-hD_1-S65A using DA in the presence of 0.6% DMSO (vehicle) or 30 μM Dyngo4a. Curves are representative of one experiment done in duplicates. Inhibition constants (K_I, nM) of DA were as follows: (A) 11030 (FLAG-hD_1R in 0.6% DMSO) (B) 1773 (FLAG-hD_1-S65A in 0.6% DMSO). K_I values of DA for FLAG-hD_1R and FLAG-hD_1-S65A in the presence of 30 μM Dyngo4a could not be determined.

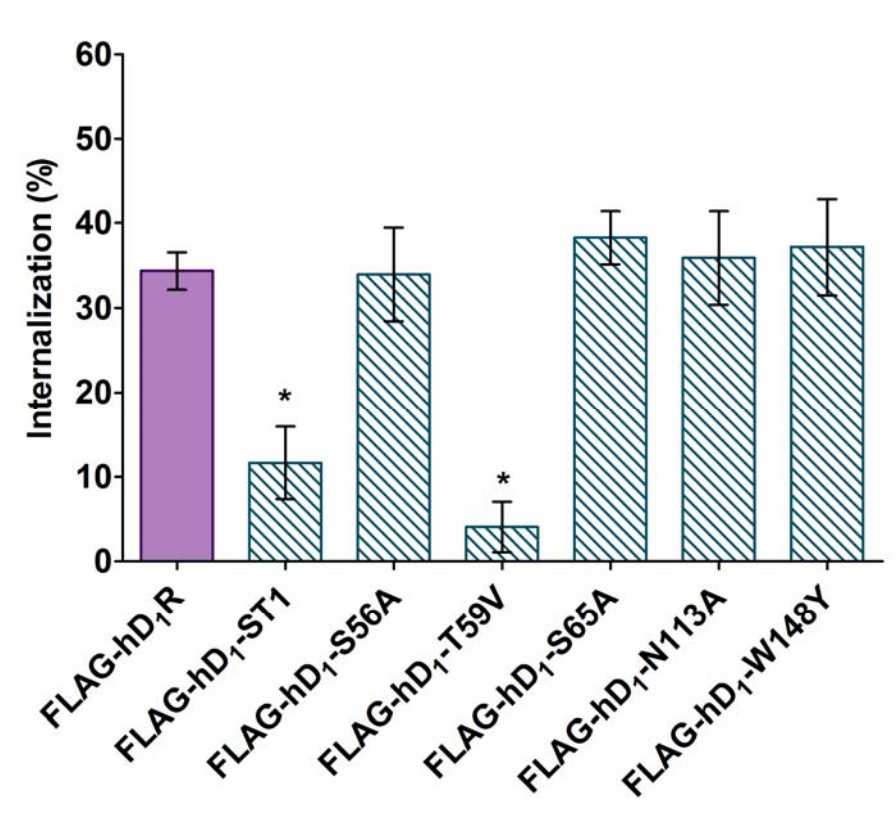

Figure 44. Agonist-induced internalization of hD_1R and mutant receptors assessed using ELISA.

For every receptor condition, % internalization was calculated by the % decrease in cell surface expression following 10 mins treatment with 10 μM of DA (or 10 mM of DA for hD_1-ST1 and hD_1-T59V) relative to that of 10 mins treatment with 0.1 mM AA (vehicle). Each bar represents the arithmetic mean ± S.E. from four to eleven experiments. B_{max} values (pmol/mg of membrane proteins) in arithmetic means ± S.E. were: 1.73 ± 0.19 (FLAG-hD_1R), 1.60 ± 0.19 (FLAG-hD_1-ST1), 2.37 ± 0.33 (FLAG-hD_1-S56A), 2.25 ± 0.31 (FLAG-hD_1-T59V), 0.305 ± 0.024 (FLAG-hD_1-S65A), 0.560 ± 0.077 (FLAG-hD_1-N113A), and 0.985 ± 0.16 (FLAG-hD_1-W148Y). *, $p < 0.05$ when compared with wild-type using multiple *t*-tests with Holm-Sidak correction method.

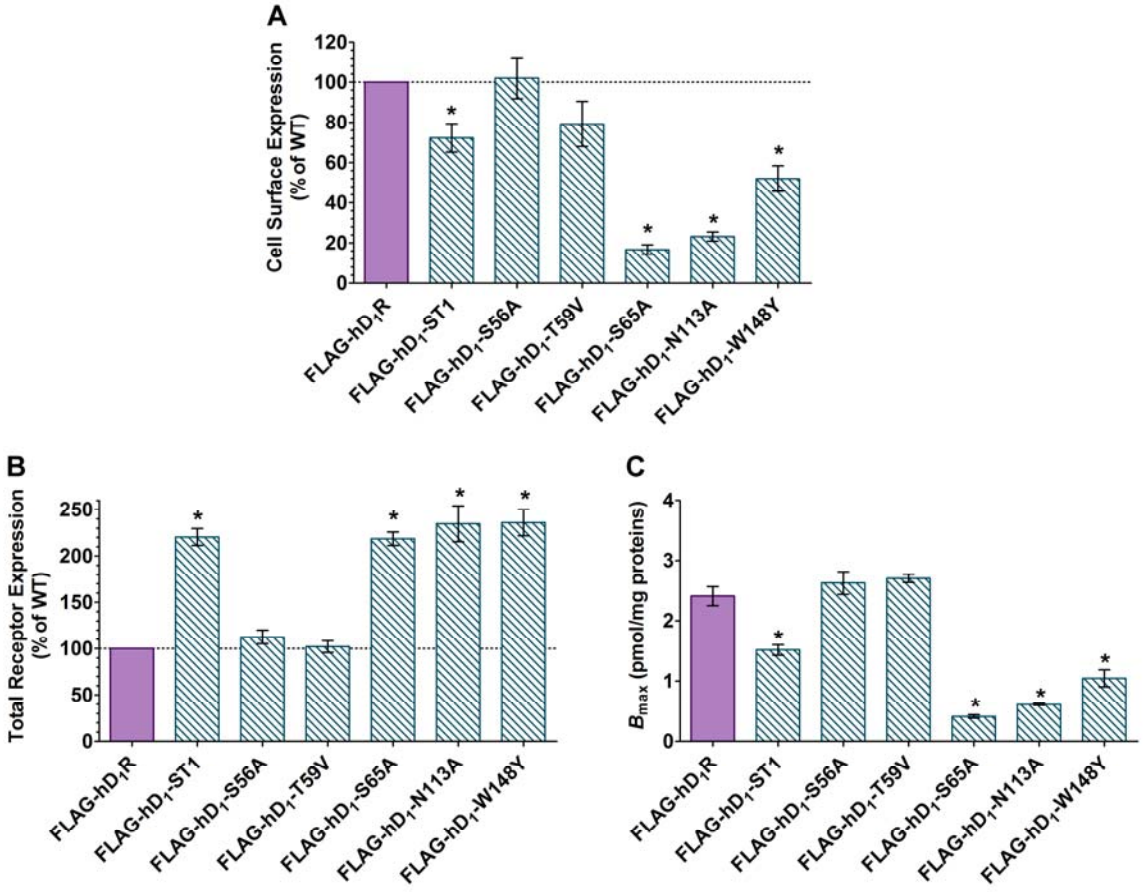

Figure 45. Comparing receptor expression between hD_1R and mutant receptors. (A), (B), and (C) were performed concurrently. Each bar represents the arithmetic mean ± S.E. from three to four experiments. (A and B) Values were calculated by dividing ELISA absorbance at 490 nm (subtracted from mock) relative to that of hD_1R. *, $p < 0.05$ when compared with wild-type (100%) using one sample *t*-test (A and B) or multiple *t*-tests with Holm-Sidak correction method (C). WT, wild-type.

.

Discussion

In the quest to understand the roles of IC1 and IC2 for D_1-class receptors, I have focused on Ser/Thr spanning these regions and have uncovered their functional importance and structural implications. Key findings from my thesis can be grouped into three topics, which are the subtype-specific role of IC2 Ser/Thr, the role of Thr59, and the role of Ser65. Insights into these topics are discussed in this section as well as future studies stemming from my thesis.

1. Comparing functional and structural roles of Ser/Thr in IC2 and IC2/TM3 membrane juncture between D_1-class receptors

Some previous studies have already highlighted the importance of Ser/Thr of IC2. For example, one study has demonstrated a role for $Thr^{3.65}$ in regulating calcium signalling via βγ subunits for the serotonin 1A receptor (Lembo *et al.*, 1997). Another study has implicated $Ser^{3.65}$ in agonist-induced desensitization for serotonin 2A receptor (Gray *et al.*, 2003). However, mutating the positionally equivalent $Thr^{3.65}$ to Ala for the rat D_1R was not found to affect this regulatory machinery (Jiang & Sibley, 1999).

For hD_5R, removing the hydroxyl side-chains of all Ser/Thr of IC2 and IC2/TM3 membrane juncture (i.e. hD_5-ST2) resulted in a significant loss in affinity for DA and DHX. In contrast, this approach for hD_1R (i.e. hD_1-ST2) induced only a slight increase of DA affinity. This could be caused by mutating $Ser^{3.55}$ and $Thr^{3.65}$ to hydrophobic residues within IC2 that may translate into upward perturbations in the TM3 and TM4 regions. Furthermore, as noted previously, the hydroxyl side-chain of $Ser^{3.47}$ adopted a gauche (-) conformation, allowing it to form hydrogen bonds with the main chain of the α-helix (i.e. carbonyl group of $Leu^{3.43}$). Because this intrahelical interaction among Ser/Thr has been

hypothesized to bend α-helices (Ballesteros *et al.*, 2000), the absence of $Ser^{3.47}$ could induce TM3 deviations and also alter the agonist binding pocket.

The ablated basal activity and decreased DA potency of the hD_5-ST2 altogether indicate a loss in G protein coupling. Because the thermodynamic equilibrium of hD_5-ST2 is shifted towards the R state, this may also account for its decreased affinity for agonists. Homology modelling and subsequent refinement using brief MD simulations revealed that $Ser^{3.55}$ and $Thr^{3.65}$ possessed molecular interactions (via their hydroxyl side-chains), which anchor the ends of the loop region of IC2 to the cytoplasmic ends of TM3 and 4 (**Figure 21**). It is possible these interactions serve as "molecular hinges" that are important for IC2 movement during receptor activation. Indeed, spectroscopy studies on rhodopsin report that IC2 moves as a rigid body following photoactivation of rhodopsin (Farahbakhsh *et al.*, 1995). Through mutating these "pivotal" Ser/Thr to Ala/Val and thereby eliminating their side-chain interactions, IC2 movement is not controlled properly and thus prevents the proper positioning of IC2 residues with the G protein. For instance, in the β_2AR-G_s complex, the carbonyl backbone of $Thr^{3.55}$ (i.e. $Ser^{3.55}$ in D_1-class receptors) contacts Arg380 of α5-helix of $G\alpha_s$ subunit, while $Phe^{3.58}$ (conserved in D_1-class receptors) in the middle of IC2 is inserted into the hydrophobic pocket within $G\alpha_s$ (Rasmussen *et al.*, 2011). The IC2 loop of hD_5R was observed to move outward during simulation, but the IC2 loop of hD_5-ST2 did not. Such outward flexibility of IC2 loop may be attributed to the "molecular hinges" of $Ser^{3.55}$ and $Thr^{3.65}$ present in hD_5R but not in hD_5-ST2. A caveat to this interpretation, however, is the short simulation period (10 ns).

In contrast, the hD_1-ST2 demonstrated DA potency and efficacy values that did not indicate a loss in coupling properties relative to hD_1R. Apart from its additional $Ser^{3.56}$, which was not observed to play any structural roles within the receptor during simulation, the hD_1-ST2 possessed the same Ser/Thr mutations and the same loss of Ser/Thr side-chain interactions as hD_5-ST2. Nevertheless, as mentioned previously, hD_5-ST2 was found to lose side-chain interactions between $Ser^{3.55}$ and $Arg^{3.56}$. These contacts were not able to form in either hD_1R or hD_1-ST2 due to the shorter side-chain of Ser3.56. Although it is still unknown how structurally losing $Arg^{3.56}$ contacts within IC2 can be translated functionally, it is possible that the distinct hD_1R and hD_5R landscape can be a contributing factor influencing the subtype-distinct functions of conserved Ser/Thr in IC2 and IC2/TM3 membrane juncture.

In addition to the molecular interactions of IC2 Ser/Thr and their functional implications, the phosphorylation status of these residues should also be mentioned. I have begun to address this matter by performing desensitization assays and demonstrating that both hD_1-ST2 and hD_5-ST2 showed reduced desensitizing capabilities compared to wild-type. This raises the possibility that IC2 Ser/Thr may be either phosphorylated or indirectly affect the phosphorylation of other residues within hD_1R and hD_5R. Even though there are no consensus sites, GRK isoforms tend to phosphorylate Ser/Thr residues with adjacent acidic residues or neighbouring basic residues on the proximal side (Kunapuli & Benovic, 1993, Loudon & Benovic, 1994, Onorato *et al.*, 1991). These criteria are not found for IC2 Ser/Thr of hD_1R and hD_5R. It is also notable to mention that $Thr^{3.65}$ for both hD_1R and hD_5R is situated in a predicted consensus sequence for kinases such as protein kinase A, protein kinase C, protein kinase G, and

p38 mitogen-activated protein kinase (NetPhos 3.1 server; www.cbs.dtu.dk/services/NetPhos/). From a structural standpoint, the impaired desensitization capabilities of hD_1-ST2 and hD_5-ST2 could also be linked to the loss of "molecular hinges" of $Ser^{3.55}$ and $Thr^{3.65}$. For instance, proper IC2 movement may provide better access for kinases (if IC2 is phosphorylated) or "open the door" to kinases to reach their target sites (such as IC3 and CT) in both hD_1R and hD_5R. As noted before, IC2 of Family A GPCRs has been shown to promote β-arrestin binding and β-arrestin-induced internalization (Marion *et al.*, 2006). Intriguingly, the absence of IC2 Ser/Thr did not affect agonist-induced internalization of D_1-class receptors. This adds further evidence from previous studies demonstrating that D_1R desensitization and internalization can be dissociated into independent events (Lamey *et al.*, 2002, Ng *et al.*, 1995).

Although both ST2 mutant receptors exhibited impaired desensitization, the desensitizing response was completely absent in hD_1-ST2 but still present, albeit greatly reduced, in hD_5-ST2. Such subtype-specific differences may contribute towards the increased E_{max} of hD_1-ST2 relative to wild-type, which was not observed in hD_5-ST2. It is also worth mentioning that D_1R has been previously shown to potentially undergo phosphorylation-independent desensitization. Upon truncating its CT, D_1R did not show any detectable basal and DA-induced phosphorylation, but underwent DA-induced desensitization (Jackson *et al.*, 2002). Phosphorylation-independent desensitization has also been reported for other GPCRs including the metabotropic glutamate receptor 1 (mGluR1), which uses its IC2 to directly associate with GRK2 to attenuate signaling independent of kinase activity (Dhami *et al.*, 2005). In another case, intracellular delivery

of IC2 peptides derived from the gonadotropin-releasing hormone (GnRH) receptor suggest that IC2 acts as a phosphorylation-independent inhibitory domain for GnRH receptor coupling to G_q (Shacham *et al.*, 2005). Whether the increased E_{max} of hD_1R-ST2 is related to a defect of similar IC2 mechanisms remains to be established.

2. Functional consequences of breaking the putative molecular interactions of Thr59 in hD_1R

My screening studies with ST1 mutant receptors revealed that Ser/Thr residues in IC1 and IC1/TM2 membrane juncture function similarly among D_1-class receptors. Both ST1 mutant receptors displayed decreased affinities for agonists, ablated basal activities, increased potencies for DA, and elevated E_{max}. The B_{max} was also reduced for both ST1 mutant receptors, which was later reiterated in hD_1-S65A. ELISA and Western blot data indicated that there was a small population of these receptors that traffick from inside the cell to the cell surface. Mutating Thr59 and Ser65 but not Ser56 were primarily responsible for the pleitropic effects of hD_1-ST1. Given Thr59 and Ser65 are conserved in hD_5R (and among other GPCRs; see **Figure 9B**), it is likely for these residues to also dictate the functional traits of hD_5-ST1.

The T59V mutation fully recapitulated the ablated basal activity and drastic loss in DA potency that was initially observed for hD_1-ST1. These pharmacological changes strongly indicate a loss in G protein coupling; however, IC1 is not known to contact the G protein directly as shown by the β_2AR-G_s complex (Rasmussen *et al.*, 2011). Nevertheless, the recurrent molecular interactions of Thr59 among crystallized structures **(Table 9)** may provide mechanistic clues. Upon receptor activation, $Thr^{2.39}$ breaks free

from the (E)DRY motif, and moves closer to interact with $Tyr^{3.60}$ near the centre of IC2. $Tyr^{3.60}$ also interacts with $Asp^{3.49}$ of the (E)DRY motif (regardless of R or R* states). These three residues form a tripartite network that stabilizes IC2 to allow contacts between IC2 and $G\alpha_s$ (Carpenter *et al.*, 2016, Rasmussen *et al.*, 2011). Specifically, this allows for the insertion of $Phe^{3.58}$ of IC2 into a hydrophobic pocket of $G\alpha_s$. Given that $Phe^{3.58}$ and $Tyr^{3.60}$ are conserved in D_1-class receptors (and among other biogenic amine GPCRs; see **Figure 9A),** I propose that by mutating $Thr^{2.39}$ to Val in hD_1R, $Phe^{3.58}$ loses proper support due to the loss of $Thr^{2.39}$-$Tyr^{3.60}$ interaction and consequently, this impairs the insertion of $Phe^{3.58}$ into the hydrophobic pocket of $G\alpha_s$ **(Figure 46)**. The increased uncoupling from the G protein by hD_1-T59V and hD_1-ST1 may also account for their decreased agonist affinities. It is also possible for the T59V mutation to impose topological changes to IC1, which translate into rearrangements of TM1 and TM2. $Asp^{2.50}$ in TM2, which is well conserved among Family A GPCRs, is known to bind to monovalent cations and allosterically modulate agonist binding (Fenalti *et al.*, 2014). Furthermore, TM2 has been demonstrated to dictate the distinct agonist affinities among β_1- and β_2AR (Isogaya *et al.*, 1999).

Another striking feature of hD_1-T59V and hD_1-ST1 is their impaired ability to undergo agonist-induced endocytosis. This could be explained based on the recent crystal structure of rhodopsin bound to arrestin—the only available structure of a GPCR-full arrestin complex to date. When aligned to R* rhodopsin (bound to $G\alpha_t$ fragment), there is remarkable resemblance with a RMSD less than 0.6 Å between the two receptors **(Figure 47A)**. This indicates that arrestin and G protein binds to the same conformation, and potentially via same contacts, of the activated receptor. Likewise, for hD_1-T59V and hD_1-

ST1, their loss in agonist-induced endocytosis may result from losing Phe$^{3.58}$-G protein contacts, which prevents the R* conformation preferred by arrestin or through losing direct contact between Phe$^{3.58}$ and arrestin. In both cases, there would be a loss of arrestin binding. Indeed, the crystal structure of rhodopsin-arrestin complex shows that Met$^{3.58}$ of rhodopsin makes hydrophobic interactions with Val248 and Tyr256 in the C domain of arrestin (Kang *et al.*, 2015) **(Figure 47B)**. Interactions between Met$^{3.58}$ and G protein are currently unknown because the crystal structure of rhodopsin bound to a full G protein has not been solved.

The other arm in the aforementioned tripartite network is the interaction between Tyr$^{3.60}$ and Asp$^{3.49}$. Would breaking this interaction destabilize the insertion of Phe$^{3.58}$ into the G protein and recapitulate the hD$_1$-T59V phenotype? In attempt to address this question, I have constructed and characterized the hD$_1$-D120A mutant receptor. Contrary to hD$_1$-T59V, the hD$_1$-D120A exhibited hallmark properties of a constitutively active mutant receptor (i.e. increases in basal activity, agonist affinity and potency). In fact, for many GPCRs, Ala mutation of Asp$^{3.49}$ leads to a constitutively active mutant receptor (Rovati *et al.*, 2007). Even though the potential Asp$^{3.49}$-Tyr$^{3.60}$ interaction is likely to be broken in hD$_1$-D120A, one must consider the loss of other conserved molecular interactions of Asp$^{3.49}$ and other conserved receptor-G protein contacts. For all crystallized Family A GPCRs either in their R or intermediate R* states, Asp$^{3.49}$ forms an ionic lock with Arg$^{3.50}$. Only in the G protein bound structures does Arg$^{3.50}$ break free from Asp$^{3.49}$ and directly interact with the G protein (Katritch *et al.*, 2013). Removing the inhibitory brake imposed by Asp$^{3.49}$ on Arg$^{3.50}$ (as in hD$_1$-D120A) potentially allows Arg$^{3.50}$ to interact more freely with the G protein. MD simulations have also shown that

charge-neutralizing mutations of $Asp^{3.49}$ increase the disruption of $Arg^{3.50}$-$Glu^{6.30}$ ionic lock and increase the separation of TM3 and TM6 (Dror *et al.*, 2009). This is supported by methanethiosulfonate reagent assays, which show greater accessibility of TM6 cysteine ($Cys^{6.47}$) in $Asp^{3.49}$ mutant receptors (Rasmussen *et al.*, 1999). Increased separation between TM3 and TM6 consequently opens the intracellular cavity of the receptor to allow for extensive interactions between the receptor and the G protein (Rasmussen *et al.*, 2011). These are some possible underlying causes for the constitutively active properties of hD_1-D120A, which counteracts—and overcompensates—the potential loss of contact between $Phe^{3.58}$ and the G protein. Furthermore, $Asp^{3.49}$ already interacts with $Tyr^{3.60}$ in the R state conformations ($A_{2A}R$ (3EML) (see **Figure 31A** for example), β_1AR (2VT4), D_3R (3PBL)). This further alludes to the different facets of receptor activation played by $Asp^{3.49}$ and $Thr^{2.39}$.

Although the hD_1-Y131A mutant receptor recapitulated the ablated basal activity of hD_1-T59V, it also differed from hD_1-T59V by exhibiting increased agonist affinities and only a 10-fold decrease in DA potency. Once again, in an attempt to break the putative Thr59-Tyr131 interaction in hD_1R (during R*), the Y131A mutation may have also affected other molecular interactions of Tyr131 that could have culminated into a functional phenotype distinct from hD_1-T59V. For instance, the $Asp^{3.49}$-$Tyr^{3.60}$ interaction, found in R and R* states of crystallized GPCR structures, is likely to be broken in hD_1-Y131A if it exists in hD_1R. Moreover, $Tyr^{3.60}$ can interact with $Arg^{3.50}$ during the inactive states of β_1AR (2VT4), β_2AR (2RH1), $A_{2A}R$ (3EML), and D_3R (3PBL). The loss of these two potential interactions may affect how the loss of Thr59-Tyr131 interaction shapes the thermodynamic equilibrium of hD_1-Y131A.

The functional activity of hD_1-R121A was investigated because $Thr^{2.39}$ was found to interact with $Arg^{3.50}$ in some GPCR crystal structures (D_3R, δ and κ opioid receptors; see **Table 9**). Interestingly, unlike the hD_1-D120A, the hD_1-R121A did not show any obvious elevations to its basal activity nor did it show a pronounced rightward EC_{50} shift of DA like hD_1-T59V. Rather, the thermodynamic equilibrium of hD_1-R121A was near the middle of these two polar opposites because it displayed DA affinity and potency comparable to wild-type, albeit an elevated E_{max}. One possible explanation for the lack of functional changes in hD_1-R121A could be that $Arg121^{3.50}$ stabilizes both the inactive conformation via ionic locks with $Asp^{3.49}$/$Glu^{6.30}$ and the active conformation through direct interactions with the G protein. Mutating $Arg^{3.50}$ in hD_1R would eliminate these two opposing stabilizing forces, but their absence would functionally balance one another. Indeed, mutating $Arg^{3.50}$ to Ala in the prototypical β_2AR also produced mild affects to receptor function (Valentin-Hansen *et al.*, 2012).

In retrospect, although none of the point mutant receptors fully recapitulated the hD_1-T59V phenotype, the existence of molecular interactions between Thr59 with the (E)DRY motif and Tyr131 of IC2 cannot be ruled out. Rather, my studies underscore the complexity of a network of molecular interactions that connect these residues.

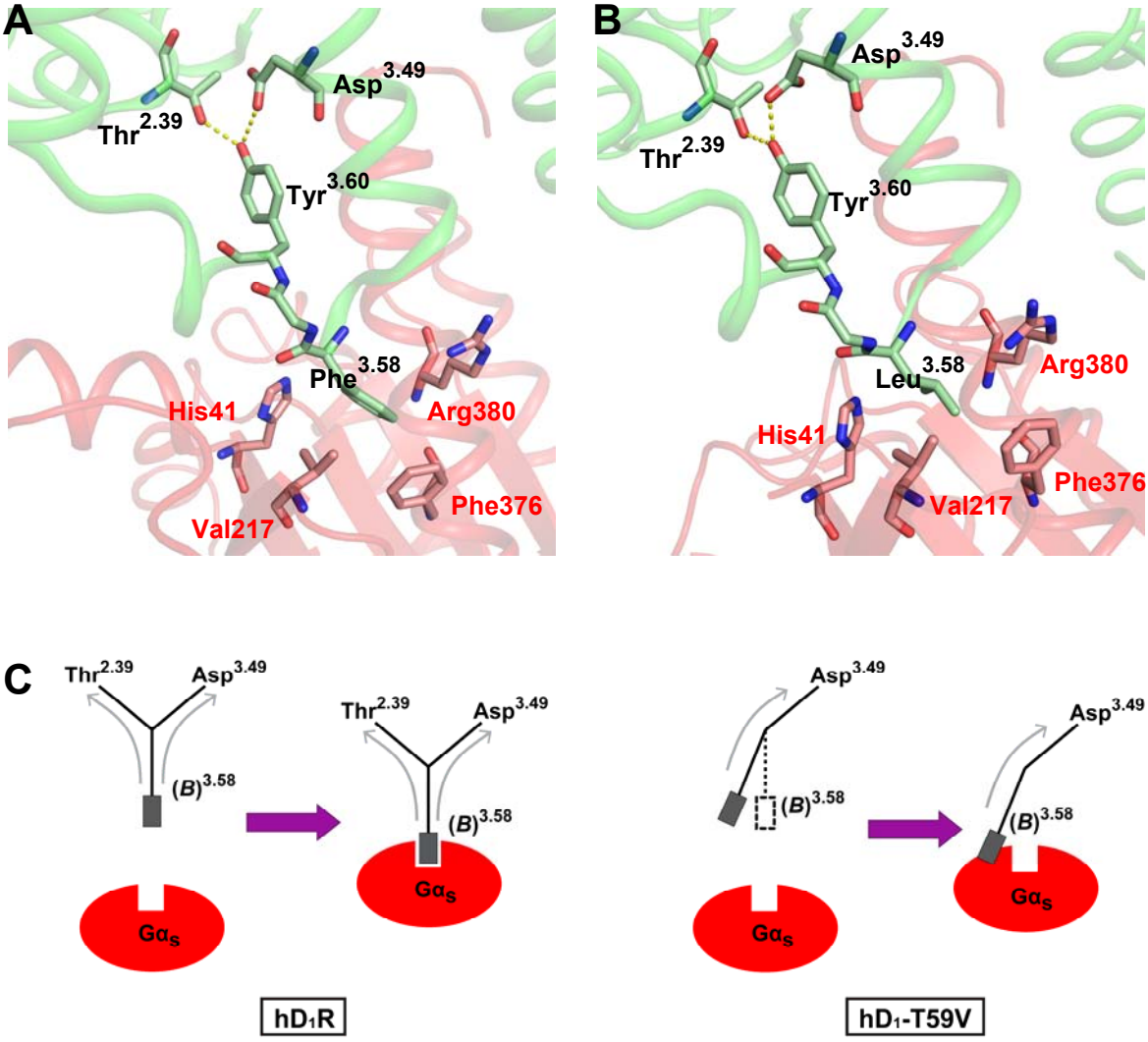

Figure 46. Potential role of conserved Thr$^{2.39}$ among Family A GPCRs.
In the G protein bounds states of β_2AR (A) (3SN6) and A_2AR (B) (5G53), the side-chain of Thr$^{2.39}$, along with Asp$^{3.49}$, interacts with Tyr$^{3.60}$ of IC2 to not only stabilize the helical conformation of IC2 but to also position the helix to facilitate the insertion of a hydrophobic residue at 3.58 into a hydrophobic pocket created by His41, Val217, Phe376, and Arg380 of Gα_s. Peptide backbone linking Tyr$^{3.60}$ to (A) Phe$^{3.58}$ and (B) Leu$^{3.58}$ is also shown. (C) In my proposed model, removing the Thr$^{2.39}$-Tyr$^{3.60}$ interaction causes the hydrophobic residue at 3.58 (denoted by *B*) to lose proper support. Consequently, this impairs the insertion of *B*$^{3.58}$ into the hydrophobic pocket of Gα_s and can account for the abolished basal activity and 260-fold decrease in DA potency in hD$_1$-T59V.

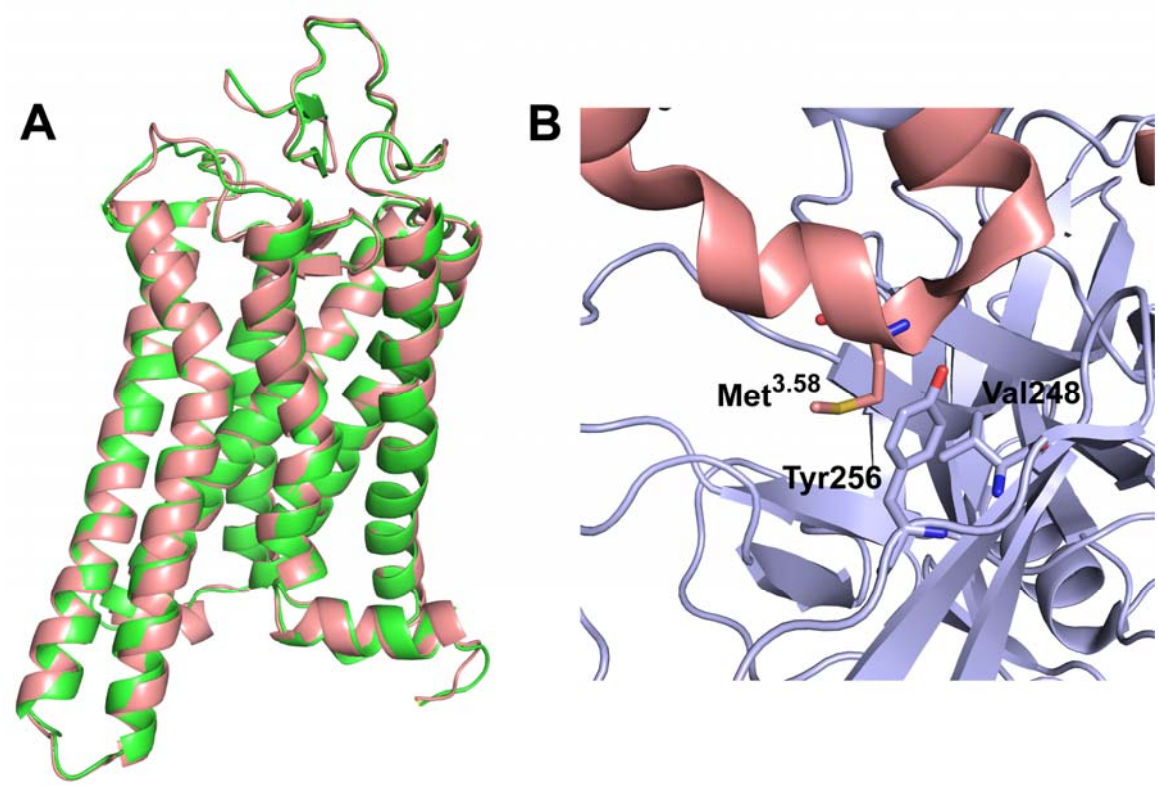

Figure 47. Examining the recent crystal structure of rhodopsin bound to arrestin (4ZWJ).
(A) Structural alignment between rhodopsin bound to $G\alpha_t$ fragment (shown in green; 3PQR) and rhodopsin bound to arrestin (shown in pink; 4ZWJ). G protein and arrestin have been removed for clarity. (B) In the crystal structure of rhodopsin bound to arrestin (4ZWJ), $Met^{3.58}$ within IC2 of rhodopsin (shown in pink) makes hydrophobic interactions with Val248 and Tyr256 in the C domain of arrestin (shown in light blue).

3. Contributions of the Ser65 molecular network towards hD_1R function

The S65A mutation was found solely responsible for the elevated E_{max} of hD_1-ST1. Based on the recurring theme observed in numerous crystallized GPCR structures, the side-chain of Ser65 in hD_1R was predicted to interact with Asn113$^{3.42}$ and/or Trp148$^{4.50}$. The hD_1-N113A resembled the hD_1-S65A in every pharmacological parameter examined (B_{max}, ligand affinity, cAMP signaling, etc.). This strongly indicates that Ser65-Asn113 interaction exists in the hD_1R and contributes towards hD_1R function. Because the hD_1-W148Y exhibited similar properties as the hD_1-S65A including increased agonist affinity and elevated E_{max}, the Ser65-Trp148 interaction is likely to exist in hD_1R and play functional roles analogous to the Ser65-Asn113 interaction. Subtle differences between hD_1-W148Y and hD_1-S65A such as higher B_{max} and DA potency may be reflected by a novel TM2-TM4 interaction by Tyr148 in hD_1-W148Y (**Figure 37**) as a consequence of Tyr148 breaking free from the side-chain of Ser65. Trp$^{4.50}$ has been previously demonstrated to contribute towards ligand binding for cannabinoid CB_2 receptor (Rhee *et al.*, 2000), D_2R (Javitch *et al.*, 2000), and the adenosine A_1 receptor (Suzuki *et al.*, 2009). Trp$^{4.50}$ has also been shown to interact with cholesterol for β_2AR (Hanson *et al.*, 2008). To my knowledge, the functional role of a polar residue at 3.42 is currently unknown.

It seems breaking either the Ser65-Trp148 or the Ser65-Asn113 interaction is sufficient to produce an elevated E_{max} in hD_1R. Although the underlying cellular mechanism has yet to be fully defined, I have shown that some explanations may be ruled out. First, the elevated E_{max} of hD_1-S65A is not due to a higher cell surface expression compared to hD_1R. At a reduced B_{max} level compared to hD_1R, hD_1-S65A produced a

greater cAMP response (**Figure 29B**). Under these circumstances, ELISA detected lower cell surface levels of hD_1-S65A relative to hD_1R. When the B_{max} of hD_1R was lowered to similar levels matching the B_{max} of hD_1-S65A, ELISA detected statistically indistinguishable cell-surface levels between the two receptors (**Figure 29C**). Second, it is unlikely for the hD_1-S65A to possess an enhanced coupling to G_s. Concomitant with its elevated E_{max}, the hD_1-ST1 demonstrated the 260-fold rightward potency shift in DA observed in hD_1-T59V, which I propose is due to a loss in G protein coupling. Nonetheless, to directly validate this claim, future studies employing GTPγS or BRET (bioluminescence resonance energy transfer) are needed. Third, the elevated E_{max} of hD_1-S65A is not attributed by an altered ability to desensitize in the presence of DA compared to wild-type. The desensitizing response for both hD_1R and hD_1-S65A included a 2- to 3-fold decrease in DA potency and a 10% reduction in E_{max}. It should be noted that the 10% decrease in E_{max} for hD_1R is lower compared to **Figure 18**. This could be related to differences in cell confluency and the batch of cells. Fourth, several experiments were repeated to show that hD_1-S65A (as well as hD_1-ST1, hD_1-N113A, and hD_1-W148Y) displayed wild-type abilities to undergo agonist-induced internalization. This regulatory step therefore is not the controlling factor for the elevated E_{max} of hD_1-S65A.

My finding that Dyngo4A interfered with ligand binding to hD_1R and hD_1-S65A is unexpected and to my knowledge, has not been reported by any published studies. I had initially reasoned that Dyngo4a, by blunting cAMP responses of hD_1R and hD_1-S65A, may at least demonstrate the abilities for both receptors to initiate endosomal signalling. Because Dyngo4a lowered [^{3}H]-SCH23390 binding, it may act as a competitive antagonist (like SCH23390), thereby impairing DA binding and diminishing

signalling of hD_1R and hD_1-S65A. Given Pitstop2 also blunted cAMP responses in a similar fashion as Dyngo4a, these non-specific effects may possibly apply to Pitstop2 as well. Furthermore, the chemical structures of Pitstop2 and Dyngo4a do not bear any resemblance towards SCH23390 or negative allosteric modulators (NAMs) of DA receptors such as amiloride and its derivatives (Hoare & Strange, 1996, Hoare *et al.*, 2000) **(Figure 48)**. Interestingly, a portion of Dyngo4a is very similar to the chemical structure of DA.

Nonetheless, one cannot dismiss that Dyngo4a and Pitstop2 indeed prevents agonist-induced endocytosis. Electron micrographs have indicated these compounds do impair the trafficking of synaptic vesicles, which utilize the clathrin machinery (McCluskey *et al.*, 2013, von Kleist *et al.*, 2011). It is possible for Dyngo4a and Pitstop2 to trap D_1R on the cell surface, but as a consequence, transform D_1R into an inactive state—i.e. lowering its agonist affinity and G protein coupling capabilities. Indeed, one study has demonstrated that the D_2R, prior to undergoing endocytosis, reverts to a low-affinity state (Ko *et al.*, 2002).

As implied from **Figure 45**, it is possible for hD_1-S65A to have a greater population of intracellular receptors compared to hD_1R. In fact, an intracellular pool of hD_1R was never detected because mock-corrected ELISA readings in permeabilized cells expressing hD_1R never increased relative to those in non-permeabilized cells expressing hD_1R (not shown in **Figure 45**). The total receptor expression of hD_1-S65A was higher compared to hD_1R most likely because transfected receptor DNA for hD_1-S65A (5 μg) was greater than hD_1R (0.02 μg). Such disparate amounts had been consistently used for hD_1-S65A and hD_1R throughout my studies; for instance, dose-response curves (e.g.

Figure 29B) and assays examining agonist-induced desensitization and internalization. A greater amount of receptor DNA was necessary for the hD_1-S65A due to its low B_{max} and cell-surface levels compared to hD_1R—even at 5 μg of receptor DNA for hD_1-S65A. Furthermore, immunoblot of hD_1-S65A produced bands near 49 kDA (theoretical molecular weight of hD_1R) that was not present in hD_1R lane, and therefore also indicated more intracellular hD_1-S65A receptors compared to the hD_1R population. It is possible for this increased intracellular pool of hD_1-S65A to be linked to the elevated cAMP response of hD_1-S65A (**Figure 49**). If so, determining how this intracellular pool becomes activated may provide answers to unravelling the elevated E_{max} of hD_1-S65A. One scenario could involve activation through signalling crosstalk from activated receptors at cell surface and/or from endosomes. While it is unclear how endosomal receptors become activated, based on diagrams by Kotowski *et al.* and Irannejad *et al.*, DA is transported into the cell through binding to membrane receptors that have been internalized (Irannejad *et al.*, 2013, Kotowski *et al.*, 2011). Thus, another scenario could involve activation using this internalized DA.

On the other hand, it is also possible for cell surface hD_1-S65A receptors to contribute to the elevated E_{max} through either increased endosomal signalling or faster recycling upon internalization. If so, and if only agonist-internalization is blocked, then the elevated E_{max} of hD_1-S65A should decrease to a greater extent compared to the decreased E_{max} of hD_1R relative to control. Unfortunately, due to the non-specific effects of Dyngo4a and potentially Pitstop2, these scenarios remain to be validated.

Pitstop2
(LogP: 4.36)

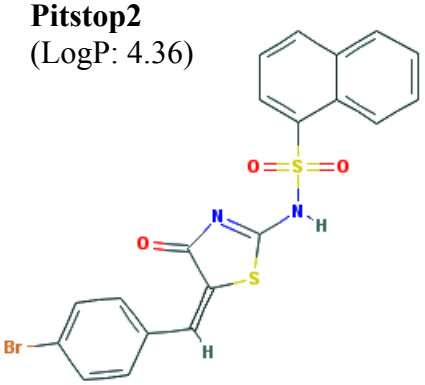

Dyngo4a (LogP: 3.38)

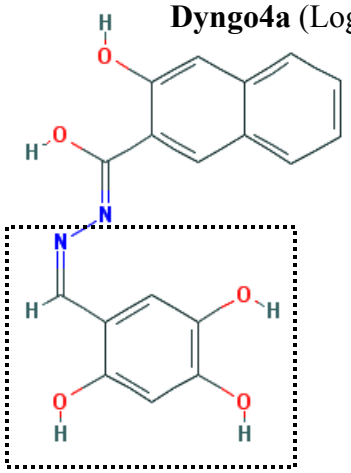

SCH23390 (LogP: 3.94)

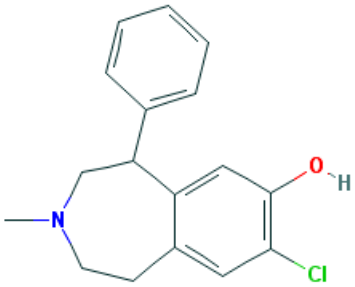

Amiloride (LogP: -0.72)

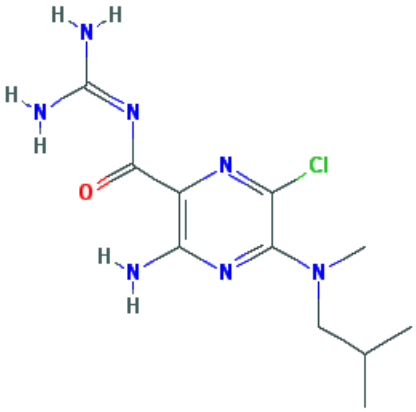

Dopamine (LogP: -0.4)

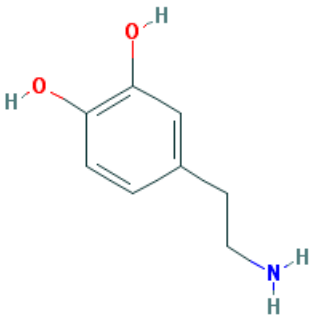

Methylisobutylamiloride
(LogP: 1.37)

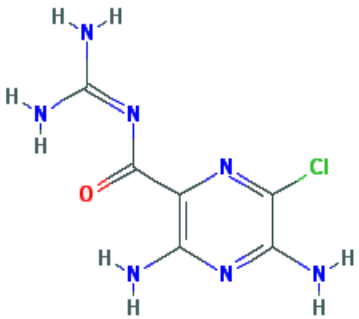

Figure 48. Chemical structure of Pitstop2 and Dyngo4a compared to those of other ligands.
Dashed box indicate similarity to dopamine. Structures were obtained from https://pubchem.ncbi.nlm.nih.gov/. They were then submitted (in .sdf format) to an online version of ALOGPS 2.1 for calculation of LogP values (Tetko *et al.*, 2005). In general, compounds with LogP values below 0.5 are highly water-soluble and may not cross the lipid membrane. Compounds with LogP values above 3 are considered highly lipid-soluble (Kenakin, 2012).

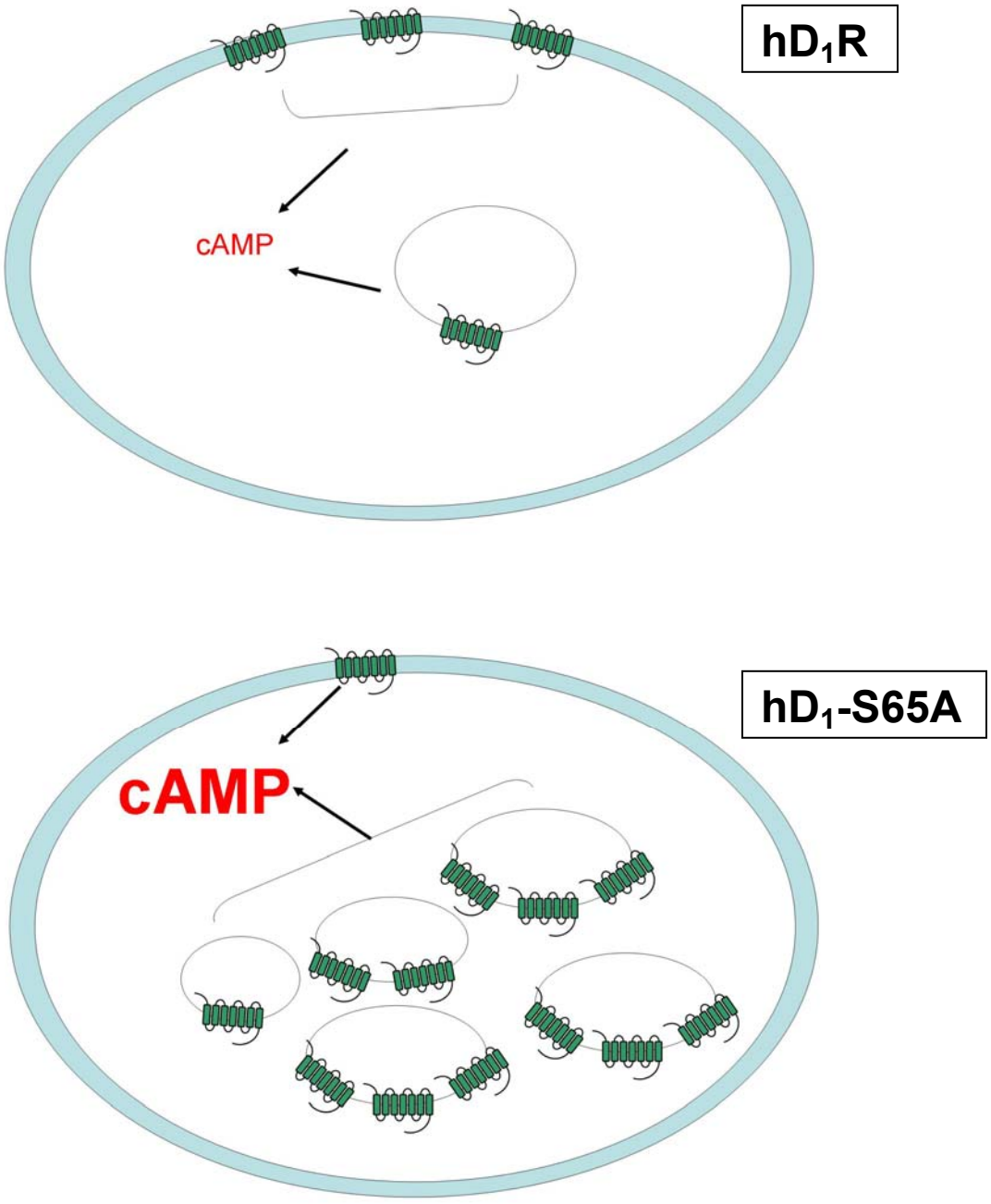

Figure 49. The elevated cAMP response of hD_1-S65A.
As indicated by ELISA, the hD_1-S65A possesses more total receptors compared to hD_1R. Since its cell surface levels are lower than hD_1R, this implies a greater number of hD_1-S65A inside the cell compared to hD_1R.Through an unknown mechanism of activation, this increased intracellular pool may contribute to elevated cAMP response of hD_1-S65A.

4. Concluding Remarks

In my studies of IC1 and IC2 function, I have found that Ser/Thr residues in IC2 and IC2/TM3 membrane juncture play contrasting roles for hD_1R and hD_5R in controlling agonist affinity, basal activity, and DA-mediated cAMP signalling. These findings are significant not only because of their striking differences but also because all Ser/Thr in this region for hD_5R are conserved in hD_1R, with the exception of $Ser^{3.56}$ in hD_1R, which was not observed to make any consistent interactions with its side-chain with other residues during simulation. Refined homology models of hD_1R and hD_5R predicted $Thr^{3.65}$ and $Ser^{3.55}$ are positioned at the ends of the loop region of IC2, which may allow their side-chains to serve as "molecular hinges" stabilizing IC2 loop conformations. Given the short simulation time and the same choice of templates, it is expected for IC2 to adopt similar conformations for hD_1R and hD_5R. Whether this is true remains to be confirmed by crystal structures of hD_1R and hD_5R in the future. Notably, despite high IC2 sequence identity between β_1AR and β_2AR, the loop region of IC2 adopts an α-helical conformation in the inactive crystallized structure of β_1AR (2VT4) compared to an extended conformation in the inactive crystallized structure of β_2AR (2RH1) (Cherezov *et al.*, 2007, Warne *et al.*, 2008). If IC2 is indeed structurally different between hD_1R and hD_5R, this may shed further light into the subtype-specific roles of IC2 Ser/Thr that I have found for these receptors.

In IC1, I have identified Thr59 as a critical residue for hD_1R activation. Mutating Thr59 to Val produced a receptor "locked" in the inactive state and exhibited reduced agonist affinity, basal activity, and DA potency. I propose $Thr59^{2.39}$ utilizes its side-chain to interact with $Tyr131^{3.60}$ to allow the proper insertion of $Phe129^{3.58}$ into a hydrophobic

pocket in $G\alpha_s$. Near the IC1/TM2 membrane juncture, I have discovered that Ser65 is an important regulatory site for hD_1R signalling. Mutating Ser65 to Ala increased the E_{max} induced by DA in hD_1R by over 2-fold. My results strongly implicate this response is a consequence from breaking the side-chain interaction of $Ser65^{2.45}$ with the side-chain of either $Asn113^{3.42}$ or $Trp148^{4.50}$. My results further suggest the elevated E_{max} of hD_1-S65A is not due to higher cell-surface expression, enhanced G protein coupling, or altered agonist-induced desensitization and internalization compared to hD_1R. Given $Thr^{2.39}$ and $Ser^{2.45}$ are conserved among many Family A GPCRs and make recurring molecular interactions in crystal structures, novel findings for $Thr^{2.39}$ and $Ser^{2.45}$ reported herein may be applicable to other Family A GPCRs. Therefore, $Thr^{2.39}$ and $Ser^{2.45}$ may pose as conserved molecular switches within and near IC1, which needs to be accounted for in our current canonical models of GPCR signalling.

While this research has helped us understand the roles of IC1 and IC2 for D_1-class receptors, it has also raised questions, which I hope will serve as catalysts for future studies. One avenue of research is to explore if these Ser/Thr are phosphorylated. Methods can involve detecting the incorporation of [^{32}P]-orthophosphate or employing mass spectrophotometry. It is important to note, based on their predicted position above the plasma membrane, $Ser^{3.47}$ and $Ser^{2.45}$ are not accessible to kinases. Unless $Thr^{2.39}$, $Ser^{3.55}$, and $Thr^{3.65}$ are constitutively phosphorylated, I envision the structural ramifications that I have described for these residues to be related to the initial wave of signalling (i.e. agonist binding and G protein coupling) and should not temporally overlap with agonist-induced phosphorylation and desensitization since the latter processes are thought to occur once the initial wave of signalling is finished (i.e. after G protein

coupling). It will also be interesting to dissect the hD_1-ST2 and hD_5-ST2 by characterizing single point mutant receptors and examining their trajectories during MD simulations. This will provide a more detailed understanding of the subtype-specific roles imposed collectively by Ser/Thr in IC2 and IC2/TM3 membrane juncture that were originally found by the screening study. Regarding the elevated E_{max} of hD_1-S65A, one of my theories involved activation of the intracellular pool of hD_1-S65A with internalized DA. Although this intracellular pool does not bind well to [^{3}H]-SCH23390, as indicated by the lower B_{max} of hD_1-S65A relative to hD_1R, future radioligand binding studies using [^{3}H]-DA should be conducted to examine if the specific binding of hD_1-S65A is higher compared to hD_1R. If so, this will provide the basis for DA-induced activation of a greater intracellular pool of hD_1-S65A compared to hD_1R.

By bridging functional and structural information can we fully appreciate how a receptor works. This will enable us to develop more comprehensive applications in the future. Presently, there are no ligands selective for D_1R or D_5R. A viable alternative in the future may come from the intracellular side in the form of pepducins, which are intracellular loops of GPCRs bound to a lipid moiety that are capable of modulating receptor function (O'Callaghan *et al.*, 2012). Already, some pepducins have been tested with promising results in clinical trials (Gurbel *et al.*, 2016). Because of the contrasting effects of ST2 mutations among D_1-class receptors, one may incorporate such mutations into the design of pepducins to differentially modulate hD_1R and hD_5R signalling. One can also take advantage of the T59V phenotype to make pepducins that act as "off switches". This is important in treating diseases associated with enhanced D_1R signalling such in L-dopa induced dyskinesia—a prevalent and incurable side effect among L-dopa

treated patients with Parkinson's disease (Murer & Moratalla, 2011). Likewise, pepducins serving as "on-switches" may benefit from the increased D_1R signalling in the S65A mutation to alleviate diseases associated with D_1R hypoactivity. For example in the prefrontal cortex, D_1R hypoactivity has been implicated in the cognitive dysfunction of schizophrenia (Barch *et al.*, 2002, Goldman-Rakic *et al.*, 2004). As our knowledge of science and medicine continue to rapidly grow and evolve hand in hand, these ideas and other similar applications, despite seemingly preliminary at the moment, may come to fruition in the future.

References

Adinoff, B. (2004) Neurobiologic processes in drug reward and addiction. *Harv Rev Psychiatry* **12**, 305-320

Alberts, B., Johnson, A., Lewis, J., Raff, M., Roberts, K., Walter, P., Wilson, J., and Hunt, T. (2008) *Molecular biology of the cell*, 5th ed., Garland Science, New York

Alexander, S. P., Davenport, A. P., Kelly, E., Marrion, N., Peters, J. A., Benson, H. E., Faccenda, E., Pawson, A. J., Sharman, J. L., Southan, C., and Davies, J. A. (2015) The Concise Guide to PHARMACOLOGY 2015/16: G protein-coupled receptors. *Br J Pharmacol* **172**, 5744-5869

Ballesteros, J. A., and Weinstein, H. (1995) Integrated methods for the construction of three dimensional models and computational probing of structure-function relations in G-protein coupled receptors. *Methods Neurosci.* **25**, 366-428

Ballesteros, J. A., Deupi, X., Olivella, M., Haaksma, E. E., and Pardo, L. (2000) Serine and threonine residues bend alpha-helices in the chi(1) = g(-) conformation. *Biophys J* **79**, 2754-2760

Barch, D. M., Csernansky, J. G., Conturo, T., and Snyder, A. Z. (2002) Working and long-term memory deficits in schizophrenia: is there a common prefrontal mechanism? *J Abnorm Psychol* **111**, 478-494

Beaulieu, J. M., and Gainetdinov, R. R. (2011) The physiology, signaling, and pharmacology of dopamine receptors. *Pharmacol Rev* **63**, 182-217

Bergson, C., Mrzljak, L., Lidow, M. S., Goldman-Rakic, P. S., and Levenson, R. (1995a) Characterization of subtype-specific antibodies to the human D5 dopamine receptor: studies in primate brain and transfected mammalian cells. *Proc Natl Acad Sci U S A* **92**, 3468-3472

Bergson, C., Mrzljak, L., Smiley, J. F., Pappy, M., Levenson, R., and Goldman-Rakic, P. S. (1995b) Regional, cellular, and subcellular variations in the distribution of D1 and D5 dopamine receptors in primate brain. *J Neurosci* **15**, 7821-7836

Bermak, J. C., Li, M., Bullock, C., and Zhou, Q. Y. (2001) Regulation of transport of the dopamine D1 receptor by a new membrane-associated ER protein. *Nat Cell Biol* **3**, 492-498

Blank, T., Nijholt, I., Teichert, U., Kugler, H., Behrsing, H., Fienberg, A., Greengard, P., and Spiess, J. (1997) The phosphoprotein DARPP-32 mediates cAMP-dependent potentiation of striatal N-methyl-D-aspartate responses. *Proc Natl Acad Sci U S A* **94**, 14859-14864

Brisch, R., Saniotis, A., Wolf, R., Bielau, H., Bernstein, H. G., Steiner, J., Bogerts, B., Braun, K., Jankowski, Z., Kumaratilake, J., Henneberg, M., and Gos, T. (2014) The role of dopamine in schizophrenia from a neurobiological and evolutionary perspective: old fashioned, but still in vogue. *Front Psychiatry* **5**, 47

Burstein, E. S., Spalding, T. A., and Brann, M. R. (1998) The second intracellular loop of the m5 muscarinic receptor is the switch which enables G-protein coupling. *J Biol Chem* **273**, 24322-24327

Calebiro, D., Nikolaev, V. O., Gagliani, M. C., de Filippis, T., Dees, C., Tacchetti, C., Persani, L., and Lohse, M. J. (2009) Persistent cAMP-signals triggered by internalized G-protein-coupled receptors. *PLoS Biol* **7**, e1000172

Carlsson, A., Lindqvist, M., and Magnusson, T. (1957) 3,4-Dihydroxyphenylalanine and 5-hydroxytryptophan as reserpine antagonists. *Nature* **180**, 1200

Carlsson, A., Lindqvist, M., Magnusson, T., and Waldeck, B. (1958) On the presence of 3-hydroxytyramine in brain. *Science* **127**, 471

Carpenter, B., Nehme, R., Warne, T., Leslie, A. G., and Tate, C. G. (2016) Structure of the adenosine A(2A) receptor bound to an engineered G protein. *Nature* **536**, 104-107

Castner, S. A., Goldman-Rakic, P. S., and Williams, G. V. (2004) Animal models of working memory: insights for targeting cognitive dysfunction in schizophrenia. *Psychopharmacology (Berl)* **174**, 111-125

Charpentier, S., Jarvie, K. R., Severynse, D. M., Caron, M. G., and Tiberi, M. (1996) Silencing of the constitutive activity of the dopamine D1B receptor. Reciprocal mutations between D1 receptor subtypes delineate residues underlying activation properties. *J Biol Chem* **271**, 28071-28076

Cherezov, V., Rosenbaum, D. M., Hanson, M. A., Rasmussen, S. G., Thian, F. S., Kobilka, T. S., Choi, H. J., Kuhn, P., Weis, W. I., Kobilka, B. K., and Stevens, R. C. (2007) High-resolution crystal structure of an engineered human beta2-adrenergic G protein-coupled receptor. *Science* **318**, 1258-1265

Chini, B., and Parenti, M. (2004) G-protein coupled receptors in lipid rafts and caveolae: how, when and why do they go there? *J Mol Endocrinol* **32**, 325-338

Cho, W., Taylor, L. P., Mansour, A., and Akil, H. (1995) Hydrophobic residues of the D2 dopamine receptor are important for binding and signal transduction. *J Neurochem* **65**, 2105-2115

Choe, H. W., Kim, Y. J., Park, J. H., Morizumi, T., Pai, E. F., Krauss, N., Hofmann, K. P., Scheerer, P., and Ernst, O. P. (2011) Crystal structure of metarhodopsin II. *Nature* **471**, 651-655

Ciliax, B. J., Nash, N., Heilman, C., Sunahara, R., Hartney, A., Tiberi, M., Rye, D. B., Caron, M. G., Niznik, H. B., and Levey, A. I. (2000) Dopamine D(5) receptor immunolocalization in rat and monkey brain. *Synapse* **37**, 125-145

Cornell, W. D., Cieplak, P., Bayly, C. I., Gould, I. R., Merz, K. M., Ferguson, D. M., Spellmeyer, D. C., Fox, T., Caldwell, J. W., and Kollman, P. A. (1994) A Second Generation Force Field for the Simulation of Proteins, Nucleic Acids, and Organic Molecules. *J. Am. Chem. Soc.* **117**, 5179–5197

Corvol, J. C., Studler, J. M., Schonn, J. S., Girault, J. A., and Herve, D. (2001) Galpha(olf) is necessary for coupling D1 and A2a receptors to adenylyl cyclase in the striatum. *J Neurochem* **76**, 1585-1588

Costa, E. M., Bedecarrats, G. Y., Mendonca, B. B., Arnhold, I. J., Kaiser, U. B., and Latronico, A. C. (2001) Two novel mutations in the gonadotropin-releasing hormone receptor gene in Brazilian patients with hypogonadotropic hypogonadism and normal olfaction. *J Clin Endocrinol Metab* **86**, 2680-2686

D'Aoust, J. P., and Tiberi, M. (2010) Role of the extracellular amino terminus and first membrane-spanning helix of dopamine D1 and D5 receptors in shaping ligand selectivity and efficacy. *Cell Signal* **22**, 106-116

Daubner, S. C., Le, T., and Wang, S. (2011) Tyrosine hydroxylase and regulation of dopamine synthesis. *Arch Biochem Biophys* **508**, 1-12

Dauer, W., and Przedborski, S. (2003) Parkinson's disease: mechanisms and models. *Neuron* **39**, 889-909

Dhami, G. K., Babwah, A. V., Sterne-Marr, R., and Ferguson, S. S. (2005) Phosphorylation-independent regulation of metabotropic glutamate receptor 1 signaling requires g protein-coupled receptor kinase 2 binding to the second intracellular loop. *J Biol Chem* **280**, 24420-24427

Dohlman, H. G., and Thorner, J. (1997) RGS proteins and signaling by heterotrimeric G proteins. *J Biol Chem* **272**, 3871-3874

Downes, G. B., and Gautam, N. (1999) The G protein subunit gene families. *Genomics* **62**, 544-552

Dror, R. O., Arlow, D. H., Borhani, D. W., Jensen, M. O., Piana, S., and Shaw, D. E. (2009) Identification of two distinct inactive conformations of the beta2-adrenergic receptor reconciles structural and biochemical observations. *Proc Natl Acad Sci U S A* **106**, 4689-4694

Dumartin, B., Caille, I., Gonon, F., and Bloch, B. (1998) Internalization of D1 dopamine receptor in striatal neurons in vivo as evidence of activation by dopamine agonists. *J Neurosci* **18**, 1650-1661

Dutta, D., Williamson, C. D., Cole, N. B., and Donaldson, J. G. (2012) Pitstop 2 is a potent inhibitor of clathrin-independent endocytosis. *PLoS One* **7**, e45799

Duvernay, M. T., Dong, C., Zhang, X., Robitaille, M., Hebert, T. E., and Wu, G. (2009) A single conserved leucine residue on the first intracellular loop regulates ER export of G protein-coupled receptors. *Traffic* **10**, 552-566

Fan, Y., Li, C., Guo, J., Hu, G., and Wu, G. (2012) A single lys residue on the first intracellular loop modulates the endoplasmic reticulum export and cell-surface expression of alpha2A-adrenergic receptor. *PLoS One* **7**, e50416

Farahbakhsh, Z. T., Ridge, K. D., Khorana, H. G., and Hubbell, W. L. (1995) Mapping light-dependent structural changes in the cytoplasmic loop connecting helices C and D in rhodopsin: a site-directed spin labeling study. *Biochemistry* **34**, 8812-8819

Feinstein, T. N., Wehbi, V. L., Ardura, J. A., Wheeler, D. S., Ferrandon, S., Gardella, T. J., and Vilardaga, J. P. (2011) Retromer terminates the generation of cAMP by internalized PTH receptors. *Nat Chem Biol* **7**, 278-284

Feinstein, T. N., Yui, N., Webber, M. J., Wehbi, V. L., Stevenson, H. P., King, J. D., Jr., Hallows, K. R., Brown, D., Bouley, R., and Vilardaga, J. P. (2013) Noncanonical control of vasopressin receptor type 2 signaling by retromer and arrestin. *J Biol Chem* **288**, 27849-27860

Felder, C. C., Jose, P. A., and Axelrod, J. (1988) The dopamine-1 agonist, SKF82526, stimulates phospholipase-C activity independent of adenylate cyclase. *J Pharmaco Exp Ther* **248**, 171-175

Fenalti, G., Giguere, P. M., Katritch, V., Huang, X. P., Thompson, A. A., Cherezov, V., Roth, B. L., and Stevens, R. C. (2014) Molecular control of delta-opioid receptor signalling. *Nature* **506**, 191-196

Ferrandon, S., Feinstein, T. N., Castro, M., Wang, B., Bouley, R., Potts, J. T., Gardella, T. J., and Vilardaga, J. P. (2009) Sustained cyclic AMP production by parathyroid hormone receptor endocytosis. *Nat Chem Biol* **5**, 734-742

Fredriksson, R., Lagerstrom, M. C., Lundin, L. G., and Schioth, H. B. (2003) The G-protein-coupled receptors in the human genome form five main families. Phylogenetic analysis, paralogon groups, and fingerprints. *Mol Pharmacol* **63**, 1256-1272

Free, R. B., Hazelwood, L. A., Cabrera, D. M., Spalding, H. N., Namkung, Y., Rankin, M. L., and Sibley, D. R. (2007) D1 and D2 dopamine receptor expression is regulated by direct interaction with the chaperone protein calnexin. *J Biol Chem* **282**, 21285-21300

Friedman, E., Jin, L. Q., Cai, G. P., Hollon, T. R., Drago, J., Sibley, D. R., and Wang, H. Y. (1997) D1-like dopaminergic activation of phosphoinositide hydrolysis is independent of D1A dopamine receptors: evidence from D1A knockout mice. *Mol Pharmacol* **51**, 6-11

Fuxe, K. (1964) Cellular Localization of Monoamines in the Median Eminence and the Infundibular Stem of Some Mammals. *Z Zellforsch Mikrosk Anat* **61**, 710-724

Gainetdinov, R. R., Premont, R. T., Bohn, L. M., Lefkowitz, R. J., and Caron, M. G. (2004) Desensitization of G protein-coupled receptors and neuronal functions. *Annu Rev Neurosci* **27**, 107-144

Gardner, B., Liu, Z. F., Jiang, D., and Sibley, D. R. (2001) The role of phosphorylation/dephosphorylation in agonist-induced desensitization of D1 dopamine receptor function: evidence for a novel pathway for receptor dephosphorylation. *Mol Pharmacol* **59**, 310-321

Gether, U., and Kobilka, B. K. (1998) G protein-coupled receptors. II. Mechanism of agonist activation. *J Biol Chem* **273**, 17979-17982

Giros, B., Sokoloff, P., Martres, M. P., Riou, J. F., Emorine, L. J., and Schwartz, J. C. (1989) Alternative splicing directs the expression of two D2 dopamine receptor isoforms. *Nature* **342**, 923-926

Goldman-Rakic, P. S., Castner, S. A., Svensson, T. H., Siever, L. J., and Williams, G. V. (2004) Targeting the dopamine D1 receptor in schizophrenia: insights for cognitive dysfunction. *Psychopharmacology (Berl)* **174**, 3-16

Gray, J. A., Compton-Toth, B. A., and Roth, B. L. (2003) Identification of two serine residues essential for agonist-induced 5-HT2A receptor desensitization. *Biochemistry* **42**, 10853-10862

Greengard, P., Allen, P. B., and Nairn, A. C. (1999) Beyond the dopamine receptor: the DARPP-32/protein phosphatase-1 cascade. *Neuron* **23**, 435-447

Guo, S., Zhang, X., Zheng, M., Min, C., Wang, Z., Cheon, S. H., Oak, M. H., Nah, S. Y., and Kim, K. M. (2015) Selectivity of commonly used inhibitors of clathrin-mediated and caveolae-dependent endocytosis of G protein-coupled receptors. *Biochim Biophys Acta* **1848**, 2101-2110

Gurbel, P. A., Bliden, K. P., Turner, S. E., Tantry, U. S., Gesheff, M. G., Barr, T. P., Covic, L., and Kuliopulos, A. (2016) Cell-Penetrating Pepducin Therapy Targeting PAR1 in Subjects With Coronary Artery Disease. *Arterioscler Thromb Vasc Biol* **36**, 189-197

Hajjhussein, H., Gardner, L. A., Fujii, N., Anderson, N. M., and Bahouth, S. W. (2013) The hydrophobic amino acid cluster at the cytoplasmic end of transmembrane

helix III modulates the coupling of the beta(1)-adrenergic receptor to G(s). *J Recept Signal Transduct Res* **33**, 79-88

Hanson, M. A., Cherezov, V., Griffith, M. T., Roth, C. B., Jaakola, V. P., Chien, E. Y., Velasquez, J., Kuhn, P., and Stevens, R. C. (2008) A specific cholesterol binding site is established by the 2.8 A structure of the human beta2-adrenergic receptor. *Structure* **16**, 897-905

Herve, D., Le Moine, C., Corvol, J. C., Belluscio, L., Ledent, C., Fienberg, A. A., Jaber, M., Studler, J. M., and Girault, J. A. (2001) Galpha(olf) levels are regulated by receptor usage and control dopamine and adenosine action in the striatum. *J Neurosci* **21**, 4390-4399

Hoare, S. R., and Strange, P. G. (1996) Regulation of D2 dopamine receptors by amiloride and amiloride analogs. *Mol Pharmacol* **50**, 1295-1308

Hoare, S. R., Coldwell, M. C., Armstrong, D., and Strange, P. G. (2000) Regulation of human D(1), d(2(long)), d(2(short)), D(3) and D(4) dopamine receptors by amiloride and amiloride analogues. *Br J Pharmacol* **130**, 1045-1059

Irannejad, R., Tomshine, J. C., Tomshine, J. R., Chevalier, M., Mahoney, J. P., Steyaert, J., Rasmussen, S. G., Sunahara, R. K., El-Samad, H., Huang, B., and von Zastrow, M. (2013) Conformational biosensors reveal GPCR signalling from endosomes. *Nature* **495**, 534-538

Isberg, V., de Graaf, C., Bortolato, A., Cherezov, V., Katritch, V., Marshall, F. H., Mordalski, S., Pin, J. P., Stevens, R. C., Vriend, G., and Gloriam, D. E. (2015) Generic GPCR residue numbers - aligning topology maps while minding the gaps. *Trends Pharmacol Sci* **36**, 22-31

Isogaya, M., Sugimoto, Y., Tanimura, R., Tanaka, R., Kikkawa, H., Nagao, T., and Kurose, H. (1999) Binding pockets of the beta(1)- and beta(2)-adrenergic receptors for subtype-selective agonists. *Mol Pharmacol* **56**, 875-885

Jackson, A., Iwasiow, R. M., and Tiberi, M. (2000) Distinct function of the cytoplasmic tail in human D1-like receptor ligand binding and coupling. *FEBS Lett* **470**, 183-188

Jackson, A., Iwasiow, R. M., Chaar, Z. Y., Nantel, M. F., and Tiberi, M. (2002) Homologous regulation of the heptahelical D1A receptor responsiveness: specific cytoplasmic tail regions mediate dopamine-induced phosphorylation, desensitization and endocytosis. *J Neurochem* **82**, 683-697

Jackson, A., Sedaghat, K., Minerds, K., James, C., and Tiberi, M. (2005) Opposing effects of phorbol-12-myristate-13-acetate, an activator of protein kinase C, on the signaling of structurally related human dopamine D1 and D5 receptors. *J Neurochem* **95**, 1387-1400

Javitch, J. A., Shi, L., Simpson, M. M., Chen, J., Chiappa, V., Visiers, I., Weinstein, H., and Ballesteros, J. A. (2000) The fourth transmembrane segment of the dopamine D2 receptor: accessibility in the binding-site crevice and position in the transmembrane bundle. *Biochemistry* **39**, 12190-12199

Jiang, D., and Sibley, D. R. (1999) Regulation of D(1) dopamine receptors with mutations of protein kinase phosphorylation sites: attenuation of the rate of agonist-induced desensitization. *Mol Pharmacol* **56**, 675-683

Jin, H., Nip, S., O'Dowd, B. F., and George, S. R. (1998) D1 dopamine receptor activity is not altered by a mutation in the first intracellular loop. *Biochim Biophys Acta* **1402**, 165-170

Jin, L. Q., Wang, H. Y., and Friedman, E. (2001) Stimulated D(1) dopamine receptors couple to multiple Galpha proteins in different brain regions. *J Neurochem* **78**, 981-990

Kang, Y., Zhou, X. E., Gao, X., He, Y., Liu, W., Ishchenko, A., Barty, A., White, T. A., Yefanov, O., Han, G. W., Xu, Q., de Waal, P. W., Ke, J., Tan, M. H., Zhang, C., Moeller, A., West, G. M., Pascal, B. D., Van Eps, N., Caro, L. N., Vishnivetskiy, S. A., Lee, R. J., Suino-Powell, K. M., Gu, X., Pal, K., Ma, J., Zhi, X., Boutet, S., Williams, G. J., Messerschmidt, M., Gati, C., Zatsepin, N. A., Wang, D., James, D., Basu, S., Roy-Chowdhury, S., Conrad, C. E., Coe, J., Liu, H., Lisova, S., Kupitz, C., Grotjohann, I., Fromme, R., Jiang, Y., Tan, M., Yang, H., Li, J., Wang, M., Zheng, Z., Li, D., Howe, N., Zhao, Y., Standfuss, J., Diederichs, K., Dong, Y., Potter, C. S., Carragher, B., Caffrey, M., Jiang, H., Chapman, H. N., Spence, J. C., Fromme, P., Weierstall, U., Ernst, O. P., Katritch, V., Gurevich, V. V., Griffin, P. R., Hubbell, W. L., Stevens, R. C., Cherezov, V., Melcher, K., and Xu, H. E. (2015) Crystal structure of rhodopsin bound to arrestin by femtosecond X-ray laser. *Nature* **523**, 561-567

Katritch, V., Cherezov, V., and Stevens, R. C. (2013) Structure-function of the G protein-coupled receptor superfamily. *Annu Rev Pharmacol Toxicol* **53**, 531-556

Kebabian, J. W., and Calne, D. B. (1979) Multiple receptors for dopamine. *Nature* **277**, 93-96

Kelly, E., Bailey, C. P., and Henderson, G. (2008) Agonist-selective mechanisms of GPCR desensitization. *Br J Pharmacol* **153 Suppl 1**, S379-388

Kenakin, T. (2012) *Pharmacology in drug discovery: understanding drug response*, 1st ed., Elsevier, New York

Kim, O. J., Ariano, M. A., Lazzarini, R. A., Levine, M. S., and Sibley, D. R. (2002) Neurofilament-M interacts with the D1 dopamine receptor to regulate cell surface expression and desensitization. *J Neurosci* **22**, 5920-5930

Kim, O. J., Gardner, B. R., Williams, D. B., Marinec, P. S., Cabrera, D. M., Peters, J. D., Mak, C. C., Kim, K. M., and Sibley, D. R. (2004) The role of phosphorylation in D1 dopamine receptor desensitization: evidence for a novel mechanism of arrestin association. *J Biol Chem* **279**, 7999-8010

Ko, F., Seeman, P., Sun, W. S., and Kapur, S. (2002) Dopamine D2 receptors internalize in their low-affinity state. *Neuroreport* **13**, 1017-1020

Kotowski, S. J., Hopf, F. W., Seif, T., Bonci, A., and von Zastrow, M. (2011) Endocytosis promotes rapid dopaminergic signaling. *Neuron* **71**, 278-290

Krieger, E., Darden, T., Nabuurs, S. B., Finkelstein, A., and Vriend, G. (2004) Making optimal use of empirical energy functions: force-field parameterization in crystal space. *Proteins* **57**, 678-683

Kunapuli, P., and Benovic, J. L. (1993) Cloning and expression of GRK5: a member of the G protein-coupled receptor kinase family. *Proc Natl Acad Sci U S A* **90**, 5588-5592

Kwon, Y. G., Huang, H. B., Desdouits, F., Girault, J. A., Greengard, P., and Nairn, A. C. (1997) Characterization of the interaction between DARPP-32 and protein phosphatase 1 (PP-1): DARPP-32 peptides antagonize the interaction of PP-1 with binding proteins. *Proc Natl Acad Sci U S A* **94**, 3536-3541

Lamb, M. E., De Weerd, W. F., and Leeb-Lundberg, L. M. (2001) Agonist-promoted trafficking of human bradykinin receptors: arrestin- and dynamin-independent sequestration of the B2 receptor and bradykinin in HEK293 cells. *Biochem J* **355**, 741-750

Lamey, M., Thompson, M., Varghese, G., Chi, H., Sawzdargo, M., George, S. R., and O'Dowd, B. F. (2002) Distinct residues in the carboxyl tail mediate agonist-induced desensitization and internalization of the human dopamine D1 receptor. *J Biol Chem* **277**, 9415-9421

Laskowski, R. A., MacArthur, M. W., Moss, D. S., and Thornton, J. M. (1993) PROCHECK - a program to check the stereochemical quality of protein structures. *J. App. Cryst.* **26**, 283-291

Lee, F. J., Xue, S., Pei, L., Vukusic, B., Chery, N., Wang, Y., Wang, Y. T., Niznik, H. B., Yu, X. M., and Liu, F. (2002) Dual regulation of NMDA receptor functions by direct protein-protein interactions with the dopamine D1 receptor. *Cell* **111**, 219-230

Lee, S. M., Yang, Y., and Mailman, R. B. (2014) Dopamine D1 receptor signaling: does GalphaQ-phospholipase C actually play a role? *J Pharmacol Exp Ther* **351**, 9-17

Lee, S. P., So, C. H., Rashid, A. J., Varghese, G., Cheng, R., Lanca, A. J., O'Dowd, B. F., and George, S. R. (2004) Dopamine D1 and D2 receptor Co-activation generates a novel phospholipase C-mediated calcium signal. *J Biol Chem* **279**, 35671-35678

Lembo, P. M., Ghahremani, M. H., Morris, S. J., and Albert, P. R. (1997) A conserved threonine residue in the second intracellular loop of the 5-hydroxytryptamine 1A receptor directs signaling specificity. *Mol Pharmacol* **52**, 164-171

Lewis, M. M., Watts, V. J., Lawler, C. P., Nichols, D. E., and Mailman, R. B. (1998) Homologous desensitization of the D1A dopamine receptor: efficacy in causing desensitization dissociates from both receptor occupancy and functional potency. *J Pharmacol Exp Ther* **286**, 345-353

Liashkovich, I., Pasrednik, D., Prystopiuk, V., Rosso, G., Oberleithner, H., and Shahin, V. (2015) Clathrin inhibitor Pitstop-2 disrupts the nuclear pore complex permeability barrier. *Sci Rep* **5**, 9994

Liu, F., Wan, Q., Pristupa, Z. B., Yu, X. M., Wang, Y. T., and Niznik, H. B. (2000) Direct protein-protein coupling enables cross-talk between dopamine D5 and gamma-aminobutyric acid A receptors. *Nature* **403**, 274-280

Lomize, M. A., Pogozheva, I. D., Joo, H., Mosberg, H. I., and Lomize, A. L. (2012) OPM database and PPM web server: resources for positioning of proteins in membranes. *Nucleic Acids Res* **40**, D370-376

Loudon, R. P., and Benovic, J. L. (1994) Expression, purification, and characterization of the G protein-coupled receptor kinase GRK6. *J Biol Chem* **269**, 22691-22697

Luttrell, L. M., and Lefkowitz, R. J. (2002) The role of beta-arrestins in the termination and transduction of G-protein-coupled receptor signals. *J Cell Sci* **115**, 455-465

Luttrell, L. M. (2008) Reviews in molecular biology and biotechnology: transmembrane signaling by G protein-coupled receptors. *Mol Biotechnol* **39**, 239-264

Lyons, D. J., Hellysaz, A., and Broberger, C. (2012) Prolactin regulates tuberoinfundibular dopamine neuron discharge pattern: novel feedback control mechanisms in the lactotrophic axis. *J Neurosci* **32**, 8074-8083

Macey, T. A., Liu, Y., Gurevich, V. V., and Neve, K. A. (2005) Dopamine D1 receptor interaction with arrestin3 in neostriatal neurons. *J Neurochem* **93**, 128-134

Malo, M., Brive, L., Luthman, K., and Svensson, P. (2012) Investigation of D(1) receptor-agonist interactions and D(1)/D(2) agonist selectivity using a combination of pharmacophore and receptor homology modeling. *ChemMedChem* **7**, 483-494

Marion, S., Oakley, R. H., Kim, K. M., Caron, M. G., and Barak, L. S. (2006) A beta-arrestin binding determinant common to the second intracellular loops of rhodopsin family G protein-coupled receptors. *J Biol Chem* **281**, 2932-2938

Martin-Negrier, M., Charron, G., and Bloch, B. (2000) Agonist stimulation provokes dendritic and axonal dopamine D(1) receptor redistribution in primary cultures of striatal neurons. *Neuroscience* **99**, 257-266

Martin-Negrier, M. L., Charron, G., and Bloch, B. (2006) Receptor recycling mediates plasma membrane recovery of dopamine D1 receptors in dendrites and axons after agonist-induced endocytosis in primary cultures of striatal neurons. *Synapse* **60**, 194-204

Mason, J. N., Kozell, L. B., and Neve, K. A. (2002) Regulation of dopamine D(1) receptor trafficking by protein kinase A-dependent phosphorylation. *Mol Pharmacol* **61**, 806-816

McCluskey, A., Daniel, J. A., Hadzic, G., Chau, N., Clayton, E. L., Mariana, A., Whiting, A., Gorgani, N. N., Lloyd, J., Quan, A., Moshkanbaryans, L., Krishnan, S., Perera, S., Chircop, M., von Kleist, L., McGeachie, A. B., Howes, M. T., Parton, R. G., Campbell, M., Sakoff, J. A., Wang, X., Sun, J. Y., Robertson, M. J., Deane, F. M., Nguyen, T. H., Meunier, F. A., Cousin, M. A., and Robinson, P. J. (2013) Building a better dynasore: the dyngo compounds potently inhibit dynamin and endocytosis. *Traffic* **14**, 1272-1289

McDonald, I. K., and Thornton, J. M. (1994) Satisfying hydrogen bonding potential in proteins. *J Mol Biol* **238**, 777-793

Meador-Woodruff, J. H., Mansour, A., Healy, D. J., Kuehn, R., Zhou, Q. Y., Bunzow, J. R., Akil, H., Civelli, O., and Watson, S. J., Jr. (1991) Comparison of the distributions of D1 and D2 dopamine receptor mRNAs in rat brain. *Neuropsychopharmacology* **5**, 231-242

Meador-Woodruff, J. H., Mansour, A., Grandy, D. K., Damask, S. P., Civelli, O., and Watson, S. J., Jr. (1992) Distribution of D5 dopamine receptor mRNA in rat brain. *Neurosci Lett* **145**, 209-212

Mente, S., Guilmette, E., Salafia, M., and Gray, D. (2015) Dopamine D1 receptor-agonist interactions: A mutagenesis and homology modeling study. *Bioorg Med Chem Lett* **25**, 2106-2111

Missale, C., Nash, S. R., Robinson, S. W., Jaber, M., and Caron, M. G. (1998) Dopamine receptors: from structure to function. *Physiol Rev* **78**, 189-225

Moro, O., Lameh, J., Hogger, P., and Sadee, W. (1993) Hydrophobic amino acid in the i2 loop plays a key role in receptor-G protein coupling. *J Biol Chem* **268**, 22273-22276

Munoz, P., Huenchuguala, S., Paris, I., and Segura-Aguilar, J. (2012) Dopamine oxidation and autophagy. *Parkinsons Dis* **2012**, 920953

Murer, M. G., and Moratalla, R. (2011) Striatal Signaling in L-DOPA-Induced Dyskinesia: Common Mechanisms with Drug Abuse and Long Term Memory Involving D1 Dopamine Receptor Stimulation. *Front Neuroanat* **5**, 51

Neve, K. A., Seamans, J. K., and Trantham-Davidson, H. (2004) Dopamine receptor signaling. *J Recept Signal Transduct Res* **24**, 165-205

New, D. C., and Wong, Y. H. (2007) Molecular mechanisms mediating the G protein-coupled receptor regulation of cell cycle progression. *J Mol Signal* **2**, 2

Ng, G. Y., Trogadis, J., Stevens, J., Bouvier, M., O'Dowd, B. F., and George, S. R. (1995) Agonist-induced desensitization of dopamine D1 receptor-stimulated adenylyl cyclase activity is temporally and biochemically separated from D1 receptor internalization. *Proc Natl Acad Sci U S A* **92**, 10157-10161

O'Callaghan, K., Kuliopulos, A., and Covic, L. (2012) Turning receptors on and off with intracellular pepducins: new insights into G-protein-coupled receptor drug development. *J Biol Chem* **287**, 12787-12796

Oakley, R. H., Laporte, S. A., Holt, J. A., Barak, L. S., and Caron, M. G. (1999) Association of beta-arrestin with G protein-coupled receptors during clathrin-mediated endocytosis dictates the profile of receptor resensitization. *J Biol Chem* **274**, 32248-32257

Oakley, R. H., Laporte, S. A., Holt, J. A., Caron, M. G., and Barak, L. S. (2000) Differential affinities of visual arrestin, beta arrestin1, and beta arrestin2 for G protein-coupled receptors delineate two major classes of receptors. *J Biol Chem* **275**, 17201-17210

Oakley, R. H., Laporte, S. A., Holt, J. A., Barak, L. S., and Caron, M. G. (2001) Molecular determinants underlying the formation of stable intracellular G protein-coupled receptor-beta-arrestin complexes after receptor endocytosis*. *J Biol Chem* **276**, 19452-19460

Onorato, J. J., Palczewski, K., Regan, J. W., Caron, M. G., Lefkowitz, R. J., and Benovic, J. L. (1991) Role of acidic amino acids in peptide substrates of the beta-adrenergic receptor kinase and rhodopsin kinase. *Biochemistry* **30**, 5118-5125

Palczewski, K., Kumasaka, T., Hori, T., Behnke, C. A., Motoshima, H., Fox, B. A., Le Trong, I., Teller, D. C., Okada, T., Stenkamp, R. E., Yamamoto, M., and Miyano, M. (2000) Crystal structure of rhodopsin: A G protein-coupled receptor. *Science* **289**, 739-745

Paolillo, M., Montecucco, A., Zanassi, P., and Schinelli, S. (1998) Potentiation of dopamine-induced cAMP formation by group I metabotropic glutamate receptors via protein kinase C in cultured striatal neurons. *Eur J Neurosci* **10**, 1937-1945

Parent, A., Laroche, G., Hamelin, E., and Parent, J. L. (2008) RACK1 regulates the cell surface expression of the G protein-coupled receptor for thromboxane A(2). *Traffic* **9**, 394-407

Park, R. J., Shen, H., Liu, L., Liu, X., Ferguson, S. M., and De Camilli, P. (2013) Dynamin triple knockout cells reveal off target effects of commonly used dynamin inhibitors. *J Cell Sci* **126**, 5305-5312

Pei, L., Lee, F. J., Moszczynska, A., Vukusic, B., and Liu, F. (2004) Regulation of dopamine D1 receptor function by physical interaction with the NMDA receptors. *J Neurosci* **24**, 1149-1158

Pierce, K. L., and Lefkowitz, R. J. (2001) Classical and new roles of beta-arrestins in the regulation of G-protein-coupled receptors. *Nat Rev Neurosci* **2**, 727-733

Pierce, K. L., Premont, R. T., and Lefkowitz, R. J. (2002) Seven-transmembrane receptors. *Nat Rev Mol Cell Biol* **3**, 639-650

Plonk, S. G., Park, S. K., and Exton, J. H. (1998) The alpha-subunit of the heterotrimeric G protein G13 activates a phospholipase D isozyme by a pathway requiring Rho family GTPases. *J Biol Chem* **273**, 4823-4826

Plouffe, B., D'Aoust, J. P., Laquerre, V., Liang, B., and Tiberi, M. (2010) Probing the constitutive activity among dopamine D1 and D5 receptors and their mutants. *Methods Enzymol* **484**, 295-328

Plouffe, B., Yang, X., and Tiberi, M. (2012) The third intracellular loop of D1 and D5 dopaminergic receptors dictates their subtype-specific PKC-induced sensitization and desensitization in a receptor conformation-dependent manner. *Cell Signal* **24**, 106-118

Pollock, N. J., Manelli, A. M., Hutchins, C. W., Steffey, M. E., MacKenzie, R. G., and Frail, D. E. (1992) Serine mutations in transmembrane V of the dopamine D1 receptor affect ligand interactions and receptor activation. *J Biol Chem* **267**, 17780-17786

Preta, G., Cronin, J. G., and Sheldon, I. M. (2015) Dynasore - not just a dynamin inhibitor. *Cell Commun Signal* **13**, 24

Rajagopal, S., Rajagopal, K., and Lefkowitz, R. J. (2010) Teaching old receptors new tricks: biasing seven-transmembrane receptors. *Nat Rev Drug Discov* **9**, 373-386

Rankin, M. L., Marinec, P. S., Cabrera, D. M., Wang, Z., Jose, P. A., and Sibley, D. R. (2006) The D1 dopamine receptor is constitutively phosphorylated by G protein-coupled receptor kinase 4. *Mol Pharmacol* **69**, 759-769

Rashid, A. J., So, C. H., Kong, M. M., Furtak, T., El-Ghundi, M., Cheng, R., O'Dowd, B. F., and George, S. R. (2007) D1-D2 dopamine receptor heterooligomers with unique pharmacology are coupled to rapid activation of Gq/11 in the striatum. *Proc Natl Acad Sci U S A* **104**, 654-659

Rasmussen, S. G., Jensen, A. D., Liapakis, G., Ghanouni, P., Javitch, J. A., and Gether, U. (1999) Mutation of a highly conserved aspartic acid in the beta2 adrenergic receptor: constitutive activation, structural instability, and conformational rearrangement of transmembrane segment 6. *Mol Pharmacol* **56**, 175-184

Rasmussen, S. G., DeVree, B. T., Zou, Y., Kruse, A. C., Chung, K. Y., Kobilka, T. S., Thian, F. S., Chae, P. S., Pardon, E., Calinski, D., Mathiesen, J. M., Shah, S. T., Lyons, J. A., Caffrey, M., Gellman, S. H., Steyaert, J., Skiniotis, G., Weis, W. I., Sunahara, R. K., and Kobilka, B. K. (2011) Crystal structure of the beta2 adrenergic receptor-Gs protein complex. *Nature* **477**, 549-555

Rhee, M. H., Nevo, I., Bayewitch, M. L., Zagoory, O., and Vogel, Z. (2000) Functional role of tryptophan residues in the fourth transmembrane domain of the CB(2) cannabinoid receptor. *J Neurochem* **75**, 2485-2491

Rosenthal, W., Antaramian, A., Gilbert, S., and Birnbaumer, M. (1993) Nephrogenic diabetes insipidus. A V2 vasopressin receptor unable to stimulate adenylyl cyclase. *J Biol Chem* **268**, 13030-13033

Ross, E. M., and Wilkie, T. M. (2000) GTPase-activating proteins for heterotrimeric G proteins: regulators of G protein signaling (RGS) and RGS-like proteins. *Annu Rev Biochem* **69**, 795-827

Rovati, G. E., Capra, V., and Neubig, R. R. (2007) The highly conserved DRY motif of class A G protein-coupled receptors: beyond the ground state. *Mol Pharmacol* **71**, 959-964

Sahu, A., Tyeryar, K. R., Vongtau, H. O., Sibley, D. R., and Undieh, A. S. (2009) D5 dopamine receptors are required for dopaminergic activation of phospholipase C. *Mol Pharmacol* **75**, 447-453

Samama, P., Cotecchia, S., Costa, T., and Lefkowitz, R. J. (1993) A mutation-induced activated state of the beta 2-adrenergic receptor. Extending the ternary complex model. *J Biol Chem* **268**, 4625-4636

Scheerer, P., Park, J. H., Hildebrand, P. W., Kim, Y. J., Krauss, N., Choe, H. W., Hofmann, K. P., and Ernst, O. P. (2008) Crystal structure of opsin in its G-protein-interacting conformation. *Nature* **455**, 497-502

Schiffmann, S. N., Lledo, P. M., and Vincent, J. D. (1995) Dopamine D1 receptor modulates the voltage-gated sodium current in rat striatal neurones through a protein kinase A. *J Physiol* **483 (Pt 1)**, 95-107

Schiffmann, S. N., Desdouits, F., Menu, R., Greengard, P., Vincent, J. D., Vanderhaeghen, J. J., and Girault, J. A. (1998) Modulation of the voltage-gated sodium current in rat striatal neurons by DARPP-32, an inhibitor of protein phosphatase. *Eur J Neurosci* **10**, 1312-1320

Schinelli, S., Paolillo, M., and Corona, G. L. (1994) Modulation of dopamine-induced cAMP production in rat striatal cultures by the calcium ionophore A23187 and by phorbol-12-myristate-13-acetate. *Brain Res Mol Brain Res* **21**, 162-166

Schoneberg, T., Schulz, A., Biebermann, H., Hermsdorf, T., Rompler, H., and Sangkuhl, K. (2004) Mutant G-protein-coupled receptors as a cause of human diseases. *Pharmacol Ther* **104**, 173-206

Scott, L., Zelenin, S., Malmersjo, S., Kowalewski, J. M., Markus, E. Z., Nairn, A. C., Greengard, P., Brismar, H., and Aperia, A. (2006) Allosteric changes of the NMDA receptor trap diffusible dopamine 1 receptors in spines. *Proc Natl Acad Sci U S A* **103**, 762-767

Seachrist, J. L., and Ferguson, S. S. (2003) Regulation of G protein-coupled receptor endocytosis and trafficking by Rab GTPases. *Life Sci* **74**, 225-235

Sedaghat, K., and Tiberi, M. (2011) Cytoplasmic tail of D1 dopaminergic receptor differentially regulates desensitization and phosphorylation by G protein-coupled receptor kinase 2 and 3. *Cell Signal* **23**, 180-192

Shacham, S., Cheifetz, M. N., Fridkin, M., Pawson, A. J., Millar, R. P., and Naor, Z. (2005) Identification of Ser153 in ICL2 of the gonadotropin-releasing hormone

(GnRH) receptor as a phosphorylation-independent site for inhibition of Gq coupling. *J Biol Chem* **280**, 28981-28988

Shaywitz, A. J., and Greenberg, M. E. (1999) CREB: a stimulus-induced transcription factor activated by a diverse array of extracellular signals. *Annu Rev Biochem* **68**, 821-861

Sherman, W., Day, T., Jacobson, M. P., Friesner, R. A., and Farid, R. (2006) Novel procedure for modeling ligand/receptor induced fit effects. *Journal of Medicinal Chemistry* **49**, 534-553

Siehler, S. (2009) Regulation of RhoGEF proteins by G12/13-coupled receptors. *Br J Pharmacol* **158**, 41-49

Smith, C. M., Haucke, V., McCluskey, A., Robinson, P. J., and Chircop, M. (2013) Inhibition of clathrin by pitstop 2 activates the spindle assembly checkpoint and induces cell death in dividing HeLa cancer cells. *Mol Cancer* **12**, 4

Sugamori, K. S., Scheideler, M. A., Vernier, P., and Niznik, H. B. (1998) Dopamine D1B receptor chimeras reveal modulation of partial agonist activity by carboxyl-terminal tail sequences. *J Neurochem* **71**, 2593-2599

Sung, C. H., Davenport, C. M., Hennessey, J. C., Maumenee, I. H., Jacobson, S. G., Heckenlively, J. R., Nowakowski, R., Fishman, G., Gouras, P., and Nathans, J. (1991) Rhodopsin mutations in autosomal dominant retinitis pigmentosa. *Proc Natl Acad Sci U S A* **88**, 6481-6485

Sung, C. H., Makino, C., Baylor, D., and Nathans, J. (1994) A rhodopsin gene mutation responsible for autosomal dominant retinitis pigmentosa results in a protein that is defective in localization to the photoreceptor outer segment. *J Neurosci* **14**, 5818-5833

Surmeier, D. J., Bargas, J., Hemmings, H. C., Jr., Nairn, A. C., and Greengard, P. (1995) Modulation of calcium currents by a D1 dopaminergic protein kinase/phosphatase cascade in rat neostriatal neurons. *Neuron* **14**, 385-397

Suzuki, T., Namba, K., Yamagishi, R., Kaneko, H., Haga, T., and Nakata, H. (2009) A highly conserved tryptophan residue in the fourth transmembrane domain of the A adenosine receptor is essential for ligand binding but not receptor homodimerization. *J Neurochem* **110**, 1352-1362

Tam, B. M., Moritz, O. L., Hurd, L. B., and Papermaster, D. S. (2000) Identification of an outer segment targeting signal in the COOH terminus of rhodopsin using transgenic Xenopus laevis. *J Cell Biol* **151**, 1369-1380

Tetko, I. V., Gasteiger, J., Todeschini, R., Mauri, A., Livingstone, D., Ertl, P., Palyulin, V. A., Radchenko, E. V., Zefirov, N. S., Makarenko, A. S., Tanchuk, V. Y., and Prokopenko, V. V. (2005) Virtual computational chemistry laboratory--design and description. *J Comput Aided Mol Des* **19**, 453-463

Thompson, D., and Whistler, J. L. (2011) Trafficking properties of the D5 dopamine receptor. *Traffic* **12**, 644-656

Thomsen, A. R., Plouffe, B., Cahill, T. J., 3rd, Shukla, A. K., Tarrasch, J. T., Dosey, A. M., Kahsai, A. W., Strachan, R. T., Pani, B., Mahoney, J. P., Huang, L., Breton, B., Heydenreich, F. M., Sunahara, R. K., Skiniotis, G., Bouvier, M., and Lefkowitz, R. J. (2016) GPCR-G Protein-beta-Arrestin Super-Complex Mediates Sustained G Protein Signaling. *Cell* **166**, 907-919

Tiberi, M., Jarvie, K. R., Silvia, C., Falardeau, P., Gingrich, J. A., Godinot, N., Bertrand, L., Yang-Feng, T. L., Fremeau, R. T., Jr., and Caron, M. G. (1991) Cloning, molecular characterization, and chromosomal assignment of a gene encoding a second D1 dopamine receptor subtype: differential expression pattern in rat brain compared with the D1A receptor. *Proc Natl Acad Sci U S A* **88**, 7491-7495

Tiberi, M., and Caron, M. G. (1994) High agonist-independent activity is a distinguishing feature of the dopamine D1B receptor subtype. *J Biol Chem* **269**, 27925-27931

Tiberi, M., Nash, S. R., Bertrand, L., Lefkowitz, R. J., and Caron, M. G. (1996) Differential regulation of dopamine D1A receptor responsiveness by various G protein-coupled receptor kinases. *J Biol Chem* **271**, 3771-3778

Tumova, K., Zhang, D., and Tiberi, M. (2004) Role of the fourth intracellular loop of D1-like dopaminergic receptors in conferring subtype-specific signaling properties. *FEBS Lett* **576**, 461-467

Undie, A. S., and Friedman, E. (1990) Stimulation of a dopamine D1 receptor enhances inositol phosphates formation in rat brain. *J Pharmacol Exp Ther* **253**, 987-992

Usiello, A., Baik, J. H., Rouge-Pont, F., Picetti, R., Dierich, A., LeMeur, M., Piazza, P. V., and Borrelli, E. (2000) Distinct functions of the two isoforms of dopamine D2 receptors. *Nature* **408**, 199-203

Valentin-Hansen, L., Groenen, M., Nygaard, R., Frimurer, T. M., Holliday, N. D., and Schwartz, T. W. (2012) The arginine of the DRY motif in transmembrane segment III functions as a balancing micro-switch in the activation of the beta2-adrenergic receptor. *J Biol Chem* **287**, 31973-31982

Valjent, E., Pascoli, V., Svenningsson, P., Paul, S., Enslen, H., Corvol, J. C., Stipanovich, A., Caboche, J., Lombroso, P. J., Nairn, A. C., Greengard, P., Herve, D., and Girault, J. A. (2005) Regulation of a protein phosphatase cascade allows convergent dopamine and glutamate signals to activate ERK in the striatum. *Proc Natl Acad Sci U S A* **102**, 491-496

Vanni, S., Neri, M., Tavernelli, I., and Rothlisberger, U. (2009) Observation of "ionic lock" formation in molecular dynamics simulations of wild-type beta 1 and beta 2 adrenergic receptors. *Biochemistry* **48**, 4789-4797

Vargas, G. A., and Von Zastrow, M. (2004) Identification of a novel endocytic recycling signal in the D1 dopamine receptor. *J Biol Chem* **279**, 37461-37469

Vassilatis, D. K., Hohmann, J. G., Zeng, H., Li, F., Ranchalis, J. E., Mortrud, M. T., Brown, A., Rodriguez, S. S., Weller, J. R., Wright, A. C., Bergmann, J. E., and Gaitanaris, G. A. (2003) The G protein-coupled receptor repertoires of human and mouse. *Proc Natl Acad Sci U S A* **100**, 4903-4908

Ventura, A. L., and Sibley, D. R. (2000) Altered regulation of the D(1) dopamine receptor in mutant Chinese hamster ovary cells deficient in cyclic AMP-dependent protein kinase activity. *J Pharmacol Exp Ther* **293**, 426-434

Vickery, R. G., and von Zastrow, M. (1999) Distinct dynamin-dependent and -independent mechanisms target structurally homologous dopamine receptors to different endocytic membranes. *J Cell Biol* **144**, 31-43

von Kleist, L., Stahlschmidt, W., Bulut, H., Gromova, K., Puchkov, D., Robertson, M. J., MacGregor, K. A., Tomilin, N., Pechstein, A., Chau, N., Chircop, M., Sakoff, J., von Kries, J. P., Saenger, W., Krausslich, H. G., Shupliakov, O., Robinson, P. J.,

McCluskey, A., and Haucke, V. (2011) Role of the clathrin terminal domain in regulating coated pit dynamics revealed by small molecule inhibition. *Cell* **146**, 471-484

Wang, Q., Jolly, J. P., Surmeier, J. D., Mullah, B. M., Lidow, M. S., Bergson, C. M., and Robishaw, J. D. (2001) Differential dependence of the D1 and D5 dopamine receptors on the G protein gamma 7 subunit for activation of adenylylcyclase. *J Biol Chem* **276**, 39386-39393

Warne, T., Serrano-Vega, M. J., Baker, J. G., Moukhametzianov, R., Edwards, P. C., Henderson, R., Leslie, A. G., Tate, C. G., and Schertler, G. F. (2008) Structure of a beta1-adrenergic G-protein-coupled receptor. *Nature* **454**, 486-491

Wess, J. (1998) Molecular basis of receptor/G-protein-coupling selectivity. *Pharmacol Ther* **80**, 231-264

Wettschureck, N., and Offermanns, S. (2005) Mammalian G proteins and their cell type specific functions. *Physiol Rev* **85**, 1159-1204

Willox, A. K., Sahraoui, Y. M., and Royle, S. J. (2014) Non-specificity of Pitstop 2 in clathrin-mediated endocytosis. *Biol Open* **3**, 326-331

Yan, Z., Hsieh-Wilson, L., Feng, J., Tomizawa, K., Allen, P. B., Fienberg, A. A., Nairn, A. C., and Greengard, P. (1999) Protein phosphatase 1 modulation of neostriatal AMPA channels: regulation by DARPP-32 and spinophilin. *Nat Neurosci* **2**, 13-17

Zhang, B., Yang, X., and Tiberi, M. (2015) Functional importance of two conserved residues in intracellular loop 1 and transmembrane region 2 of Family A GPCRs: insights from ligand binding and signal transduction responses of D1 and D5 dopaminergic receptor mutants. *Cell Signal* **27**, 2014-2025

Zhang, J., Ferguson, S. S., Barak, L. S., Menard, L., and Caron, M. G. (1996) Dynamin and beta-arrestin reveal distinct mechanisms for G protein-coupled receptor internalization. *J Biol Chem* **271**, 18302-18305

Zhang, J., Barak, L. S., Anborgh, P. H., Laporte, S. A., Caron, M. G., and Ferguson, S. S. (1999) Cellular trafficking of G protein-coupled receptor/beta-arrestin endocytic complexes. *J Biol Chem* **274**, 10999-11006

Zhang, J., Vinuela, A., Neely, M. H., Hallett, P. J., Grant, S. G., Miller, G. M., Isacson, O., Caron, M. G., and Yao, W. D. (2007) Inhibition of the dopamine D1 receptor signaling by PSD-95. *J Biol Chem* **282**, 15778-15789

Zhou, X. M., Sidhu, A., and Fishman, P. H. (1991) Desensitization of the human D(1) dopamine receptor: Evidence for Involvement of both cyclic AMP-dependent and receptor-specific protein kinases. *Mol Cell Neurosci* **2**, 464-472

Zhuang, X., Belluscio, L., and Hen, R. (2000) G(olf)alpha mediates dopamine D1 receptor signaling. *J Neurosci* **20**, RC91